

FABRICATION AND LIGHT SCATTERING STUDY OF MULTI-RESPONSIVE  
NANOSTRUCTURED HYDROGELS AND WATER-SOLUBLE POLYMERS

Xiaohu Xia, B.E.

Dissertation Prepared for the Degree of  
DOCTOR OF PHILOSOPHY

UNIVERSITY OF NORTH TEXAS

December 2003

APPROVED:

Zhibing Hu, Major Professor

Martin Schwartz, Committee Member

Paul Marshall, Committee Member

William E. Acree Jr., Committee Member

Tom Cundari, Chair of Graduate Studies in  
Department of Chemistry

Ruthanne D. Thomas, Chair of the Department of  
Chemistry

Sandra L. Terrell, Interim Dean of the Robert B.  
Toulouse School of Graduate Studies

Xia, Xiaohu, Fabrication and light scattering study of multi-responsive nanostructured hydrogels and water-soluble polymers. Doctor of Philosophy (Analytical Chemistry), December 2003, 112 pages, 2 tables, 31 illustrations, 121 references.

Monodispersed microgels composed of poly-acrylic acid (PAAc) and poly(N-isopropylacrylamide) (PNIPAM) interpenetrating networks were synthesized by 2-step method with first preparing PNIPAM microgel and then polymerizing acrylic acid that interpenetrates into the PNIPAM network. The semi-dilute aqueous solutions of the PNIPAM-PAAc IPN microgels exhibit an inverse thermo-reversible gelation. Furthermore, IPN microgels undergo the reversible volume phase transitions in response to both pH and temperature changes associated to PAAc and PNIPAM, respectively. Three applications based on this novel hydrogel system are presented: a rich phase diagram that opens a door for fundamental study of phase behavior of colloidal systems, a thermally induced viscosity change, and *in situ* hydrogel formation for controlled drug release.

Clay-polymer hydrogel composites have been synthesized based on PNIPAM gels containing 0.25 to 4 wt% of the expandable smectic clay Na-montmorillonite layered silicates (Na-MLS). For Na-MLS concentrations ranging from 2.0 to 3.2 wt%, the composite gels have larger swelling ratio and stronger mechanical strength than those for a pure PNIPAM. The presence of Na-MLS does not affect the value of the lower critical solution temperature (LCST) of the PNIPAM.

Surfactant-free hydroxypropyl cellulose (HPC) microgels have been synthesized in salt solution. In a narrow sodium chloride concentration range from 1.3 to 1.4 M, HPC

chains can self-associate into colloidal particles at room temperature. The microgel particles were then obtained in situ by bonding self-associated HPC chains at 23 °C using divinyl sulfone as a cross-linker. The volume phase transition of the resultant HPC microgels has been studied as a function of temperature at various salt concentrations. A theoretical model based on Flory-Huggins free energy consideration has been used to explain the experimental results.

Self-association behavior and conformation variation of long chain branched (LCB) poly (2-ethyloxazoline) (PEO<sub>x</sub>) with a CH<sub>3</sub>-(CH<sub>2</sub>)<sub>17</sub> (C<sub>18</sub>) modified surface are investigated using light scattering techniques in various solvents. The polymer critical aggregation concentration (cac) strongly depends on solvent polarity, decreasing as the solvent becomes more hydrophobic.

## ACKNOWLEDGMENTS

I am grateful to many people in the University of North Texas for their help and guidance. In particular, I would like to thank my supervisor Professor Zhibing Hu for his encouragement, friendship and countless hours of conversation, including many ideas presented here.

My appreciation also extends to Dr. Martin Schwartz, Dr. Paul Marshall, Dr. Oliver Chyan and Dr. William E. Acree Jr. who served my doctoral committee.

I gratefully acknowledge financial support from U. S. Army Research Office, National Science Foundation and the Petroleum Research Fund.

I would like to express my deepest gratitude to my parents for their wisdom, guidance, and support. My passion toward chemistry was originated from the profound influence of their highly instructive education since my childhood.

Finally, I would like to thank my wife Zhiling Zhang for her patience and love.

## TABLE OF CONTENTS

ACKNOWLEDGEMENTS .....	ii
LIST OF TABLES .....	iv
LIST OF ILLUSTRATIONS .....	v
CHAPTER 1 INTRODUCTION .....	1
CHAPTER 2 THEORETICAL BACKGROUND OF LASER LIGHT SCATTERING .....	13
CHAPTER 3 SYNTHESIS AND LIGHT SCATTERING STUDY OF MICROGELS WITH INTERPENETRATING POLYMER NETWORKS.....	25
CHAPTER 4 SWELLING AND MECHANICAL BEHAVIOR OF POLY(N- ISOPROPYLACRYLAMIDE)/Na-MONTMORILLONITE LAYERED SILICATES COMPOSITE GELS .....	51
CHAPTER 5 FORMATION AND VOLUME PHASE TRANSITION OF HYDROXYPROPYL CELLULOSE MICROGELS IN SALT SOLUTION .....	66
CHAPTER 6 LIGHT SCATTERING STUDY OF SELF-ASSOCIATION BEHAVIOR OF LONG CHAIN BRANCHED POLY(2-ETHYLOXAZOLINE) IN SOLVENTS .....	81
CHAPTER 7 CONCLUSION.....	101
BIBLIOGRAPHY .....	103
APPENDIX.....	112

## LIST OF TABLES

TABLE 3.1 PNIPAM AND IPN MICROGELS COMPARISON SUMMARY .....	36
TABLE 4.1 COMPOSITION AND CHARACTERIZATION RESULTS FOR Na- MLS/PNIPAM SAMPLES .....	53

## LIST OF ILLUSTRATIONS

2.1 SCHEMATIC SETUP OF THE LASER LIGHT SCATTERING INSTRUMENT .....	23
2.2 A COMMERCIAL ALV/DLS/SLS-5000 LASER LIGHT SCATTERING (LLS) .....	23
3.1 HYDRODYNAMIC RADIUS $R_h$ VARIATION OF THE PARTICLES DURING IPN SYNTHESIS .....	29
3.2 TURBIDITY CHANGE OF REACTING SOLUTION DURING IPN SYNTHESIS .....	30
3.3 IPN NANOPARTICLE SYNTHESIS .....	32
3.4 SIZE DISTRIBUTIONS OF IPN MICROGEL AND ITS PRECURSOR PNIPAM NANOPARTICLES .....	33
3.5 ZIMM PLOT OF STATIC LIGHT SCATTERING FOR (A) PNIPAM NANOPARTICLES; (B) IPN NANOPARTICLES .....	34
3.6 TEMPERATURE INDUCED PHASE TRANSITION FOR PNIPAM AND IPN NANOPARTICLES .....	37
3.7 IMAGES OF IPN SEMI-DILUTE AQUEOUS SOLUTION BELOW AND ABOVE THE LCST OF PNIPAM ( $\sim 34^{\circ}\text{C}$ ) .....	38
3.8 THE pH INDUCED PHASE TRANSITION FOR PNIPAM AND IPN NANOPARTICLES .....	40
3.9 SIZE DISTRIBUTIONS OF IPN NANOPARTICLES AT DIFFERENT pH ENVIRONMENTS .....	41
3.10 THE PHASE BEHAVIOR OF THE PNIPAM-PAA IPN NANOPARTICLES IN WATER .....	42

3.11 TEMPERATURE-DEPENDENT VISCOSITY. VISCOSITIES OF AQUEOUS SOLUTIONS OF IPN (C=1.97 WT%), IPN (C= 3.27 WT%) AND PNIPAM (C=3.27 WT%) WERE MEASURED AS A FUNCTION OF TEMPERATURE USING A BROOKFIELD VISCOMETER .....	44
3.12 A CUMULATIVE RELEASE OF MODEL DRUGS FROM AN <i>in situ</i> FORMED GEL DEPOT .....	46
4.1 OPTICAL IMAGES OF COMPOSITE GELS BY AXIOPLAN POLARIZING OPTICAL MICROSCOPE .....	55
4.2 SWELLING RATIO ( $d/d_o$ ) FOR THE PNIPAM GEL AND ITS COMPOSITES AT 23°C, WHERE $d$ IS THE EQUILIBRIUM GEL FILAMENT DIAMETER AND $d_o$ IS THE CAPILLARY DIAMETER. THE SHEAR MODULI OF NA-MLS/PNIPAM COMPOSITES ARE ALSO SHOWN IN THE FIGURE, MEASURED AT 23°C .....	57
4.3 TEMPERATURE DEPENDENCE PHASE TRANSITION OF THE PNIPAM GEL AND ITS COMPOSITE WITH UP TO 4.0 WT% OF NA-MLS IN WATER .....	59
4.4 THE RELATIVE SIZE CHANGE ( $\Delta l/l_o$ ) OVER THE VOLUME PHASE TRANSITION TEMPERATURE FOR THE PNIPAM GEL AND ITS COMPOSITES.....	61
4.5 THE pH SENSITIVITY OF NIPA-SA COPOLYMER, PURE PNIPAM AND NA-MLS/PNIPAM COMPOSITE GELS .....	62
5.1 THE LCST OF UN-CROSS-LINKED HPC DECREASES WITH INCREASING SODIUM CHLORIDE CONCENTRATION .....	69
5.2 HYDRODYNAMIC RADIUS DISTRIBUTIONS ( $f(R_h)$ ) OF HPC MICROGEL PARTICLES ( $C = 5.0 \times 10^{-5}$ g/mL) IN DEIONIZED WATER AT 23.5°C .....	71



5.3 SODIUM CHLORIDE INDUCED HPC MICROGEL PARTICLES ( $C = 5.0 \times 10^{-5}$ G/ML)	
VOLUME PHASE TRANSITION AT 23.5 <sup>o</sup> C .....	74
5.4 TEMPERATURE-INDUCED VOLUME PHASE TRANSITION OF HPC MICROGEL	
PARTICLES ( $C = 5.0 \times 10^{-5}$ G/ML) UNDER DIFFERENT SODIUM CHLORIDE	
CONCENTRATIONS .....	75
6.1 A SCHEMATIC DIAGRAM OF THE CHEMICAL STRUCTURE OF THE LONG CHAIN	
BRANCHED POLY(2-ETHYLOXAZOLINE) .....	83
6.2 HYDRODYNAMIC RADIUS DISTRIBUTION PROFILES OF THE LONG CHAIN	
BRANCHED-PEOX IN ETHANOL AT 23 <sup>o</sup> C .....	85
6.3 THE CHANGE IN HYDRODYNAMIC RADIUS $\langle R_h \rangle$ AND NORMALIZED	
SCATTERING LIGHT INTENSITY ( $I/C$ ) OF LONG CHAIN BRANCHED-PEOX IN	
ETHANOL AS A FUNCTION OF POLYMER CONCENTRATION AT 23 <sup>o</sup> C .....	86
6.4 COMPARISON OF THE HYDRODYNAMIC RADIUS $\langle R_h \rangle$ AND NORMALIZED	
LIGHT SCATTERING INTENSITY AS A FUNCTION OF POLYMER	
CONCENTRATION FOR WATER, METHANOL, ETHANOL, AND THF AT 23 <sup>o</sup> C .....	88
6.5 THE SKETCH OF CONFORMATION OF INDIVIDUAL LONG CHAIN BRANCHED-	
PEOX AND THEIR AGGREGATES IN VARIOUS SOLVENTS .....	90
6.6 ZIMM PLOT OF THE LONG CHAIN BRANCHED-PEOX IN ETHANOL AT 23 <sup>o</sup> C,	
WHERE THE POLYMER CONCENTRATION RANGES FROM $2.5 \times 10^{-5}$ G/ML TO $1.0$	
$\times 10^{-4}$ G/ML .....	93
6.7 THE TEMPERATURE DEPENDENT CONFORMATION CHANGE OF THE	
INDIVIDUAL LONG CHAIN BRANCHED-PEOX IN ETHANOL .....	95

6.8 COMPARISON OF HYDRODYNAMIC RADIUS DISTRIBUTION PROFILES FOR THE LONG CHAIN BRANCHED-PEOX IN ETHANOL, METHANOL, AND WATER AT 23 <sup>0</sup> C .....	97
---------------------------------------------------------------------------------------------------------------------------------------------------------------	----

## CHAPTER 1

### INTRODUCTION

The subject of colloid science covers an extremely broad range of seemingly different systems. What these systems have in common are their constituent units: small objects that have at least one characteristic dimension in the range of 1 nm to 1 micron. These objects are usually referred to as colloidal particles, which have long been used as the major components of industrial products such as foods, inks, paints, coatings, papers, cosmetics, biomedical materials, photographic films, and rheological fluids.<sup>1-2</sup> They are also frequently seen and studied in materials science, chemistry, and biology. Notable examples include slurries, clays, minerals, aerosols, or foams in materials science, macromolecules (including dendrimers), aggregates of surfactant molecules, semiconductor nanocrystallites, silica colloids, or polymer latexes in chemistry, and proteins, viruses, bacteria, or cells in biology.

As a special member of the colloidal family, microgels are cross-linked particles that are swollen in a good solvent and exhibit behavior ranging from that of polymer solutions to that of hard spheres.<sup>3-7</sup> In this dissertation, the synthesis and light scattering study of a series of nanostructured materials including poly(*N*-isopropylacrylamide) (PNIPAM) / poly(acrylic acid) (PAAc) interpenetrating polymer networks (IPN) microgel, PNIPAM/Na-MLS (sodium montmorillonite layered silicates) nanocomposites, FDA approved natural material hydroxypropyl cellulose (HPC) microgels and long chain branched polymer poly(2-ethylloxazoline) are illustrated. The dissertation is composed of seven chapters, in which chapters 2-7 are briefly described as follows:

The fundamental theory and application of laser light scattering technique are illustrated in chapter 2. The characterization of colloidal particles are normally being approached by two categories of laser light scattering techniques: 1) measurement of the time-average scattered intensity  $\langle I \rangle$  of photon counts  $\langle n \rangle$  and 2) the fluctuation of  $I(t)$  or  $n(t)$  with time. These two measurements are referred to as static light scattering (elastic, non-absorption) SLS and dynamic (quasi-elastic) light scattering DLS, respectively. The colloidal particle's translational diffusion coefficient ( $D$ ), relaxation rate ( $\Gamma$ ), hydrodynamic radius can be determined by DLS. In contrast, the static light scattering SLS is used to measure the time-average scattered intensity at different angles and concentrations, with which the physical parameters of macromolecules such as the weight-average molecular weight ( $M_w$ ), the z-average root-mean-square radius of gyration  $\langle R_g \rangle$  and the second-order virial coefficient ( $A_2$ ) could be determined.

Hydrogels containing two interpenetrating polymer networks (IPN) have attracted an intensive investigation.<sup>8</sup> This is because an IPN hydrogel usually exhibits properties that a hydrogel with the random co-polymerization of two monomers does not have. For example, the IPN of poly(acrylic acid) (PAAc) and polyacrylamide (PAAM) undergoes the volume phase transition driven by cooperative “zipping” interactions between the molecules which result from hydrogen bonding.<sup>8</sup> In addition to the improved mechanical properties which usually come from the reinforcement between two interpenetrating networks,<sup>9</sup> an IPN hydrogel can have a preferred direction for swelling by pre-stressing one of them (poly-*N*-isopropylacrylamide (PNIPAM)) before the gelation of the other one (polyacrylamide (PAAM)) takes place.<sup>10</sup> A well-designed hydrogel with an IPN structure shows an upper critical solution temperature without a volume change.<sup>11</sup>

Two polymer chain networks in an IPN gel can be sensitive independently to two different external stimuli. Such hydrogels have been employed for controlled drug delivery.<sup>12-14</sup> The PNIPAM gel undergoes the volume phase transition at  $T_c=34\text{ }^{\circ}\text{C}$ <sup>15-20</sup> and has been used often as one of the components in an IPN gel. Its phase transition temperature remains the same if the PNIPAM is incorporated in an IPN matrix. However, the random copolymerization results in shifting  $T_c$  depending on the hydrophilic/hydrophobic moieties of the co-monomer.<sup>14</sup>

IPN microgel particles have been synthesized because they are more effective as delivery systems than macroscopic gels for agrochemical or medical applications.<sup>21</sup> A comparison of the swelling behavior of the random P(AAc-co-AAm) particles and PAAc/PAAm IPN microgels has been made using temperature and pH as the triggers.<sup>21</sup> Jones and Lyon, on the other hand, showed multiresponsive core-shell microgels that consist of a weakly interpenetrating polymer network core and a shell<sup>22</sup>. These microgels were prepared by precipitation polymerization at  $70\text{ }^{\circ}\text{C}$  in aqueous media. In the synthesis of the shell polymer, the collapsed particles serve as nuclei for further polymerization, thereby resulting in preferential growth of the existing particles over the nucleation of new ones.<sup>22</sup>

In Chapter 3, a method to synthesize an IPN microgel of PNIPAM/PAAc is presented. I extended Jones and Lyon's method by controlling reaction time so that the reaction was stopped once the interpenetrating network was formed at room temperature.<sup>22</sup> I present the synthesis and light scattering characterization of these microgels, which displays the same  $T_c$  as the PNIPAM but shrinks less than the PNIPAM above  $T_c$ . The semi-dilute aqueous solutions of the PNIPAM-PAAc IPN microgels exhibit unusually inverse thermo-reversible gelation. In contrast to polymer solutions of poly(NIPAM-co-AAc) that have the inverse thermo-reversible gelation,<sup>23-26</sup> our system can self-assemble into an ordered structure, displaying bright colors. Three

applications based on this novel hydrogel system are presented: a rich phase diagram that opens a door for fundamental study of phase behavior of colloidal systems, a thermally induced viscosity change, and *in situ* hydrogel formation for controlled drug release.

Gels are crosslinked polymer networks swollen in a liquid medium. The liquid inside the gel allows diffusion of some solute molecules, while the polymer network serves as a matrix to hold the liquid together. Swelling and mechanical properties of PNIPAM gels have been investigated intensively.<sup>27-29</sup> It has been found that increasing crosslinker concentration can enhance PNIPAM mechanical strength.<sup>30</sup> However, a large amount of crosslinkers could result in the shift of the volume transition temperature and in the reduction of swelling capability.<sup>31-32</sup> It is well known that the properties of gels can be significantly enhanced by incorporation of inorganic ordered systems, in particular clays, into the gels.<sup>33-36</sup> As a model system, sodium montmorillonite layered silicates (Na-MLS) is widely used as an additive for plastics to improve their physical properties. The chemical structure of the Na-MLS has been reported.<sup>37</sup>

It has been found that incorporating clay into poly(acrylamide) gel enhanced the gel elastic modulus while exhibiting no significant improvement to its swelling ability.<sup>34</sup> PNIPAM/Na-MLS composite materials have been made with high Na-MLS concentrations (above 3.5 wt%) and their swelling behavior as a function of temperature has been studied.<sup>35</sup> However, despite the potential of low content Na-MLS (less than 3.5 w%) on the swelling ratio, the volume phase transition temperature and shear modulus of the PNIPAM gel has not been investigated so far. In chapter 4, we present the results of the swelling and elastic properties of a series of PNIPAM composites with Na-MLS concentrations ranging from 0.25 w% to 4.0 w%.

The volume phase transition in polymer gels can be induced by many external stimuli such as temperature, solvent composition, light, electric field, and pH value.<sup>19, 38</sup> Hydroxypropyl cellulose (HPC), one of the thermally responsive gels similar to the poly(*N*-isopropylacrylamide) (PNIPAM), has received considerable attention because of its biocompatibility.<sup>39-43</sup> Bulk HPC hydrogels and its derivatives with various forms including homogeneous gel, porous gel, and gel beads have been extensively studied.<sup>42-43</sup> Our group has reported the synthesis of HPC microgel particles<sup>44</sup> using a precipitation polymerization method. For polymer chains like the HPC that contain both hydrophobic and hydrophilic portions, changing the properties of the solvent by other ways may also induce self-association, leading to the formation of colloidal particle aggregates. It is known that addition of salt can lower the phase transition temperature in ionic and nonionic gels.<sup>45-47</sup> This effect is caused by the competing interactions between salt and water and between water and polymer chains.

In chapter 5, I show that HPC microgel particles have been synthesized at room temperature by adding salt into HPC-water solution. In contrast to a previous method<sup>44</sup> that requires one to heat a HPC-water solution above the low critical solution temperature (LCST) of the HPC at about 41°C, the current method is to first reduce the LCST of HPC polymer chains from 41°C to room temperature by adding salt into the HPC-water solution and then to bond HPC globules without surfactant at room temperature. These microgels may be used as building blocks for the formation of nanoparticle networks<sup>22, 48</sup> and as carriers for controlled drug delivery. The volume phase transition of the resultant microgels has been investigated using light scattering techniques. The results have been discussed in terms of Flory-Huggins swelling equilibrium of gels and compared with the previous study of bulk PNIPAM gels.<sup>27</sup>

A new architectural class of polymeric materials known as dendritic materials, including dendrimers and their more readily accessible but less structurally-defined counterparts known as hyperbranched polymers (HBPs) and long chain branched polymers (LCBPs) have received a great deal of interest in the last decade.<sup>49-56</sup> Work on dendrimers, HBPs and LCBPs has primarily focused on their synthesis and chemical modification with an eye toward micelle mimics, nanoscale building blocks and drug-delivery agents.<sup>57-58</sup> At the same time, intensive efforts have been made to study fundamental properties of these macromolecules using various analytic tools including NMR,<sup>59</sup> rheology,<sup>60</sup> small angle neutron scattering and light scattering,<sup>61-63</sup> atomic force microscopy,<sup>64</sup> TEM,<sup>65</sup> fluorescence Probing.<sup>66</sup>

The effect of solvent quality on dendrimer conformation has been investigated and it was found that the average dimension of dendrimers has a small but significant dependence on the solvent quality, which consequently leads to large variations of average segment density.<sup>63, 67-68</sup> Recently, a novel  $\text{CH}_3\text{-(CH}_2\text{)}_{17}$  surface modified LCB-poly (2-ethyloxazoline) (PEOx) polymer, was synthesized using a cationic polymerization method. With the internal tertiary amide functional group on repeat ethyloxazoline units and external  $\text{C}_{18}$  chains, it possesses a hydrophilic core and a hydrophobic shell. The grafted hydrophobic  $\text{C}_{18}$  chains aim to act as a smart arm to move intelligently according to solvent environment. This unique architecture may provide us a model system to study solvent quality effect on LCBP conformation and its self-association in different solvents. The study may lead to not only better understanding of self-association of macromolecules in general, but also to potential applications in the fields of nanoscale catalysts, reactors, and controlled drug delivery.



Self-association is a well-known self-assembling phenomenon often found in diblock or triblock copolymer/solvent systems,<sup>69-70</sup> where the selective solvent to specific polymer blocks can lead to the formation of nanoparticles or chain aggregates without precipitation. Linear polymer self-association processes and mechanisms have been well studied. For example, it was found that in concentrated solutions, neutral poly (*N*-isopropylacrylamide) (PNIPAM) homopolymer chains self-associate above their lower critical solution temperature (LCST, ~32°C) to stable aggregates instead of undergoing the expected precipitation.<sup>71</sup> In these processes, chain collapse accompanied chain association, forming stable aggregates of different sizes at different temperatures and concentrations. Our previous studies revealed that the driving force leading to hydropropylcellulose (HPC) self-association results from hydrophobic attraction between hydrophobic moieties of HPC linear chains when water becomes a poor solvent above the LCST of the HPC.<sup>44</sup> It is thus reasonable to rationalize that, for the hyper-branched polymers containing both hydrophobic and hydrophilic portions, changing the properties of the solvent may induce self-association, leading to the formation of stable LCBP aggregates.

In chapter 6, light scattering techniques were used to study the LCBP self-associate processes because the scattering light intensity is very sensitive to particle size. I demonstrated that long chain branched-PEOx can self-associate at different critical aggregation concentrations (*cac*) and form metastable aggregates in ethanol, methanol and tetrahydrofuran. The *cac* depends strongly on solvent polarity. Below the *cac*, static light scattering measurements revealed properties of individual long chain branched-PEOx macromolecules including its molar mass and second virial coefficient. Heating a dilute long chain branched-PEOx ethanol solution to higher temperatures leads to significant shrinkage of the hydrodynamic radius of the macromolecules.

In chapter 7, the main conclusions of the dissertation are summarized.

## CHAPTER REFERENCES:

1. Everett, D. H. *Basic Principles of Colloid Science*, London **1998**
2. Russel, W. B., Saville, D. A., Schowalter, W.R. *Colloidal Dispersions*, Cambridge University Press, Cambridge **1989**
3. Saunders, B. R.; Vincent, B. *Adv. Colloid Interface Sci.* **1999**, 80, 1
4. Murry, M. J.; Snowden, M. J. *Adv. Colloid Interface Sci.* **1995**, 54, 73
5. Senff, H.; Richtering, W. *J. Chem. Phys.* **1999**, 111, 1705
6. Senff, H.; Richtering, W. *Langmuir* **1999**, 15, 102
7. Bartsch, E.; Kirsch, S.; Lindner, P.; Scherer, T.; Stolken, S. *Ber. Bunsen-Ges. Phys. Chem.* **1998**, 102, 1597
8. Ilmain, F., Tanaka, T., Kokufuta, E. *Nature* **1991**, 349, 400
9. Sperling, L. H. *Adv. Chem. Ser.* **1994**, 239, 12
10. Wang, C. J., Hu, Z. B., Chen, Y. Y., Li, Y. *Macromolecules* **1999**, 32, 1822
11. Chen, L., Gong, J., Osada, Y. *Macromolecular Rapid Communications* **2002**, 23, 171.
12. Katono, H., Sanui, K., Ogata, N., Okano, T., Sakurai, Y. *Polym J* **1991**, 23, 1179; Katono, H., Maruyama, A., Sanui, K., Ogata, N., Okano, T., Sakurai, Y. *J Control Rel* **1991**, 16, 215
13. Gutowska, Y.H., Bae, H., Jacobs, J., Feijen, Sung Wan Kim, *Macromolecules*, **1994**, 27, 4167
14. Park, T. G., Choi, H. K. *Macromol. Rapid Commun.* **1998**, 19, 167
15. Hirotsu, S., Hirokawa, Y., Tanaka, T. *J. Chem. Phys.* **1987**, 87, 1392
16. Wu, C., Zhou, S. *Macromolecules* **1996**, 29, 1574
17. Benee, L. S., Snowden, M. J., Chowdhry, B. Z. *Langmuir* **2002**, 18, 6025
18. Routh, A. F., Vincent, B. *Langmuir* **2002**, 18, 5366

19. Woodward, N. C., Chowdhry, B. Z., Snowden, M. J., Leharne, S. A., Griffiths, P. C., Winnington, A. L. *Langmuir* **2003**, 19, 3202
20. Gao, J., Frisken, B. J. *Langmuir* **2003**, 19, 5217
21. Bouillot, P., Vincent, B. *Colloid and Polymer Science* **2000**, 278, 74
22. Jones, C. D., Lyon, L.A. *Macromolecules* **2000**, 33, 8301
23. Kato, T., Yokoyama, M., Takahashi, A. *Colloid & Polym. Sci.* **1978**, 256, 15
24. Almgren, M., Bahadur, P., Jansson, M., Li, P., Brown, W., Bahadur, A.J. *Colloid & Interface Sci.* **1992**, 151, 157; Alexandridis, P., Hatton, T. A. *Colloidal Surfaces A: Physicochem. Eng. Aspects* **1995**, 96, 1
25. Han, C. K., Bae, Y. H. *Polymer* **1998**, 39, 2809
26. Jeong, B., Kim, S. W., Bae, Y. H. *Adv. Drug Del. Rev.* **2002**, 54, 37
27. Hirotsu, S., Hirokawa, Y., Tanaka T. *J. Chem. Phys.* **1987**, 87, 1392
28. Shinde, V.S., Badiger, M.V., Lele, A.K., Mashelkar, R.A. *Langmuir* **2001**, 17, 2585
29. Zhang, X., Zhuo, R., Yang, Y. *Biomaterials*, **2002**, 23, 1313
30. Takigawa, T., Yamawaki, T., Takahashi, K., Masuda, T. *Polymer Gels and Networks*, **1997**, 5, 585
31. Xue, W., Champ, S. Huglin, M.B. *Polymer* **2001**, 42, 3665
32. Lu, X., Hu, Z., Gao, J. *Macromolecules* **2000**, 33, 8698
33. Gao, D., Heimann, R.B. *Polymer Gels and Networks* **1993**, 1, 225
34. Churochkina, N.A., Starodoubtsev, S.G., Khokhlov, AA. *Polymer Gels and Networks* **1998**, 6, 205
35. Phillip, B., Messersmith, Znidarsich, F. *Mat. Res. Soc. Symp.* **1997**, 457
36. Haraguchi, K., Takehisa, T. *Adv. Mat.* **2002**, 14, 1120

37. Lvov, Y., Ariga, K., Ichinose, I., Kunitake, T. *Langmuir* **1996**, 12, 3038
38. Tanaka, T. *Phys. Rev. Lett.* **1978**, 40, 820
39. Kluc, E. D. *J. Polym. Sci.* **1971**, 36, 491
40. Drummond, C., Albers, S., Furlong, D. N. *J. Colloids Surf.* **1992**, 62, 75
41. Winnik, F. M., Tamai, N., Yonezawa, J., Nishimura, Y., Yamazaki, I. *J. Phys. Chem.* **1992**, 96, 1967
42. Kabra, B. G., Gehrke, S. H., Spontak, R. J. *Macromolecules* **1998**, 31, 21668
43. Harsh, D. C., Gehrke, S. H. *J. Controlled Release* **1991**, 17, 175
44. Gao, J., Haidar, G., Lu, X., Hu, Z. *Macromolecules* **2001**, 34, 2242
45. Ohmine, I., Tanaka, T. *J. Chem. Phys.* **1982**, 77, 5725
46. Park, T., Hoffman, A. S. *Macromolecules* **1993**, 26, 5045
47. Zhang, X., Hu, Z., Li, Y. *J. Appl. Polym. Sci.* **1997**, 63, 1851
48. Hu, Z. B., Lu, X., Gao, J. *Adv. Mater.* **2001**, 13, 1708
49. Moore, J.S. *Acc. Chem. Res.* **1997**, 30, 402
50. Tomalia, D. A., Baker, H., Dewald, J., Hall, M., Kallos, G., Martin, S., Roeck, J., Ryder, J., Smith, P. *Polym. J.* **1985**, 17, 117
51. Tomalia, D. A., Baker, H., Dewald, J., Hall, M., Kallos, G., Martin, S., Roeck, J., Ryder, J., Smith, P. *Macromolecules* **1986**, 19, 2466
52. Hawker, C.J., Frechet, J.M. *J. Am. Chem. Soc.* **1990**, 112, 7638
53. Kawaguchi, T., Walker, K.L., Wilkins, C.L., Moore, J.S. *J. Am. Chem. Soc.* **1995**, 117, 2159
54. Yin, R., Zhu, Y., Tomalia, D.A. *J. Amer. Chem. Soc.*, **1998**, 120, 2678
55. Aoki, A., Ghosh, P., Crooks, R.M. *Langmuir* **1999**, 15, 7418
56. Guan, Z., Cotts, P. M., McCord, E. F., McLain, S. J. *Science* **1999**, 283, 2059

57. Tomalia, D.A., Naylor, A.M., Goddard, W.A. *Angew. Chem. Int. Ed. Engl.* **1990**, 29, 138
58. Dagani, R. *Chemical and Engineering News* **1996**, 1
59. Meltzer, A. D., Tirrell, D. A., Jones, A. A. *Macromolecules* **1992**, 25, 4541
60. Uppuluri, S., Keinath, S. E., Dvornic, P. R. *Macromolecules*, **1998**, 31, 4498
61. Topp, A., Bauer, B.J., Prosa, T.J., Scherrenberg, R., Amis, E.J. *Macromolecules* **1999**, 32, 8923
62. Bauer, B., Topp, A., Prosa, T.J., Amis, E.J., Yin, R., Qin, D., Tomalia, D.A. *ACS PMSE Proc.* **1997**, 77, 87
63. Topp, A., Bauer, B.J., Tomalia, D.A., Amis, E.J. *Macromolecules* **1999**, 32, 7232
64. Li, J., Piehler, L.T., Meier, D.J. *Langmuir* **2000**, 16, 5613
65. Ottaviani, M.F., Favuzza, P., Tomalia, D. A. *Langmuir* **2000**, 16, 7368
66. Pistolis, G., Malliaris, A., Tsiourvas, D. *Langmuir* **1997**, 13, 5870
67. Ishizu, K., Takeda, H., *Eur. Polym. J.* **2001**, 37, 2073
68. Bayouhd, S., Laschewsky, A., Wishcherhoff, E., *Coll. Polym. Sci.* **1999**, 277, 519
69. Zhou, Z., Chu, B., Nace, V. M. *Langmuir* **1996**, 21, 5016
70. Yu, J.M., Jerome, R. *Macromolecules* **1996**, 29, 8371
71. Li, M., Wu, C. *Macromolecules* **1999**, 32, 4311

## CHAPTER 2

### THEORETICAL BACKGROUND OF LASER LIGHT SCATTERING

#### 2.1 INTRODUCTION

The field of light scattering is a well-studied, detailed scientific discipline on which a lot of information has been published. Lord Rayleigh first described the science of light scattering at the end of the 19<sup>th</sup> century, experiments in the field have proceeded thereafter within the limitations of the technology. When monochromatic, polarized lasers became available in the early 1970s, laser light scattering (LLS) technology began to be applied to practical instruments for research and industrial use. In contrast to the well known analytical tools such as Fluorescence, Phosphorescence and Raman spectroscopy, the fundamentals of LLS is based on the elastic light scattering where the frequency of the scattering light is the same as the incident light. When a coherent laser beam passes through a dilute colloidal dispersion, the incident light will be scattered by the dispersed particles in all of the directions. The scattered light intensity at different angles, as well as its time correlation function, is related to the particle size, size distribution, molar mass and conformations in the solution. The characterization of colloidal particles are normally being approached by two categories of laser light scattering techniques: 1) measurement of the time-average scattered intensity  $\langle I \rangle$  of photon counts  $\langle n \rangle$  and 2) the fluctuation of  $I(t)$  or  $n(t)$  with time. These two measurements are referred to as static (elastic, non-absorption) SLS and dynamic (quasi-elastic) light scattering DLS, respectively.

Assume that the particles are at rest in the solution, there will be no discrimination of the scattered light intensity in each direction and the value of scattering light intensity should be independent of time. In fact, however, all the particles or scatterers in solution are undergoing

constant Brownian motion. This Brownian motion leads to a fluctuation of the scattered intensity pattern. The fluctuation rate can be related to different kinds of relaxation processes such as diffusion (translation and rotation) and internal motions of the macromolecules. Faster relaxation process may lead to the faster intensity fluctuation.

The measurement interest of dynamic light scattering DLS is the intensity fluctuation, which is essentially caused by the Doppler effect. When an incident light is scattered by a moving macromolecule or particle, the frequency of the scattered light will be slightly higher or lower than that of the incident light, depending on the relative velocity between the detected particle and the detector. As a result, the frequency distribution of the scattered light will be slightly broader than that of the incident light. DLS is technically known as quasi-elastic light scattering QELS. Compared with the incident light frequency ( $10^{15}$  Hz), the scattered light frequency broadening ( $10^5$ - $10^7$  Hz) is very small and very hard to be detected in the frequency domain. Nonetheless, it could be accurately recorded in the time domain through a time correlation function. For this reason, dynamic light scattering is sometimes referred to as photon correlation spectroscopy (PCS). The colloidal particle's translational diffusion coefficient ( $D$ ), relaxation rate ( $\Gamma$ ), hydrodynamic radius can be determined by DLS. In contrast, the static light scattering SLS is used to measure the time-average scattered intensity at different angles and concentrations, with which we may calculate other physical parameters of macromolecules: the weight-average molecular weight ( $M_w$ ), the z-average root-mean-square radius of gyration  $\langle R_g^2 \rangle^{1/2}$ , (simply  $R_g$ ), and the second-order virial coefficient ( $A_2$ ).

Laser light scattering LLS, especially dynamic light scattering DLS, has evolved from a very special instrument for fundamental research work to a routine analytical tool in polymer laboratories during the past two decades. It is even used as a quality-control device in



production lines. Commercially available LLS instruments are normally capable of making both static and dynamic measurements simultaneously to study colloidal particles or macromolecules in solutions, as well as in gels and viscous media.

## 2.2 STATIC LASER LIGHT SCATTERING <sup>1-2</sup>

In practice, two interferences should be considered for static light scattering measurement for macromolecules or particles dispersion: 1) the intra-particle interference arising from different parts of a larger particle (dimension  $> \lambda/10$ ), whereas the intra-particle interference from small particles (dimension  $< \lambda/10$ ) may be neglected. 2) The inter-particle interference. For dilute solutions, the inter-particle interference could be neglected. Rayleigh ratio is an important concept in SLS which is defined as  $R = \frac{Ir^2}{I_0}$ , where  $I$  is the scattered intensity per unit scattering volume,  $I_0$  is the incident light intensity, and  $r$  is the average distance between the scatterers and the observer. Thus, the dimension of the Rayleigh ratio  $R$  is the reciprocal of the dimension of length. Based on the electromagnetic principle and concentration fluctuation theory, we can get the excess Rayleigh ratio of the dilute solution ( $R_{\text{excess}}$ )<sup>2</sup>:

$$R_{\text{excess}} = \frac{I_{\text{excess}} r^2}{I_0} = \frac{4\pi^2 n^2}{\lambda_0^4} \left( \frac{dn}{dc} \right)^2 \frac{kTC}{\partial\Pi/\partial C} \quad (2-2)$$

Where  $I_{\text{excess}}$  ( $=I_{\text{solution}}-I_{\text{solvent}}$ ) is the net scattering intensity of the solute by subtracting the intensity of solvent from that of the solution, and  $n$ ,  $\lambda_0$ ,  $C$ ,  $k$ ,  $T$ ,  $\Pi$  are the colloidal solution refractive index, the incident light wavelength, the solute concentration, the Boltzmann constant, the absolute temperature and the osmotic pressure, respectively.

For dilute macromolecule or particle solutions, the relationship of the osmotic pressure and colloidal concentration can be written as <sup>3</sup>

$$\frac{\Pi}{C} = \frac{N_0 kT}{M} (1 + A_2 CM + \dots) \quad (2-3)$$

Thus, 
$$\frac{\partial \Pi}{\partial C} = \frac{N_0 kT}{M} (1 + 2A_2 M + \dots) \quad (2-4)$$

where  $N_0$ ,  $M$ , and  $A_2$  are the Avogadro's number, the weight-average molecular weight, and the second order virial coefficient, respectively. By substitution of equation (2-4) into equation (2-2), the excess Rayleigh ratio  $R_{excess}$  can be express as:

$$R_{excess} = \frac{4\pi^2 n^2}{N_0 \lambda_0^4} \left(\frac{dn}{dc}\right)^2 \frac{CM}{1 + 2A_2 CM + \dots} \quad (2-5)$$

For a particular colloidal solution and incident laser,  $4\pi^2 n^2 (dn/dc)^2 / (N_0 \lambda_0^4)$  is a constant and can be represented by a single parameter  $K$ , thus (2-5) transforms to:

$$\frac{KC}{R_{excess}} = \frac{1}{M} + 2A_2 C + \dots \quad (2-6)$$

For larger macromolecules or colloidal particles, a construction factor should be introduced.

Here,  $P(\theta)$  is defined as an angular scattering function

$$P(\theta) = \frac{R(\theta)}{R(0)} = 1 - \frac{1}{3} q^2 \langle R_g^2 \rangle \quad (2-7)$$

where  $q = 4\pi n \sin(\theta/2) / \lambda$  is the magnitude of the scattering vector,  $\langle R_g^2 \rangle$  is the mean square of the radius of gyration. Thus,

$$\frac{KC}{R(\theta)} = \frac{1}{MP(\theta)} + 2A_2 C + \dots \quad (2-8)$$

As concentration  $C$  approaching to 0,

$$R(\theta) = KCMP(\theta) = KCM[1 - (1/3)q^2 \langle R_g^2 \rangle + \dots]$$

$$\frac{R(\theta)}{KC} = M[1 - \frac{1}{3}q^2 \langle R_g^2 \rangle + \dots] \quad (2-9)$$

When  $q^2 \langle R_g^2 \rangle \ll 1$ , omitting the higher order ( $>2$ ) terms in series, we get

$$\frac{KC}{R(\theta)} = \frac{1}{M} \left[ 1 + \frac{1}{3} q^2 \langle R_g^2 \rangle_z \right] + 2A_2 C \quad (2-10)$$

This is the basic equation of static light scattering SLS and is frequently shown in the literature,

<sup>4-7</sup> in which the molar mass is the weight-average  $M = \sum_i C_i M_i / \sum_i C_i$ ; and the mean square

radius of gyration is the z average  $\langle R_g^2 \rangle_z = \sum_i C_i M_i R_{g,i}^2 / \sum_i C_i M_i$ . It should be noted that the

Equation (2-10) is valid under the restriction that the polymer solution exhibits no adsorption, no fluorescence, and no depolarized scattering. It can be seen that when  $R(\theta)$  is measured at a series of  $C$  and  $q$ , we are able to determine  $\langle R_g^2 \rangle_z$  from the slope of  $[KC/R(\theta)]_{c \rightarrow 0}$  versus  $q^2$ ;  $A_2$  from the slope of  $[KC/R(\theta)]_{\theta \rightarrow 0}$  versus  $C$ ; and  $M_w$  from  $[KC/R(\theta)]_{c \rightarrow 0, k \rightarrow 0}$ . In practice, the Rayleigh ratio is determined by measuring the scattering intensity of polymer solution, background solvent and a standard solvent such as benzene or toluene, as shown in the following equation:

$$R_{vv}(\theta) = R_{vv}^0(\theta) \frac{I(\theta)_{\text{solution}} - I(\theta)_{\text{solvent}}}{I(\theta)_{\text{standard}}} \left( \frac{n_{\text{solvent}}}{n_{\text{standard}}} \right)^\gamma \quad (2-11)$$

The subscript “vv” means both the incident and the scattered light are vertically polarized;  $I$  and  $n$  are, respectively, the time-averaged scattering intensity and the refractive index. The term  $(n_{\text{solvent}}/n_{\text{standard}})^\gamma$  is a refraction correction for the scattering volume and  $\gamma$  is a constant between 1 and 2, depending on the detection geometry of the light scattering instrument, because we should compare the same scattering volumes from the solution and the reference standard.

### 2.3 DYNAMIC LASER LIGHT SCATTERING

The relation of interest in dynamic light scattering is the fluctuation of the scattered intensity with time  $t$ , caused by the particle Brownian motion.<sup>8,9</sup> The motion of the particles

includes transitional, rotational or internal motion. The moving macromolecules or particles scatter the incident light passing through the macromolecules or particles and result in two main effects: the fluctuation of the scattered intensity and the broadening of the frequency distribution. In frequency domain, the frequency shift of the scattered light is very difficult to precisely detect, because the frequency broadening ( $10^5$ - $10^7$  Hz) is much smaller than the incident light frequency ( $10^{15}$  Hz). However, in the time domain, the fluctuation of the scattered intensity is closely related to the frequency broadening and can be sensed by a highly sensitive and fast response photodiode detector. It is equally efficient to have either the fluctuation of the scattered intensity or the frequency broadening because the two effects are related to each other. The most commonly used method in quasi-elastic light scattering (QELS) is the digital technique of photon correction spectroscopy (or optical mixing), which measures the intensity fluctuation of the scattered light in the time domain. There are two basic forms of the optical mixing: heterodyne and homodyne (self-beating). Heterodyne mixing is the mixture of the scattered light with a reference beam (local oscillator), which has a constant frequency same as the incident light beam. Self-beating model, however, the scattering light is not mixed with a reference signal but directly being detected. The DLS theory illustrated in the following paragraphs is based on the self-beating intensity-intensity time correction spectroscopy.

The Siegert relation is an important equation in DLS. When the scattered field is a Gaussian process, the correlation functions  $g^{(1)}(t)$  and  $g^{(2)}(t)$  are connected through the Siegert relation <sup>2</sup>

$$g^{(2)}(t) = 1 + |g^{(1)}(t)|^2 \quad (2-12)$$

where  $g^{(1)}(t) \equiv [\langle E(0)E^*(t) \rangle / \langle E(0)E^*(0) \rangle]$  and  $g^{(2)}(t) \equiv [\langle I(0)I(t) \rangle / \langle I(0) \rangle^2]$  are the normalized field-field and normalized intensity-intensity autocorrelation functions, respectively.

Thus, the intensity-intensity time autocorrelation function becomes

$$G^{(2)}(t) = \langle I(0)I(t) \rangle = \langle I(0) \rangle^2 g^{(2)}(t) = \langle I(0) \rangle^2 [1 + |g^{(1)}(t)|^2] \quad (2-13)$$

The significance of introducing  $g^{(2)}(t)$  and  $G^{(2)}(t)$  is that  $G^{(2)}(t)$  and  $\langle I(0) \rangle$  can be measured experimentally. Since the detection area cannot be zero in practice, the scattered light is not purely coherent and an instrument parameter,  $\beta$  ( $<1$ ), is introduced into equation (2-13)

$$G^{(2)}(t) = A [1 + \beta |g^{(1)}(t)|^2] \quad (2-14)$$

where  $A(\equiv \langle I(0) \rangle^2)$  is the measurement baseline,  $t$  is the decay time, and  $\beta$  is the parameter depending on the coherence of the detection optics. In Equation (2-13),  $I(t)$  is the scattered intensity, or photon counts, at time  $t$ , it includes the contributions from both the solvent and the solute. Therefore,

$G^{(2)}(t) = \langle I(0)I(t) \rangle = \langle [I_{\text{solvent}}(0) + I_{\text{solute}}(0)][I_{\text{solvent}}(t) + I_{\text{solute}}(t)] \rangle$  and equation (2-12) becomes

$$G^{(2)}(t) = A \left\{ 1 + \beta \left[ \frac{I_{\text{solvent}}}{I_{\text{solution}}} |g_{\text{solvent}}^{(1)}| + \frac{I_{\text{solute}}}{I_{\text{solution}}} |g_{\text{solute}}^{(1)}(t)| \right]^2 \right\} \quad (2-15)$$

where all the cross terms disappear since the light scattered by solvent molecules and solute particles are not correlated. It should be noted that  $|g_{\text{solvent}}^{(1)}|$  decays much faster than  $|g_{\text{solute}}^{(1)}(t)|$  because small solvent molecules diffuse faster than particles do. Thus, after a very short delay time, equation (2-13) becomes<sup>1</sup>

$$G^{(2)}(t) = A \left[ 1 + \beta \left( \frac{I_{\text{solute}}}{I_{\text{solution}}} \right)^2 |g_{\text{solute}}^{(1)}(t)|^2 \right] = A [1 + \beta_{\text{app}} |g_{\text{solute}}^{(1)}|^2] \quad (2-16)$$

where  $\beta_{\text{app}} = \beta (I_{\text{solute}} / I_{\text{solution}})^2$ . For a dilute solution, the scattered intensity from solvent molecules could become appreciable, i.e.,  $I_{\text{solute}} \leq I_{\text{solution}}$ , so that the apparent coherence  $\beta_{\text{app}}$  would be even lower, i.e.,  $G^{(2)}(0)$  appears to have a lower value than expected. We should be

aware of this situation, especially for the weakly scattered, dilute, and low molar mass polymer solutions. For example, if  $I_{\text{solute}} = I_{\text{solvent}}$ ,  $\beta_{\text{app}} = \beta/4$ . It should be noted that  $\beta$  is constant for each particular optical geometry of the scattering instrument. In fact,  $I_{\text{solute}}$  can be estimated from  $\beta_{\text{app}}$  (certainly  $I_{\text{solute}}$  can be measured in static LLS by comparing the scattered intensity of solution and solvent.) if the values of  $\beta$  at different scattering angles have been pre-calibrated with a narrowly distributed latex standard whose scattering intensity is much stronger than water (solvent).

Now we will see how to get the information about the motion of the particles from the measured intensity-intensity time correlation function  $G^{(2)}(t)$ . Generally, the relaxation of  $|g^{(1)}(t)|$  includes both diffusion (translation and rotation) and internal motions. Let us only consider the translational diffusion relaxation of the particles. For monodisperse, spherical scatterers,  $|g^{(1)}(t)|$  is theoretically represented as an exponential decay function:

$$|g^{(1)}(t)| = G e^{-\Gamma t} \quad (2-17)$$

where  $G$  and  $\Gamma$  are the factor of proportionality and the line-width, respectively and

$\Gamma^{-1} = \tau_c$ , the characteristic decay time representing the rate of dynamic relaxation in self-beating.

For a polydisperse polymer sample with a continuous distribution of molar

mass  $M$ , equation (2-17) may be generalized as

$$|g^{(1)}(t)| = \int_0^{\infty} G(\Gamma) e^{-\Gamma t} d\Gamma \quad (2-18)$$

where  $G(\Gamma)$  is the line-width distribution and  $G(\Gamma)d\Gamma$  is the statistic weight of the particles or macromolecules which possess line-width  $\Gamma$ . By using a Laplace inversion program, CONTIN,<sup>11,12</sup> the normalized distribution function of the characteristic line width  $G(\Gamma)$  was obtained. For a dilute solution,  $\Gamma$  measured at a finite scattering angle is related to  $C$  and  $q$  by

$$\frac{\Gamma}{q^2} = D(1 + K_d C)(1 + f q^2 \langle R_g^2 \rangle_z) \quad (2-19)$$

where  $D$  is the transitional diffusion coefficient of the solute molecule at  $C \rightarrow 0$ ,  $k_d$  is the diffusion second virial coefficient, and  $f$  is a dimensionless parameter depending on polymer chain structure and solvent (For polymers with flexible chains in a good solvent,  $f$  is between 0.1 and 0.2). Hence, for small  $C$  and  $q$ ,  $D$  is around  $\Gamma/q^2$ . It should be noted that by the definition of  $|g^{(1)}(t)|$ ,  $G(D) = q^2 G(\Gamma)$ , the translational diffusion coefficient distribution, is an intensity distribution. And, since  $|g^{(1)}(t)|$  approaches unity as  $t \rightarrow 0$ , we have

$$|g^{(1)}(t \rightarrow 0)| = \frac{\langle E(0)E^*(t \rightarrow 0) \rangle}{\langle E(0)E^*(0) \rangle} = \int_0^\infty G(\Gamma) d\Gamma = \int_0^\infty G(D) dD = 1$$

Here, the average diffusion coefficient  $\langle D \rangle$  is defined as

$$\langle D \rangle = \int_0^\infty G(D) D dD \quad (2-20)$$

Further, the transitional diffusion coefficient  $D$  may be related to the molecular friction factor  $f$  through the Stokes-Einstein relation

$$D = k_B T / f \quad (2-21)$$

where  $k_B$  and  $T$  are the Boltzmann constant and the absolute temperature, respectively.

For a hard sphere with a radius of  $R$ ,  $f = 6\pi\eta R$ , where  $\eta$  is the viscosity of the solvent.

For a polymer coil,  $R$  is replaced by its hydrodynamic radius  $R_h$ , so that

$$R_h = \frac{k_B T}{6\pi\eta D} \quad (2-22)$$

In dynamic light scattering, translational motion of macromolecules or particles within size range of 1-1,000 nm can be measured. The characteristic time ( $\tau_c$ ) of dynamic relaxation in self-

beating, which includes transitional, rotational, and internal motion, could vary from seconds to tens of nanoseconds.

Dynamic LLS plays a very important role in particle sizing.<sup>4-7, 10</sup> In a dilute dispersion, if the colloidal particles are spherical, or in other words, in the absence of rotational and internal motions,  $G(I)$  can be converted to the hydrodynamic size distribution  $f(R_h)$ . All the parameters in the conversion are either well-known constants or precisely measurable by the other methods. Therefore, particle sizing based on dynamic LLS can be considered as an absolute method without calibration. This is why dynamic LLS is so successful in particle sizing and many commercial instruments have been developed using the dynamic LLS principle.

## 2.4 LLS INSTRUMENTATION

A commercial laser light scattering (LLS) spectrometer (ALV/DLS/SLS-5000) equipped with an ALV-5000 digital time correlator was used with a Helium-Neon laser (Uniphase 1145P, output power of 22mW and wavelength of 632.8 nm) as the light source (Figure 2.1). The incident light was vertically polarized with respect to the scattering plane and the light intensity was regulated with a beam attenuator (Newport M-925B). The scattered light was transmitted through a very thin (~ 40  $\mu\text{m}$  in diameter) optical fiber leading to an active, quenched, avalanche photo diode (APD) as the detector. As a result, the coherent factor  $\beta$  in dynamic laser light scattering was about 0.98. The avalanche photo diode has a sensitivity of 2 orders higher than that of a normal photon multiplier tube (PMT), while its dark count increases no more than 10 times. Thus, a 22-mW laser could have a measured count rate similar to a 400 mW laser for a normal PM tube. For DLS experiments in this dissertation, the standard deviation of every



measurement of hydrodynamic radius ( $R_h$ ) can be automatically calculated and is below 1%. The schematic setup of the LLS is given in Figure 2.1.

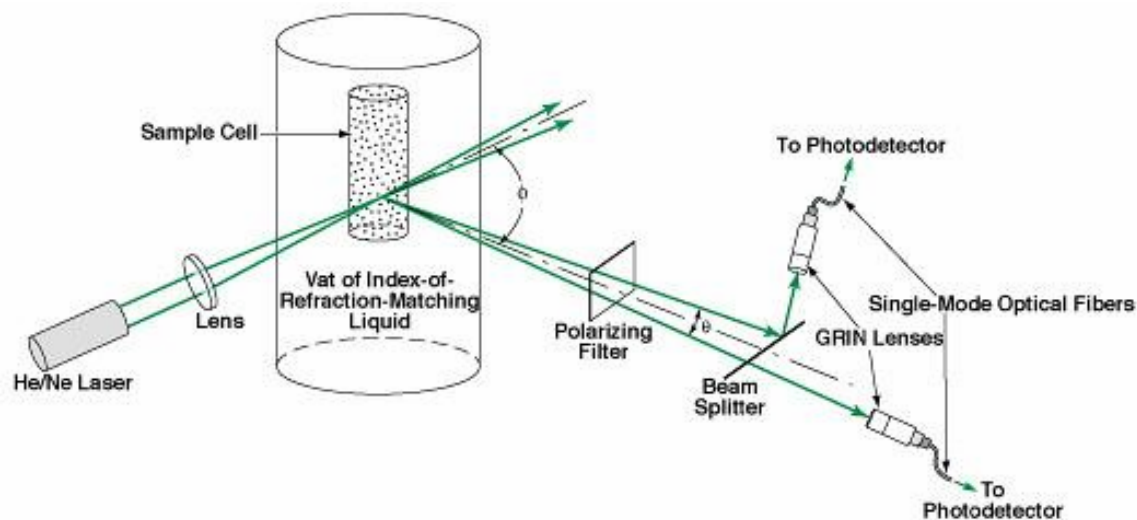


Figure 2.1 Schematic Setup of the Laser Light Scattering Instrument



Figure 2.2 A commercial ALV/DLS/SLS-5000 laser light scattering (LLS).

## CHAPTER REFERENCES

1. Tanaka, T. *Experimental Methods in Polymer Science*; Academic Press, **2000**
2. Chu, B. *Laser Light Scattering*, 2nd edition; Academic Press, **1991**
3. Allcock, H. R., Lampe, F. W. *Contemporary Polymer Chemistry*, 2nd edition; Prentice-Hall, Ins.: New Jersey, **1990**
4. Xia, X., Hu, Z., Gao, J., Qin, D., Durst, H. D., Yin, R. *Langmuir* **2002**, 18(22), 8302
5. Lu, X., Hu, Z., Gao, J. *Macromolecules* **2000**, 33, 8698
6. Wu, C., Chan, K. K., Xia, K. Q. *Macromolecules* **1995**, 28, 1032
7. Zhang, G., Wu, C. *J. Am. Chem. Soc.* **2001**, 123, 1376
8. Berne, B. J., Pecora, R. *Dynamic Light Scattering*; John Wiley & Sons, Inc: New York, **1976**
9. Brown, W. *Dynamic Light Scattering* Oxford University Press: Oxford, **1993**
10. Gao, J., Haidar, G., Lu, X. H., Hu, Z. B. *Macromolecules* **2001**, 34, 2242
11. Provencher, S. W. *Biophys. J.* **1976**, 16, 29
12. Provencher S. W. *Makromol. Chem.* **1979**, 180, 201

## CHAPTER 3

### SYNTHESIS AND STUDY OF INTERPENETRATING POLYMER NETWORK (IPN)

#### NANOPARTICLES IN WATER <sup>1</sup>

##### 3.1 INTRODUCTION

Hydrogels containing two interpenetrating polymer networks (IPN) have attracted an intensive investigation.<sup>2</sup> This is because an IPN hydrogel usually exhibits properties that a hydrogel with the random co-polymerization of two monomers does not have. For example, the IPN of poly(acrylic acid) (PAAc) and polyacrylamide (PAAM) undergoes the volume phase transition driven by cooperative “zipping” interactions between the molecules which result from hydrogen bonding.<sup>2</sup> In addition to the improved mechanical properties which usually come from the reinforcement between two interpenetrating networks,<sup>3</sup> an IPN hydrogel can have a preferred direction for swelling by pre-stressing one of them (poly-N-isopropylacrylamide (PNIPAM)) before the gelation of the other one (polyacrylamide (PAAM)) takes place.<sup>4</sup> A well-designed hydrogel with an IPN structure shows an upper critical solution temperature without a volume change.<sup>5</sup>

Two polymer chain networks in an IPN gel can be sensitive independently to two different external stimuli. Such hydrogels have been employed for controlled drug delivery.<sup>6-8</sup> The PNIPAM gel undergoes the volume phase transition at  $T_c=34\text{ }^{\circ}\text{C}$ <sup>9-14</sup> and has been used often as one of the components in a IPN gel. Its phase transition temperature remains the same if the PNIPAM is incorporated in an IPN matrix. However, the random copolymerization results in shifting  $T_c$  depending on the hydrophilic/hydrophobicity of the co-monomer.<sup>8</sup>

IPN microgel particles have been synthesized because they are more effective as delivery systems than macroscopic gels for agrochemical or medical applications.<sup>15</sup> A comparison of the swelling behavior of the random P(AAc-*co*-AAm) particles and PAAc/PAAm IPN microgels has been made using temperature and pH as the triggers.<sup>15</sup> Jones and Lyon, on the other hand, showed multiresponsive core-shell microgels that consist of a weakly interpenetrating polymer network core and a shell<sup>16</sup>. These microgels were prepared by precipitation polymerization at 70 °C in aqueous media. In the synthesis of the shell polymer, the collapsed particles serve as nuclei for further polymerization, thereby resulting in preferential growth of the existing particles over the nucleation of new ones.<sup>16</sup>

Here we show a method to synthesize an IPN microgel of PNIPAM/PAAc. We extended Jones and Lyon's method by controlling reaction time so that the reaction was stopped once the interpenetrating network was formed at room temperature.<sup>16</sup> We present the synthesis and light scattering characterization of these microgels, which displays the same  $T_c$  as the PNIPAM but shrinks less than the PNIPAM above  $T_c$ . The semi-dilute aqueous solutions of the PNIPAM-PAAc IPN microgels exhibit unusually inverse thermo-reversible gelation. In contrast to polymer solutions of poly(NIPAM-*co*-AAc) that have the inverse thermo-reversible gelation,<sup>17-20</sup> our system can self-assemble into an ordered structure, displaying bright colors. Three applications based on this novel hydrogel system are presented: a rich phase diagram that opens a door for fundamental study of phase behavior of colloidal systems, a thermally induced viscosity change, and *in situ* hydrogel formation for controlled drug release.

### 3.2 EXPERIMENTAL

*Materials:* N-isopropylacrylamide was purchased from Polysciences, Inc. Dodecyl sulfate, sodium salt 98%; potassium persulfate; acrylic acid 99%; and N,N'-methylenebisacrylamide 99% were purchased from Aldrich. TEMED; ammonium persulfate were bought from Bio-Rad Laboratories. Water for sample preparation was distilled and deionized to a resistance of 18.2 M $\Omega$  by a MILLIPORE system, and filtered through a 0.22 $\mu$ m filter to remove particulate matter.

*PNIPAM Microgel Preparation:* The polymerization of NIPAM was carried out in a flask equipped with a magnetic stirrer and a nitrogen feed: 3.8 g N-isopropylacrylamide, 0.066 g N,N'-methylenebisacrylamide and 0.15 g sodium dodecyl sulfate (SDS) were dissolved in 240 g distilled water under continuous stirring for one hour. The solution was nitrogen purged for 40 min before being placed into 70°C hot bath. Potassium persulfate (0.166 grams), which was dissolved in 20 ml water, was then added to initiate the emulsion polymerization. The reaction last for 4 hours under nitrogen atmosphere, and temperature was kept at (70 $\pm$ 0.5) °C throughout. The final PNIPAM microgel size can be well regulated by controlling the amount of surfactant: the smaller nanoparticle size can be achieved by using large amount of emulsifier SDS. I prepared two sized of PNIPAM nanoparticles (hydrodynamic radius  $R_h$  are 121 nm and 170 nm, respectively) for the next step IPN synthesis.

All PNIPAM particles were purified via dialysis (Spectra/Por 7 dialysis membrane, MWCO 10'000, VWR) against frequent changes of stirring H<sub>2</sub>O for 2 weeks at room temperature. The final PNIPAM microgel concentrations were adjusted to 1.35 x10<sup>-2</sup> g/ml for both.

*IPN Microgel Synthesis:* The preparation of IPN nanoparticle is based on the above PNIPAM microgels: 35 g PNIPAM microgel solution was diluted ten times with distilled water. 0.5 g N,

N'-methylenebisacrylamide and 2.3 g acrylic acid were then added. The solution was deaerated for 1 hour with nitrogen bubbling. The initiators (0.2 g ammonium persulfate) and accelerator (0.2 g TEMED) were separately dissolved in water and added rapidly to the solution, making the final solution volume into 370 ml. The reaction last for 120 min under nitrogen atmosphere, and temperature was well regulated at  $(21 \pm 1)$  °C with a water bath. To gather reaction kinetic information, 10 ml aliquot solution was taken from reaction container at different time since reaction started; all aliquots were dialyzed for future DLS analysis. For the reason I will give later in this dissertation, the resultant nanoparticle has the structure of PNIPAM-PAAc interpenetrating network (IPN), rather than PNIPAM-PAAc core-shell structure.

*Turbidity Measurement:* Absorbance measurements (wavelengths from 200 to 1100 nm) were made on an Agilent 8453 UV-Vis Spectrometer with a 1-cm optical path length quartz cell.

### 3.3 RESULTS AND DISCUSSIONS

Both the PNIPAM and IPN particles presented here were prepared by precipitation polymerization in aqueous media. A detailed description and explanation about PNIPAM nanoparticles synthesis may be found elsewhere.<sup>21</sup> The second step IPN formation is possible because the polymerization of acrylic acid may occur within each PNIPAM nanoparticle interior. PNIPAM nanoparticles shrank slightly under the electrolyte effects from acrylic acid, but they are still swollen enough at 21°C (below LCST) in aqueous media allowing the acrylic acid monomers exist within their interior. During the reaction, every single PNIPAM nanoparticle served as a skeleton for the polymerization of acrylic acid, thereby resulting in preferential growth of the existing particles over the nucleation of new ones. To collect the kinetic information of the reaction, 10 ml of aliquot solution was taken from the reaction container at the

time of 40 min, 80 min, 100 min and 120 min, respectively. All these aliquot solutions were purified via dialysis against frequent changes of stirring H<sub>2</sub>O for 2 weeks at room temperature, and the samples were then diluted to  $5 \times 10^{-6}$  g/ml with distilled water for dynamic light scattering analysis. The solution concentrations indicated here are all based on the PNIPAM solid content.

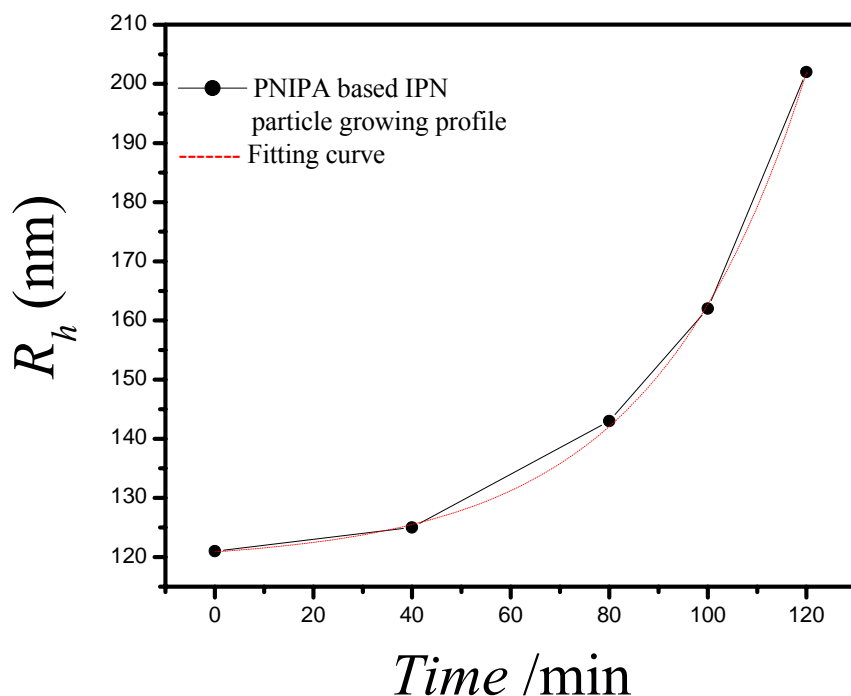


Figure 3.1. Hydrodynamic radius  $R_h$  variation of the particles during IPN synthesis. The samples were taken at different reaction moment, and dialyzed for 2 weeks to remove monomers and small molecules. For DLS measurements, all the samples are of the same concentration of  $5.0 \times 10^{-6}$  g/ml based on NIPAM solid content, and pH values were regulated between 6.5-7.0.

As the PAAc gradually interpenetrated into the particles, the polymer content of the solutions will increase correspondingly, but it had little effect on the measurement of particle hydrodynamic radius. The particle size variation as a function of reaction time is shown in Fig

3.1, measured by dynamic light scattering (DLS). Based on the PNIPAM nanoparticles with hydrodynamic radius of 121 nm at 21°C, the  $R_h$  increased little during the first one hour, but dramatically in the following 60 minutes, and further reaction for 10 more minutes lead to the precipitation. The collected data can be well represented by an equation of  $R_h = 119.1 + 1.77e^{t/\tau}$ , where the characterization time  $\tau = 31$  min. I found that the IPN growing speed varies much based on the different size of PNIPAM nanoparticles and reaction temperature. For example, the precipitation of IPN occurred at 60 minutes based on the  $R_h = 170$  nm PNIPAM nanoparticles, providing all the other reaction parameters are kept the same as described above. Raising temperature also results in a faster kinetics.

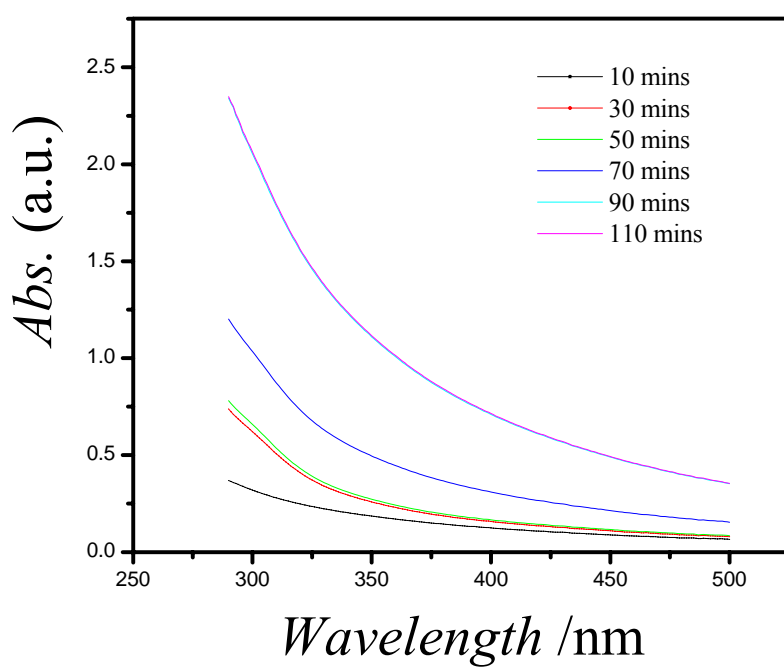


Figure 3.2. Turbidity change of reacting solution during IPN synthesis, as measured by UV/Vis spectrometer. The absorption wavelength is ranged from 290 nm to 500 nm.



Visual observation revealed that the solution turns from translucent to blurred blue to white and finally to precipitation during the IPN growth, based on  $R_h = 121$  nm PNIPAM nanoparticle as skeleton. The turbidity variation measured by UV/Vis spectrometer as a function of reaction time is shown in Fig 3.2. Since the continuous reaction for 130 minutes will lead to the precipitation as illustrated, we stopped the reaction at 120 min.

For a single PNIPAM nanoparticle, there is a higher  $-\text{CONH}-$  group density in its interior than its surface before the reaction start, therefore the interaction of the  $-\text{COOH}$  of acrylic acid and  $-\text{CONH}-$  of PNIPAM, in the form of monomeric or dimeric hydrogen bonding,<sup>22</sup> would be stronger within individual PNIPAM. It is thus reasonable to assume that the polymerization of acrylic acid was primarily happened within each single PNIPAM nanoparticle at the initial phase of the reaction. As the hydrophilic PAA gradually interpenetrated into the PNIPAM skeleton, the IPN nanoparticles would be enlarged due to the increased water absorbing ability. Later reaction mainly happened on the IPN nanoparticles surface where there has much more un-reacted acrylic acid monomers available, and result in the fast growing of the particle size. The nanoparticles therefore underwent the structure change from PNIPAM to IPN and finally to IPN-PAAc core-shell throughout the reaction. The mechanism for the IPN synthesis is schematically shown in Figure 3.3. To demonstrate the importance of hydrogen bonding for the IPN formation and growth, sodium acrylate was used to replace acrylic acid as the interpenetrating reagent. As a consequence, there is no turbidity or particle size change within 4 hours, monitored by UV/Vis spectrometry and dynamic light scattering.

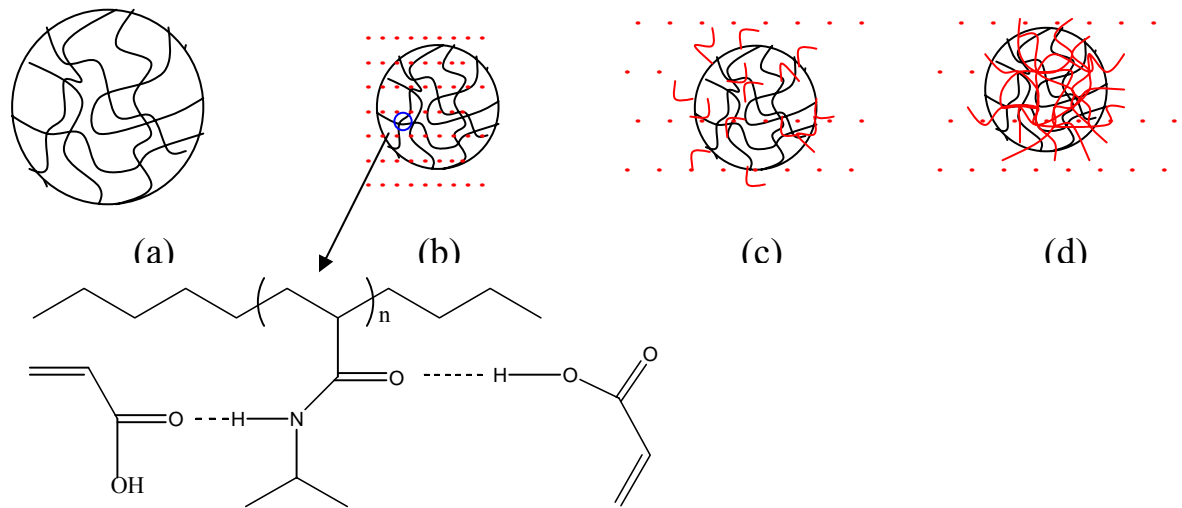


Figure 3.3. IPN nanoparticle synthesis: (a) pure PNIPAM nanoparticle; (b) shrunken PNIPAM nanoparticle under the effect of electrolyte acrylic acid, the red dots stand for the acrylic acid monomers; the hydrogen bonding between PNIPAM and acrylic acid was represented by the dot line as indicated in the enlarged chemical structure; (c) polymerization of the acrylic acid; (d) final IPN nanoparticle.

3.3.1. *Comparison of PNIPAM and IPN.* PNIPAM and IPN nanoparticles were characterized and compared using dynamic and static light scattering. Both PNIPAM and IPN nanoparticles were diluted to  $5.0 \times 10^{-6}$  g/ml with distilled water, and pH values were measured around 6.5-7.0 for all samples. The nanoparticles size and distribution are shown in Fig 3.4, measured by dynamic light scattering, in which the PNIPAM nanoparticles were very narrowly distributed with  $R_h$  around 121 nm, IPN nanoparticles were also narrowly distributed around 202 nm. The calculated polydispersities PD.I for PNIPAM and IPN were 1.068 and 1.07, respectively, PD.I is

referred as  $1 + \frac{\mu_2}{\langle \Gamma \rangle^2}$ , where  $\Gamma$  is the average line width and  $\mu_2 = \int_0^\infty G(D)(D - \langle D \rangle)^2 dD$ ,  $D =$

$\frac{K_b T}{6\pi\eta < R_h >}$ . Increased particle size and their narrow distribution demonstrate that PAAc

interpenetrated into the PNIPAM nanoparticles and the nucleation of new particles during IPN synthesis is negligible.

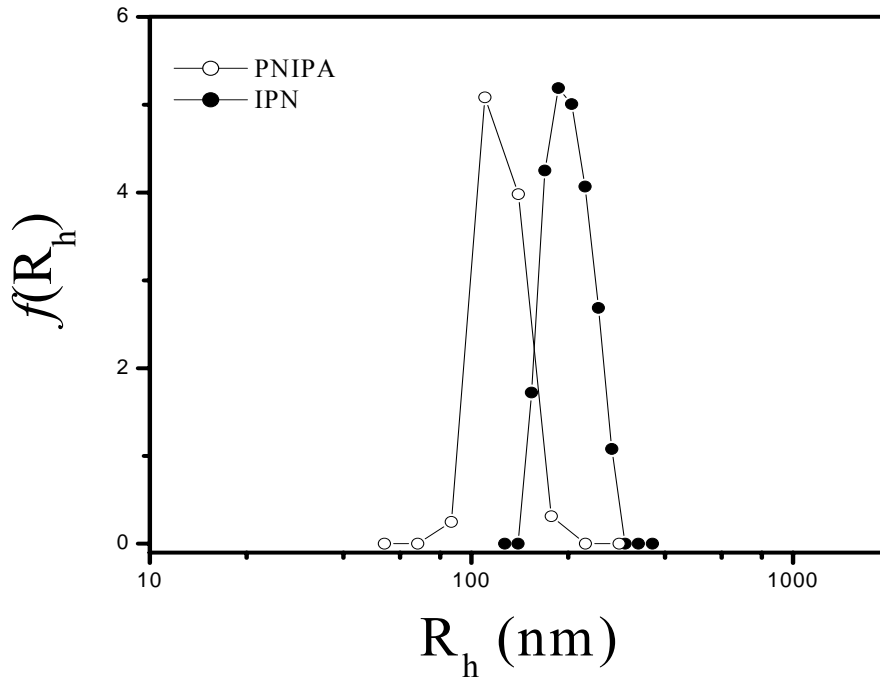
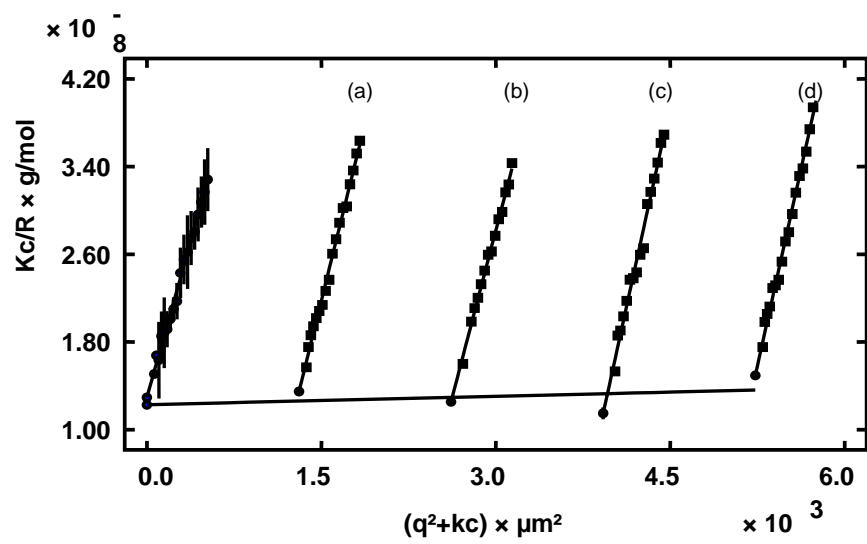
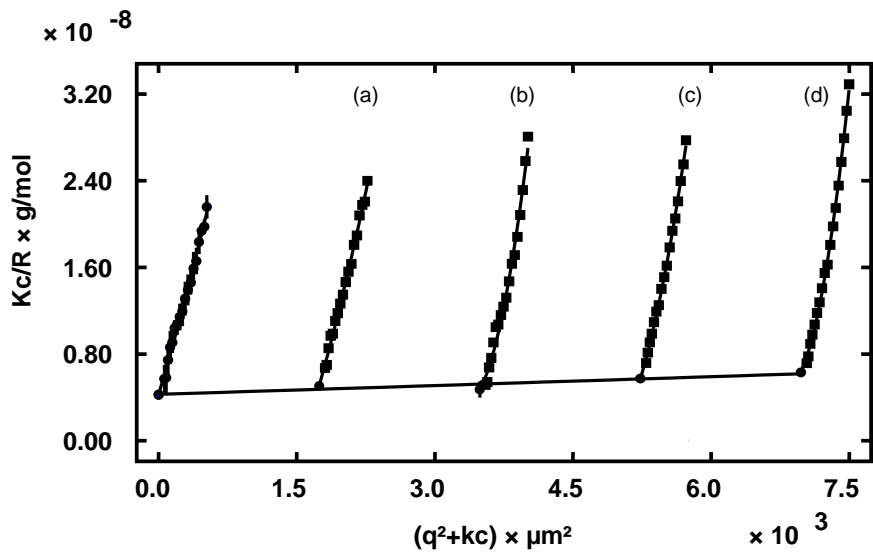


Figure 3.4. Size distributions of IPN microgel and its precursor PNIPAM nanoparticles, as measured by dynamic light scattering.



(a)



(b)

Figure 3.5. Zimm plot of static light scattering for (a) PNIPAM nanoparticles; (b) IPN nanoparticles. Sample concentration varies from  $2.5 \times 10^{-6}$  g/ml to  $1.0 \times 10^{-5}$  g/ml for both.

Static light scattering was carried out for the pure PNIPAM aqueous solution at 25°C, with sample concentration varies from  $2.5 \times 10^{-6}$  g/ml to  $1.0 \times 10^{-5}$  g/ml. The value of  $dn/dc$  used here is  $0.166 \text{ cm}^3/\text{g}$ , measured by a refractometer. Fig 3.5(a) shows the Zimm plot of PNIPAM particles aqueous solution. From the extrapolation of  $KC/R_{v\vee}(q)$  in Eq (2-10) to the zero angle and zero concentration, the molar mass  $M_w$ , the second virial coefficient  $A_2$ , and the radius of gyration  $\langle R_g \rangle$  are determined to be  $8.14 \times 10^7$  g/mol,  $8.90 \times 10^{-5} \text{ mol} \cdot \text{cm}^3/\text{g}^2$ , and 98 nm, respectively. By combining DLS and SLS results, the ratio of  $\langle R_g \rangle / \langle R_h \rangle$  was found to be 0.80, which is close to the theoretical value of  $(3/5)^{1/2}$  for uniform hard spheres. The density of pure PNIPAM nanoparticle ( $\rho$ ) in water may be estimated according to the relation  $4/3 \cdot \pi R^3 \rho = M_w / N_A$ , where  $R$  is  $R_h$  from DLS, the molar mass,  $M$ , is  $M_w$  from SLS, and  $N_A$  is Avogadro's number. Thus the calculated average polymer density in each PNIPAM sphere is about  $1.82 \times 10^{-2} \text{ g/cm}^3$  at 25°C in water.

From Zimm plot of static light scattering for IPN microgel shown in Fig 3.5(b), we got the molar mass  $M_w$ , and the radius of gyration  $\langle R_g \rangle$  and second virial coefficient  $A_2$  were  $2.341 \times 10^8$  g/mol and 143.6 nm and  $9.496 \times 10^{-5} \text{ cm}^3/\text{g}^2$ , respectively. The value of  $dn/dc$  used here is  $0.102 \text{ cm}^3/\text{g}$ . The increased  $A_2$  demonstrate that IPN nanoparticle is more hydrophilic than its PNIPAM precursor. Since PAA exhibits more hydrophilic than PNIPAM at neutral environment, IPN nanoparticles thus have more water content than pure PNIPAM nanoparticles. By combining DLS and SLS results, the ratio of  $\langle R_g \rangle / \langle R_h \rangle$  was found to be 0.71. It suggests that the polymers are uniformly distributed. The average density of this IPN nanoparticle ( $\rho$ ) was calculated with the method introduced above, it is about  $1.13 \times 10^{-2} \text{ g/cm}^3$  at 25°C in water. The detailed comparison data between PNIPAM and IPN nanoparticle are listed in the Table 3.1.

Table 3.1. PNIPAM and IPN microgels comparison summary.

	R <sub>h</sub> (nm)	R <sub>g</sub> (nm)	R <sub>g</sub> /R <sub>h</sub> (a.u.)	A <sub>2</sub> (mol*cm <sup>3</sup> /g <sup>2</sup> )	M <sub>w</sub> (g/mol)	Density (g/cm <sup>3</sup> )	PNIPA:PA A ratio	LCST
PNIPA	121	98	0.81	8.9x10 <sup>-5</sup>	8.137x10 <sup>7</sup>	1.82x10 <sup>-2</sup>	1 : Nothing	34°C
IPN	202	143	0.71	9.5x10 <sup>-5</sup>	2.341x10 <sup>8</sup>	1.13x10 <sup>-2</sup>	1 : 1.88	34°C

The weight ratio of PAA to PNIPAM in each IPN nanoparticle was determined to be 1.88:1, calculated from the IPN M<sub>w</sub> 2.34x10<sup>8</sup> g/mol, which is 2.88 times of pure PNIPA 8.137x10<sup>7</sup> g/mol. The value is very close to what we measured by evaporation method 1.82:1. If the reaction goes for longer, the ratio will increase correspondingly.

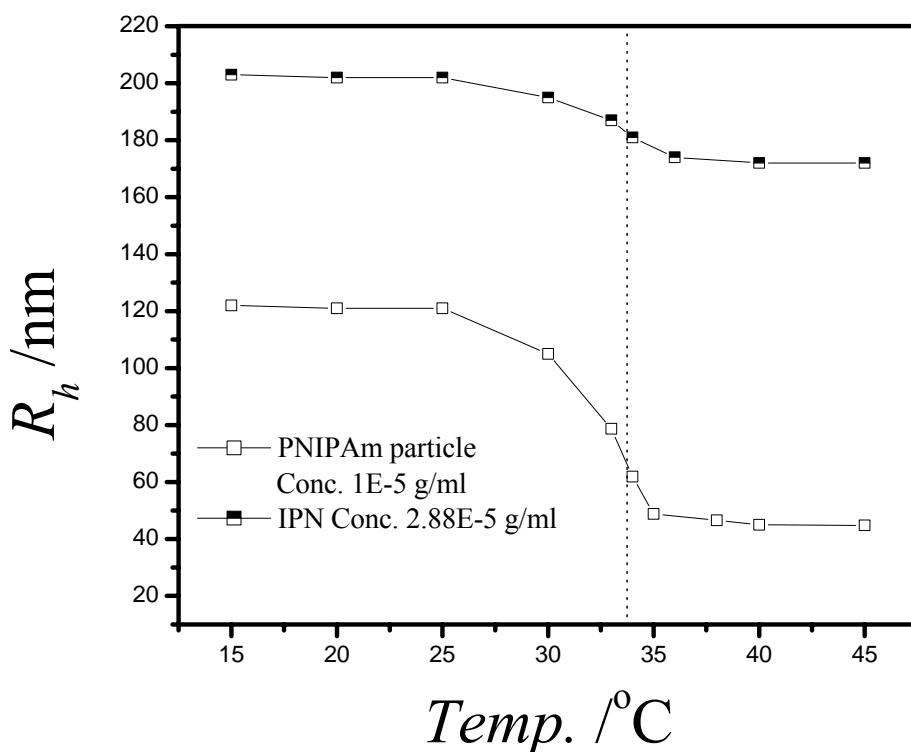


Figure 3.6. Temperature induced phase transition for PNIPAM and IPN nanoparticles.

### 3.3.2. Temperature Induced Phase Transition of IPN Microgels and the Thermo-thickening Property of Their Semi-dilute Solution.

For extremely diluted IPN and PNIPAM solution ( $5 \times 10^{-6}$  g/ml), the interaction between particles can be neglected; DLS was used to monitor the particle size variation against temperature. From Fig 3.6 we can see the IPN has approximately the same LCST  $32 \sim 34^\circ\text{C}$  as pure PNIPAM. Such property is remarkably different from poly (AA-co-NIPAM), which always brings the LCST of NIPAM to higher temperature.<sup>23</sup> The comparison of their  $R_h$  below and above LCST shows that the IPN shrinkage ratio 0.84 is much bigger than that of PNIPAM 0.37. It is rationalized by assuming the hydrophilic PAA within IPN nanoparticle hindered the further shrinking force from PNIPAM skeleton. We also observed that

the semi-diluted IPN aqueous solution (conc. 2.5% g/ml) exhibited unusual thermothickening phenomenon at pH above 5. Different from graft copolymer containing p(acrylic acid) backbone and p(NIPAM) side chains of which the semi-diluted solution viscosity increase took long time and not to the much extent,<sup>24</sup> the IPN semi-diluted solution responded very fast to the environment temperature increase and the viscosity enhancement was also tremendous. For example, when the solution was set in 40°C hot bath for 10 seconds, the viscosity of IPN solution enhanced to such an extent that the whole solution could be set upside down. Fig 3.7 shows the comparison of IPN semi-diluted solution at room temperature (left) and 40°C (right). This thermothickening behavior can be explained by the inter-particles hydrophobic attraction of PNIPAM on the IPN surface when the temperature increased above the LCST of PNIPAM 34°C. More detailed study about the rheological property of this IPN solution will be published elsewhere.

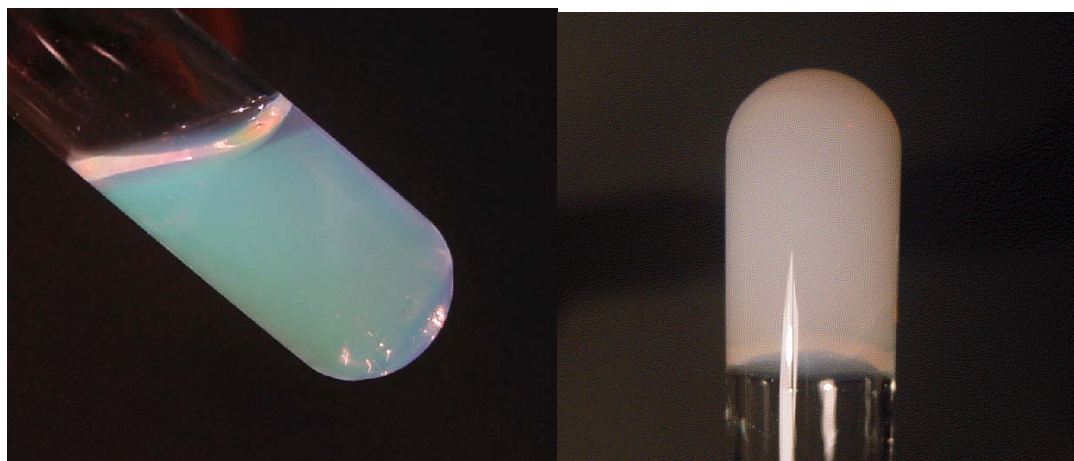


Figure 3.7. Images of IPN semi-dilute aqueous solution below and above the LCST of PNIPAM (~34°C).



*3.3.3. pH Induced Volume Phase Transition.* It is reasonable to anticipate that this IPN nanoparticle possesses pH sensitivity due to the large amount of interpenetrated PAA. The  $R_h$  variation of IPN and PNIPAM nanoparticles as a function of pH is shown in Fig 3.8, measured by dynamic light scattering. The pH for all solutions were adjusted using hydrochloric acid and sodium hydroxide and the concentrations for all solutions were  $5 \times 10^{-6}$  g/ml. DLS detector was set at  $90^\circ$  relative to the incident light and temperature was controlled at  $21^\circ\text{C}$  for all measurement. As shown in Fig 3.8, there was a sharp drop of  $R_h$  for IPN nanoparticles from 200 nm to 165 nm as the pH went from 5 to 4. In the pH range of 5-10, the particle  $R_h$  slightly fluctuated around 200 nm without aggregation demonstrated by the constant scattering light intensity. It is well known that PAA is mainly in ionic state when the environment pH is above its pKa 4.7, and exhibits much more hydrophilic property than its molecular counterpart which was dominant when the environment pH below the pKa. Therefore, as the  $\text{pH} < 4.7$ , the IPN became more hydrophobic and forced water out from its interior, rendering sharp decrease of particle size. However, with pH insensitive PNIPAM as skeleton, the shrinkage of the particle is limited. It's interesting to note that the extent of pH induced IPN shrinkage is about the same as the temperature induced IPN particle shrinkage, both from 200 nm to around 160 nm. As expected, there is no particle size variation observed for PNIPAM nanoparticles in the pH range of 4-10, the little drop occurred at  $\text{pH}=2$  are due to the electrolyte effect.

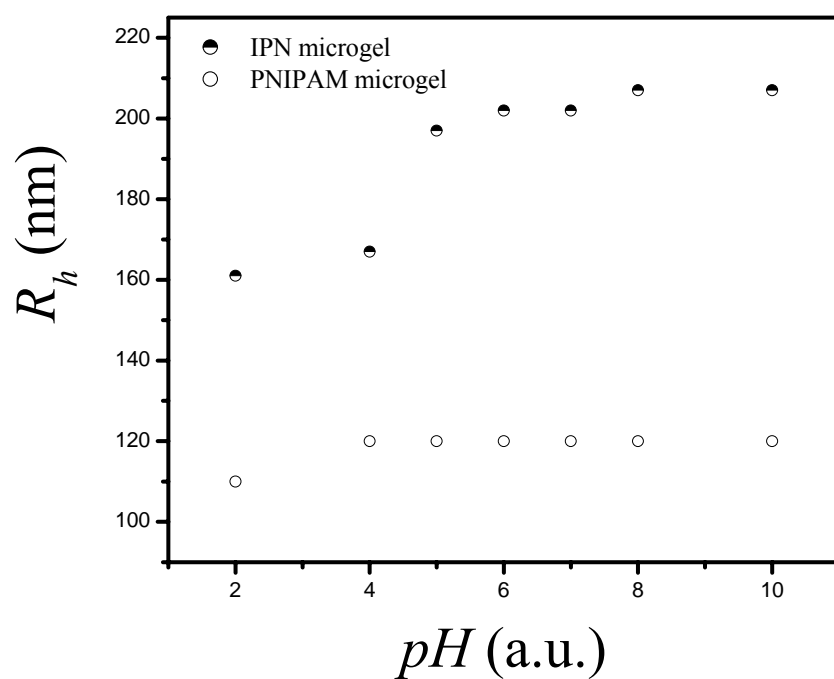


Figure 3.8. pH induced phase transition for PNIPAM and IPN nanoparticles.

The comparison of IPN nanoparticles size distributions at pH 4 and 7 are shown in Figure 3.9, we found the IPN nanoparticles have narrower dispersion at pH 4 than 7. It indicated that the nanoparticles tend to get more uniform size distribution after the shrinkage. The PD. I for IPN microgel at pH 4 and 7 are 1.02 and 1.07, respectively.

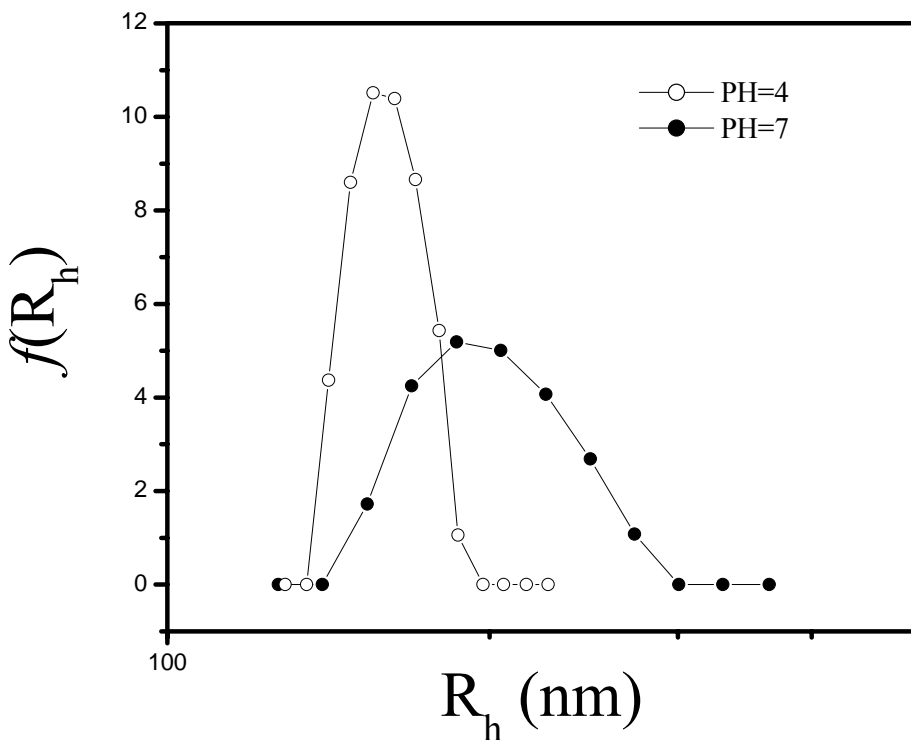
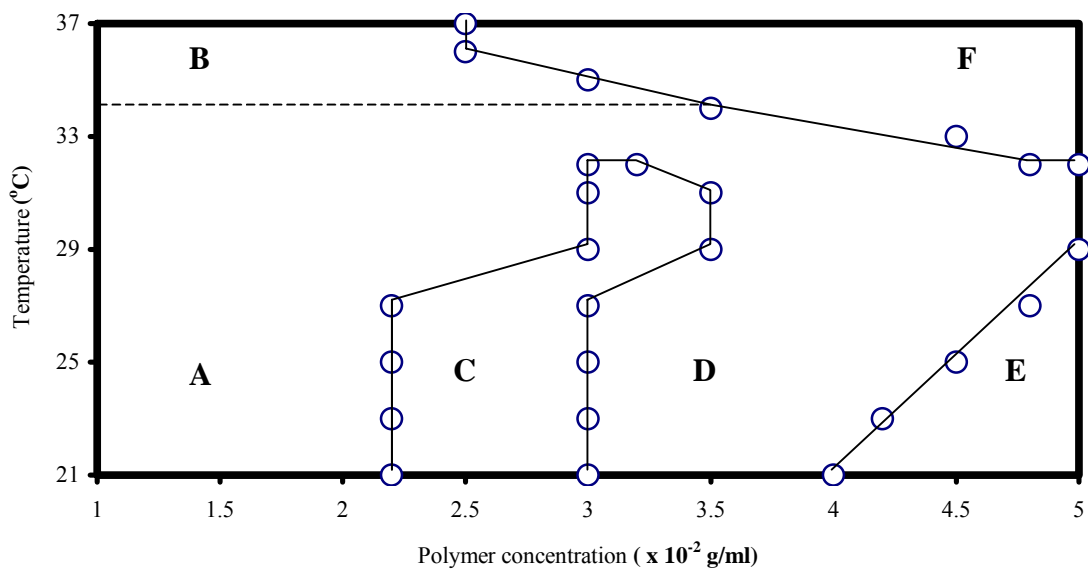
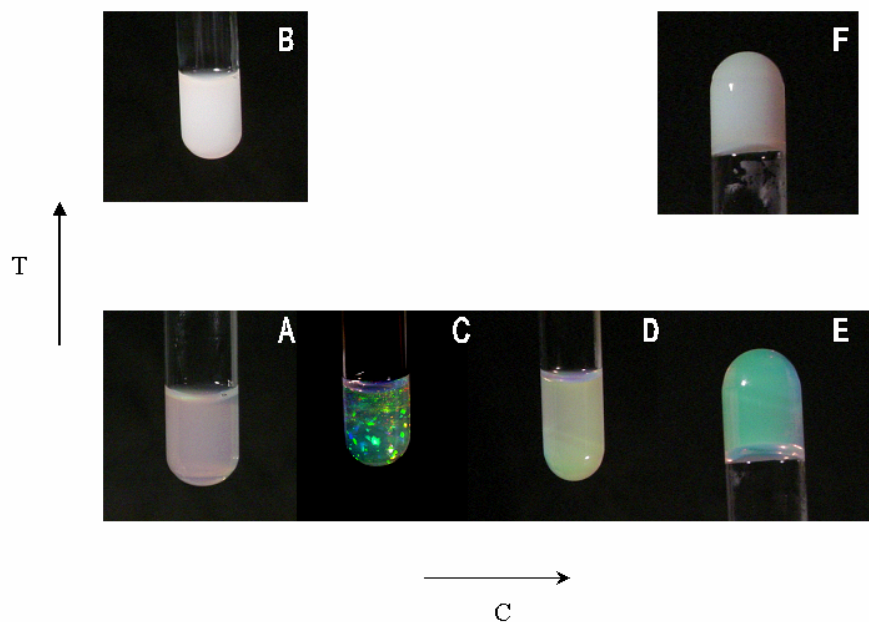


Figure 3.9. Size distributions of IPN nanoparticles at different pH environments.

*3.3.4 Phase Diagram of Semi-dilute IPN Nanoparticle Solution.* The aqueous solutions of the IPN nanoparticles exhibit rich phase behavior as shown in Figure 3.10 (a), determined by combining visual inspection, turbidity and viscosity measurements. The phase behavior has been divided into six areas with typical optical appearances as shown in Figure 3.10 (b). At low polymer concentrations ( $< 2.2 \times 10^{-2}$  g/ml, Area A), the IPN dispersions appear translucent and flow easily. The IPN nanoparticles are fully swollen.



(a)

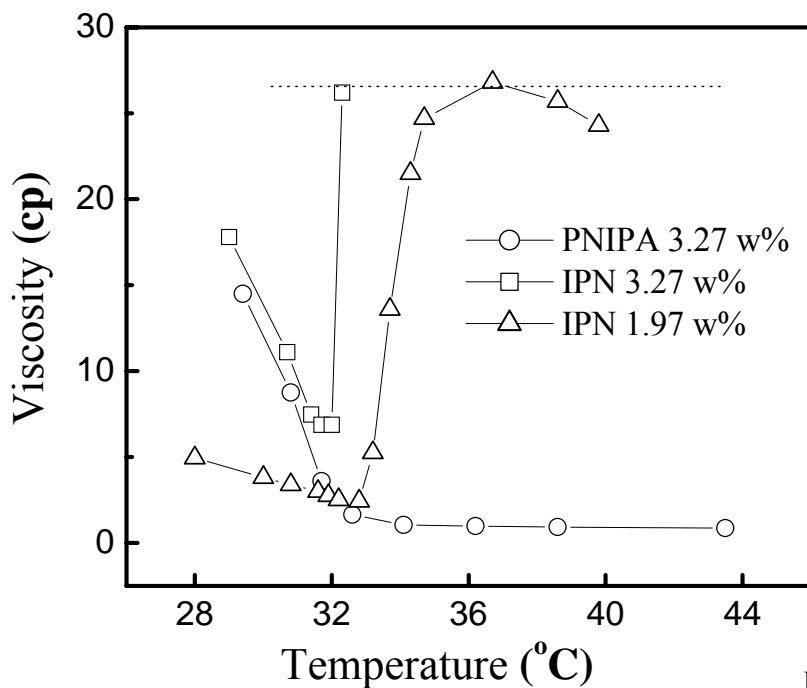


(b)

Figure 3.10. The phase behavior of the PNIPAM-PAAc IPN nanoparticles in water. (a) The temperature-concentration phase diagram. There are six areas: (A) a homogeneous colloidal

fluid, (B) a phase-separated colloidal fluid, (C) a colloidal crystal phase, (D) a colloidal glass, (E) a colloidal gel, and (F) a phase-separated colloidal gel. (b) Representative pictures of each phase. The hydrodynamic radii of the PNIPAM and IPN particles are 125 nm and 155 nm, respectively. The weight ratio of PNIPA to PAA is 2:1, determined by both evaporation method and static light scattering.

Upon increasing the temperature, the particle size shrinks and the dispersions enter into a phase-separated area (Area B). In the intermediate polymer concentration range (between  $2.2$  and  $3.0 \times 10^{-2}$  g/ml, Area C), the IPN dispersions are colloidal crystal fluids at room temperature. These crystals are easy to observe due to their iridescent patterns caused by Bragg diffraction.<sup>22</sup> Constructive interference occurs if the Bragg condition,  $2nd\sin\theta = m\lambda$ , is satisfied, where  $d$ ,  $\theta$ ,  $n$ ,  $\lambda$ , and  $m$  are the lattice spacing, the diffraction angle, the refractive index of the gel medium, the wavelength of light in vacuum and an integer, respectively. In a high polymer concentration range (between  $3.0 \times 10^{-2}$  and  $4.0 \times 10^{-2}$  g/ml, Area D), the IPN dispersions are colloidal glass fluids that are viscous fluids and exhibit a homogeneous color due to a short-range order.<sup>28</sup> At very high polymer concentrations ( $>4 \times 10^{-2}$  g/ml, area D) at room temperature, the IPN dispersions become colloidal gels. At higher temperatures, the gels become white and opaque (Area F).



Dr. Z. Hu

Figure 3.11. Temperature-dependent viscosity. Viscosities of aqueous solutions of IPN ( $C=1.97$  w%), IPN ( $C= 3.27$  w%) and PNIPAM ( $C=3.27$  wt%) were measured as a function of temperature using a Brookfield Viscometer. The hydrodynamic radii of the PNIPAM and IPN particles are 125 nm and 155 nm, respectively. The weight ratio of PNIPAM to PAAc is 2:1, determined by both evaporation method and static light scattering.

The inverse thermo-reversible gelation occurs in a broad polymer concentration above  $2.5 \times 10^{-2}$  g/ml. That is, when the system is heated to above the gelation temperature  $T_g$ , it undergoes a transformation from a low-viscous fluid to a gel. This behavior is completely reversible. A typical temperature-dependent viscosity of an IPN nanoparticle aqueous solution (3.27 wt %) is presented in Figure 3.11 in comparison with that for a PNIPAM nanoparticle dispersion with the same polymer concentration with a heating rate of  $2^\circ\text{C}/5\text{mins}$ . The viscosity was measured using a Brookfield viscometer with a shear rate of 100 rpm. The viscosity data

obtained with various heating rates between 1 and 5 °C/5mins were the same, indicating that the associative phenomenon is rather fast.

The viscosity of the PNIPAM nanoparticle dispersion (C=3.27 wt %) was observed to decrease as the temperature increased and reached a plateau above 32°C. This was due to the increase of the mobility of individual particles and the gradually shrinking particle size with the increasing temperature. In comparison, the IPN nanoparticle dispersion (C=3.27 wt %) exhibited behavior similar to the PNIPAM dispersion below 32 °C. However, when the temperature reached 32.5°C, the viscosity drastically increased and jumped beyond our viscometer's measurement range. Visual inspection revealed that the dispersion in the test tube was physically gelled and could not flow even the tube was set upside down. The thermally induced viscosity change can be tuned by changing polymer concentration. The IPN dispersion with a lower polymer concentration ( $C < 2.5 \times 10^{-2}$  g/ml) exhibits a viscosity enhancement but without gelling, as shown in Figure 3.11.

The gelation of the IPN dispersion at  $T > T_g$  is caused by the attractive interactions between particles. At room temperature, PNIPAM particles are in the swollen state and they contain 97% water by volume. The van der Waals attraction between colloidal particles is negligible due to the close match in the Hamaker constants of the particle and the water.<sup>25</sup> The reduced osmotic second virial coefficient exhibits a sharp change at the volume transition temperature, beyond which it turns negative, indicating an increase in the van der Waals attraction as the particles collapse. Thermodynamic calculation indicates that the reduced interaction potential energy between nanoparticles increases by over six orders of magnitude as temperature changes from 24°C to 36 °C, with the sharpest increase near the volume transition temperature of 34 °C.<sup>28</sup> The gelation is therefore achieved by the balance between van der Waal

interaction between PNIPAM networks and the ionic repulsion of the PAAc networks in the IPN particles.

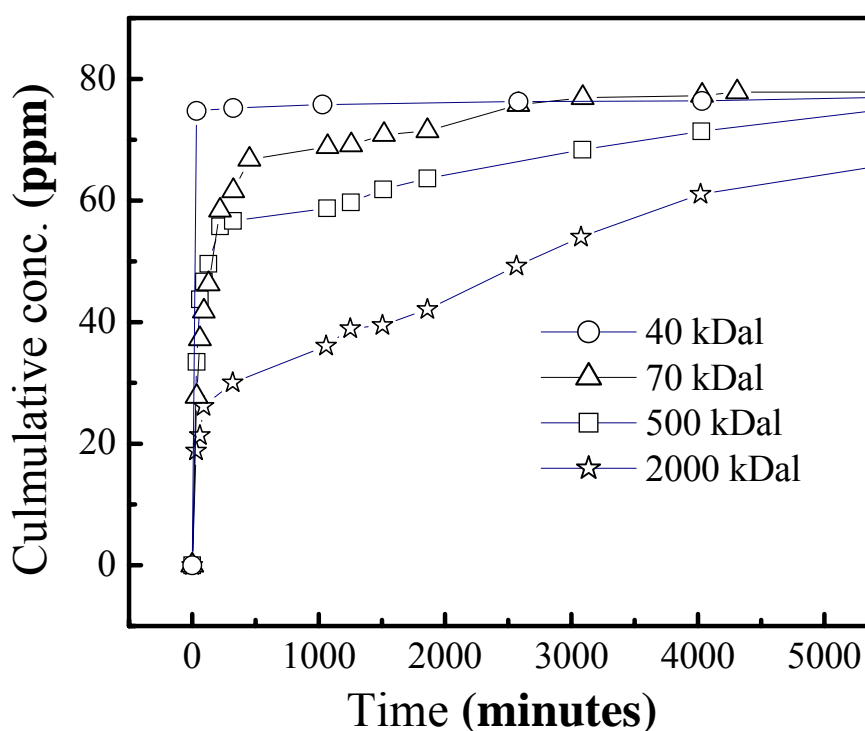


Figure 3.12. A cumulative release of model drugs from an *in situ*-formed gel depot. The dyes with molecular weights of 40, 70, 500 and 2000 k Daltons are mixed with 5.25 wt % IPN dispersion at room temperature, respectively. The weight ratio of PNIPAM to PAA is 1:0.13 and the IPN particle size is 111 nm at room temperature. The release was measured after the IPN formed a gel in 37°C PBS.

**3.3.5 Physically Crosslinked IPN Microgels Network for Drug Delivery.** One of the key applications of this novel hydrogel nanoparticle dispersion is in the area of controlled drug delivery. The mixture of the IPN nanoparticles and drugs can be prepared as an aqueous solution below the gelation temperature to form a drug delivery liquid. This liquid could be administered into a warm-blooded animal which forms *in situ* a gelled drug depot since body temperature will be above the gelation temperature of the IPN dispersion. The drug can be entrapped inside a



hydrogel by solution mixing without chemical reaction. In contrast to hydrogels obtained from polymer solutions with inverse thermoreversible gelation <sup>26</sup>, the hydrogel formed with our nanoparticle dispersions has unique two-level structural hierarchy: the primary network consists of crosslinked polymer chains inside each nanoparticle, while the secondary network is a crosslinked system of the nanoparticles. The drug could be entrapped either between the particles or inside each particle.

As a demonstration, we used dextran with different molecular weights as a model drug and mixed them with an IPN nanoparticle dispersion with a polymer concentration at 5.25 wt%. At room temperature, the dispersion is a viscous fluid can be mixed with a dextran solution very thoroughly. The drug-dispersion mixture was then heated to 37 °C at which point the dispersion becomes a gel. This gel was then taken out from the tube and immersed into a PBS solution at 37 °C. The cumulative drug release from the gel was measured using a UV-Visible spectrophotometer as a function of time as shown in Figure 3.12. It is clear that the molecules with smaller molecular weights diffuse out faster than those of higher molecular weights. The release rates slowed down gradually for 70K, 500K and 2M drug analogs in the order of their molecular weights. The drug molecules here were entrapped between IPN nanoparticles, permitting the release of molecules with very large molecular weight of 2M. It is noted that the polymer concentration used in the release experiment is about 10 times smaller than that used in a polymer solution system. <sup>27</sup>

### 3.4 CONCLUSION

Monodisperse IPN nanoparticles composed of poly-acrylic acid (PAA) and poly(*N*-isopropylacrylamide) (PNIPAM) interpenetrating networks are for the first time synthesized. The

kinetics of IPN formation is obtained by measuring the turbidity variation and particle hydrodynamic radius change as a function of time. Individual IPN and PNIPAM nanoparticles are studied and compared using both dynamic and static light scattering techniques. The semidilute IPN nanoparticle dispersion possesses the advantage of thermosensitive property. The single IPN nanoparticle exhibits a relatively high equilibrium water content and also showed the multiple and reversible sensitivity to both pH and temperature. This system exhibits a very rich phase behavior including a colloidal crystalline phase in which the system displays iridescent colors, and an inverse thermoreversible gelation for polymer concentrations above  $2.5 \times 10^{-2}$  g/mL. The gelation is achieved by the balance between van der Waal's interaction between PNIPAM networks and the ionic repulsion of the PAA networks in the IPN particles. The drug has been loaded into a hydrogel by mixing the solutions below the gelation temperature, and was released from the gel depot above  $T_g$ .

## CHAPTER REFERENCES

1. Hu, Z., Xia, X. *Adv. Mat.* **2003** (accepted)
2. Ilmain, F., Tanaka, T., Kokufuta, E. *Nature* **1991**, 349, 400
3. Sperling, L. H. *Adv. Chem. Ser.* **1994**, 239, 12
4. Wang, C. J., Hu, Z. B., Chen, Y. Y., Li, Y. *Macromolecules* **1999**, 32, 1822
5. Chen, L., Gong, J., Osada, Y. *Macromolecular Rapid Communications* **2002**, 23, 171
6. Katono, H., Sanui, K., Ogata, N., Okano, T., Sakurai, Y. *Polym J* **1991**, 23, 1179; Katono, H., Maruyama, A., Sanui, K., Ogata, N., Okano, T., Sakurai, Y. *J Control Rel* **1991**, 16, 215
7. Gutowska, Y.H., Bae, H., Jacobs, J., Feijen, Sung Wan Kim, *Macromolecules*, **1994**, 27, 4167
8. Park, T. G., Choi, H. K. *Macromol. Rapid Commun.* **1998**, 19, 167
9. Hirotsu, S., Hirokawa, Y., Tanaka, T. *J. Chem. Phys.* **1987**, 87, 1392
10. Wu, C., Zhou, S. *Macromolecules* **1996**, 29, 1574
11. Bence, L. S., Snowden, M. J., Chowdhry, B. Z., *Langmuir*, **2002**, 18, 6025
12. Routh, A. F., Vincent, B., *Langmuir*, **2002**, 18, 5366
13. Woodward, N. C., Chowdhry, B. Z., Snowden, M. J., Leharne, S. A., Griffiths, P. C., Winnington, A. L., *Langmuir*, **2003**, 19, 3202
14. Gao, J., Frisken, B. J., *Langmuir*, **2003**, 19, 5217
15. Bouillot, P., Vincent, B. *Colloid and Polymer Science* **2000**, 278, 74
16. Jones, C. D., Lyon, L.A. *Macromolecules* **2000**, 33, 8301
17. T. Kato, M. Yokoyama, A. Takahashi, *Colloid & Polym. Sci.* **1978**, 256, 15

18. M. Almgren, P. Bahadur, M. Jansson, P. Li, W. Brown, A. J. Bahadur, *Colloid & Interface Sci.* **1992**, 151, 157; P. Alexandridis, T. A. Hatton, *Colloidal Surfaces A: Physicochem. Eng. Aspects* **1995**, 96, 1
19. C. K. Han, Y. H. Bae, *Polymer* **1998**, 39, 2809
20. B. Jeong, S. W. Kim, Y. H. Bae, *Adv. Drug Del. Rev.* **2002**, 54, 37
21. Gao, J., Hu, Z. *Langmuir*, **2002**, 18, 1360
22. Jeffrey, G.A., Saenger, W. *Hydrogen Bonding in Biological Structures*. Springer-Verlag, New York, **1991**
23. Shibayama, M., Ikkai, F., Inamoto, S., Nomura, S., Han, C.C. *J. Chem. Phys.* **1996**, 105, 8
24. Durand, A., Hourdet, D. *Polymer*, **1999**, 40, 4941
25. Wu, J. Z., Zhou, B., Hu, Z. B. *Phys. Rev. Lett.* **2003**, 90, 048304; Wu, J. Z., Huang, G., Hu, Z. B. *Macromolecules* **2003**, 36, 440
26. Jeong, B., Kim S. W., Bae, Y. H. *Adv. Drug Del. Rev.* **2002**, 54, 37
27. Han C. K., Bae, Y. H. *Polymer* **1998**, 39, 2809

CHAPTER 4  
SWELLING AND MECHANICAL BEHAVIOR OF POLY(*N*-  
ISOPROPYLACRYLAMIDE)/Na-MONTMORILLONITE LAYERED SILICATES  
COMPOSITE GEL <sup>1§</sup>

#### 4.1 INTRODUCTION

Gels are crosslinked polymer networks swollen in a liquid medium. The liquid inside the gel allows diffusion of some solute molecules, while the polymer network serves as a matrix to hold the liquid together. Poly(*N*-isopropylacrylamide) (PNIPAM) gel is a temperature sensitive gel exhibiting the volume phase transition at approximately 34°C <sup>2-3</sup>. Below this volume phase transition temperature,  $T_c$ , the gel swells and it shrinks as the temperature is raised. On the other hand, un-crosslinked PNIPAM polymer chains in water exhibit the low critical solution temperature (LCST) behavior. The temperature sensitivity of the PNIPAM gel has attracted a considerable attention in the recent years due to both fundamental and technological interests <sup>4-11</sup>. The PNIPAM and its derivatives have potential applications for controlled drug delivery, chemical separation, sensors and actuators.

Swelling and mechanical properties of PNIPAM gels have been investigated intensively. <sup>3, 12-13</sup> It has been found that increasing crosslinker concentration can enhance PNIPAM mechanical strength. <sup>14</sup> However, a large amount of crosslinkers could result in the shift of the volume transition temperature and in the reduction of swelling capability. <sup>15-16</sup> It is well known that the properties of gels can be significantly enhanced by incorporation of inorganic ordered

§ Reproduced with permission from [Xia, X., Yih, M.J., Dsouza, N., Hu, Z., *Polymer*, **2003**, 44, 3387]. Copyright [2003] Polymer.

systems, in particular clays, into the gels<sup>17-20</sup>. As a model system, sodium montmorillonite layered silicates (Na-MLS) is widely used as an additive for plastics to improve their physical properties. The chemical structure of the Na-MLS has been reported.<sup>21</sup>

It has been found that the incorporating clay into poly(acrylamide) gel enhanced the gel elastic modulus while exhibited no significant improvement to its swelling ability.<sup>18</sup> PNIPAM/Na-MLS composite materials have been made with high Na-MLS concentrations (above 3.5 wt%) and their swelling behavior as a function of temperature has been studied.<sup>19</sup> However, the potential of low content Na-MLS (less than 3.5 w%) on the swelling ratio, the volume phase transition temperature and shear modulus of the PNIPAM gel has not been investigated so far. In this article, we present the results of the swelling and elastic properties of a series of PNIPAM composites with Na-MLS concentrations ranging from 0.25 w% to 4.0 w%.

## 4.2 EXPERIMENTAL

*Sample Preparation:* The gels were prepared by free radical copolymerization of monomers in aqueous suspensions of Na-MLS (Southern Clay Products, Texas). A series of gel disks and filaments were made, respectively, for shear modulus and swelling ratio measurements. 0.2 g Na-MLS was first suspended in 20 ml water thoroughly under ultrasonic irradiation. Then, 1.56 g N-isopropylacrylamide (NIPAM), 26.6 mg methylene-bis-acrylamide (BIS) as crosslinker, and 48 $\mu$ l tetra-methyl-ethylene-diamine as an accelerator were dissolved in 20 ml Na-MLS water suspension at 21°C. The solution was bubbled with nitrogen gas for 30 minutes to remove dissolved oxygen. The polymerization was initiated by adding 8 mg ammonium persulfate (APS). Three micro-liter glass capillaries with an inner diameter of 0.269 mm were inserted into the solution. The solution climbed along the capillary tubing due to the high surface tension.

After 24 hours, the micro capillaries were drawn out carefully from gelled PNIPAM. The PNIPAM filaments were obtained by carefully breaking the capillaries in de-ionized water. To make the transparent PNIPAM gel filaments more easily identified, they were dyed with brilliant blue, which stick to the filament surface without changing the gel properties. The gel disks were made in the glass test vials having a diameter of 2.54 cm. The synthetic chemical compositions were the same as described above. The vial was then broken carefully and a thin copper thread was used to cut the gel into a series of 1 mm-thick disks. The gel disks were kept in distilled water for the shear modulus measurement. The same procedure was used to prepare pure PNIPAM gel and other Na-MLS/PNIPAM gel composites with Na-MLS concentration ranging from 0.25 to 4.0 wt%. The composition and properties of Na-MLS/PNIPAM composites are listed in Table 4.1. For swelling ratio measurements, the use of filaments can substantially reduce the waiting period.

Table 4.1. Composition and characterization results for Na-MLS/PNIPAM samples, in which NIPA, BIS, APS and water amounts were 1.56 gram, 0.0266 gram, 0.048 ml and 20 grams for all the samples preparation.

Sample	Na-MLS (gram)	Na-MLS percentage in the sample (w%)	$\Delta l / l_o$ (A.U.)	$d/d_o$ (A.U.)	Shear modulus (Pa)
1	-	-	0.535	1.122	1882
2	0.05	0.25	-	1.194	1067
3	0.1	0.5	0.563	1.208	865
4	0.2	1.0	0.564	1.187	1198
5	0.3	1.5	0.622	-	1565

6	0.4	2.0	0.494	1.171	2097
7	0.5	2.5	0.43	1.151	2699
8	0.6	3.0	0.351	1.127	3304
9	0.8	4.0	-	1.098	4316

*Shear Modulus Measurements:* A Paar Physica UDS200 rheometer and a 25mm parallel plate were used for shear modulus measurements. Torque amplitude sweeps were first conducted in order to determine the linear elastic region. The torque amplitude ranged from 0 to 1 mN\*m and frequency was kept at 1 Hz for all the measurements. The sample was placed very carefully into the rheometer to prevent the disruption of the gel structure. Measurements were commenced after a waiting time of 10 min. Following this procedure, we were able to obtain reproducible results. The relative compression of the samples was in the range from 1.0 to ca. 0.5. Values of the elastic modulus G were calculated from the formula:  $\tau = G \cdot \gamma$ , where  $\tau$  is shear stress and  $\gamma$  is the shear strain of a sample. G was calculated from the slope of the linear region of the stress-strain plot.

#### 4.3 RESULTS AND DISCUSSION

The level of homogenous distribution of the Na-MLS platelets within the PNIPAM matrix is first determined using polarized optical microscopy. The presence of water limits our use of X-ray diffraction (XRD) and Transmission electron microscopy (TEM). When the montmorillonite is mixed with water, two dispersions have been commonly identified: the exfoliated (when the basal interlayer of the montmorillonite is completely disrupted) and intercalated (when the



interlayer basal spacing increases relative to the original montmorillonite). In our earlier paper<sup>22</sup>, we have demonstrated that even when Na-MLS is exfoliated, the individual clay platelets form aggregates where the face of one platelet has a face-face interaction with others at its edge. This leads to the increase of clay domain size with concentration. XRD and TEM measurement have confirmed that exfoliated dispersions show a sign of aggregation similar to clay + water suspensions.<sup>23</sup> In aggregation, two or more particles clump together, touching only at certain points. The aggregated clays retain their identity but move kinetically as a single unit.<sup>24</sup>

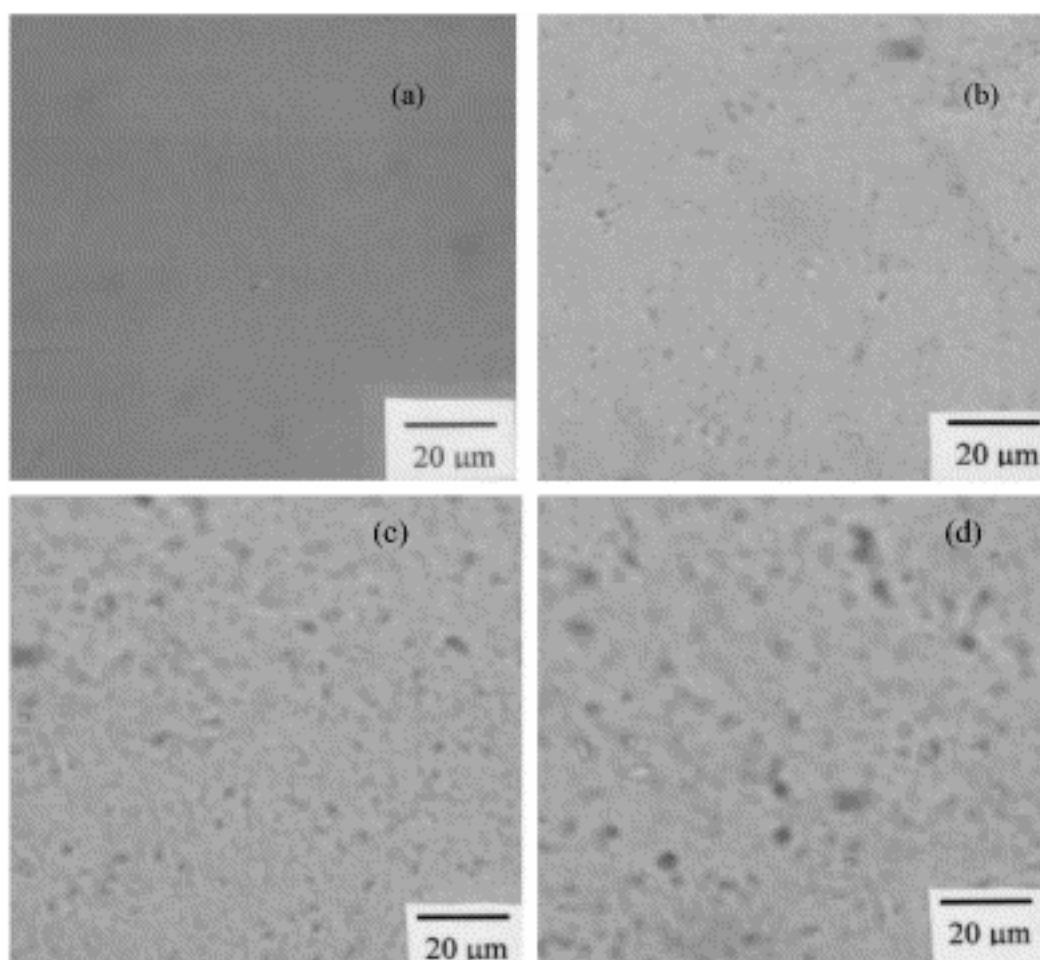
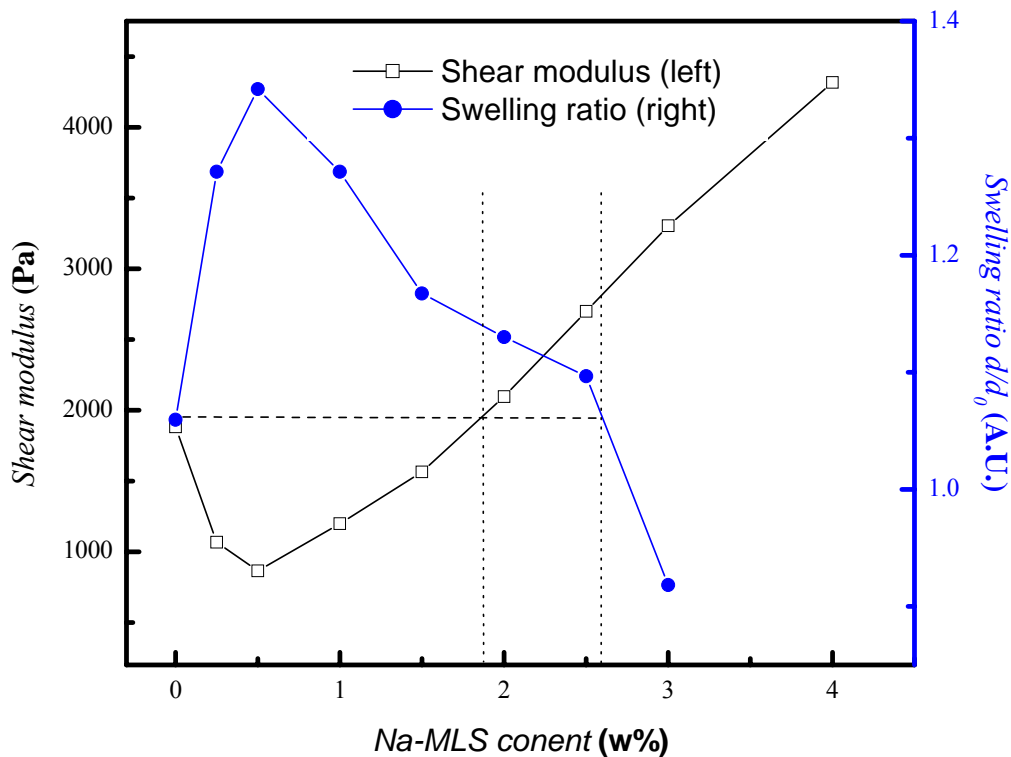


Figure 4.1. Optical images of composite gels by Axioplan polarizing optical microscope. (a) pure PNIPAM, (b) 0.5 w%, (c) 1.5 w%, and (d) 2.0 w% Na-MLS/PNIPAM composite gels.

Here, optical microscopy images for different concentration of Na-MLS/PNIPAM composites show the same phenomenon in Figure 4.1. With increasing clay concentration, the average platelet size varied from 1 to 5  $\mu\text{m}$  gradually as the concentration of Na-MLS increased from 0.5 wt% to 2.0 wt%, and an average agglomerate separation of 10, 4 and 3  $\mu\text{m}$  was observed for 0.5, 1.5, 2.0 wt% Na-nanocomposites, respectively. It revealed that Na-MLS tends to form larger aggregates in a PNIPAM gel matrix when its concentration above 1.5 w%. In the low Na-MLS concentration ranging from 0 to 1.5 w%, the small Na-MLS aggregates are well dispersed inside PNIPAM matrix as suggested by the evenly distributed small black dots in Figure 4.1 (b) and (c). When the Na-MLS concentration reached 2 w%, larger aggregates were formed as indicated by the increased concentration and dimensions of the black dots in Figure 4.1 (d). This morphology will be related to the swelling and mechanical properties of the gels. Increased turbidity of samples having more than 2% clay prevented optical analysis of the samples with higher clay concentrations.



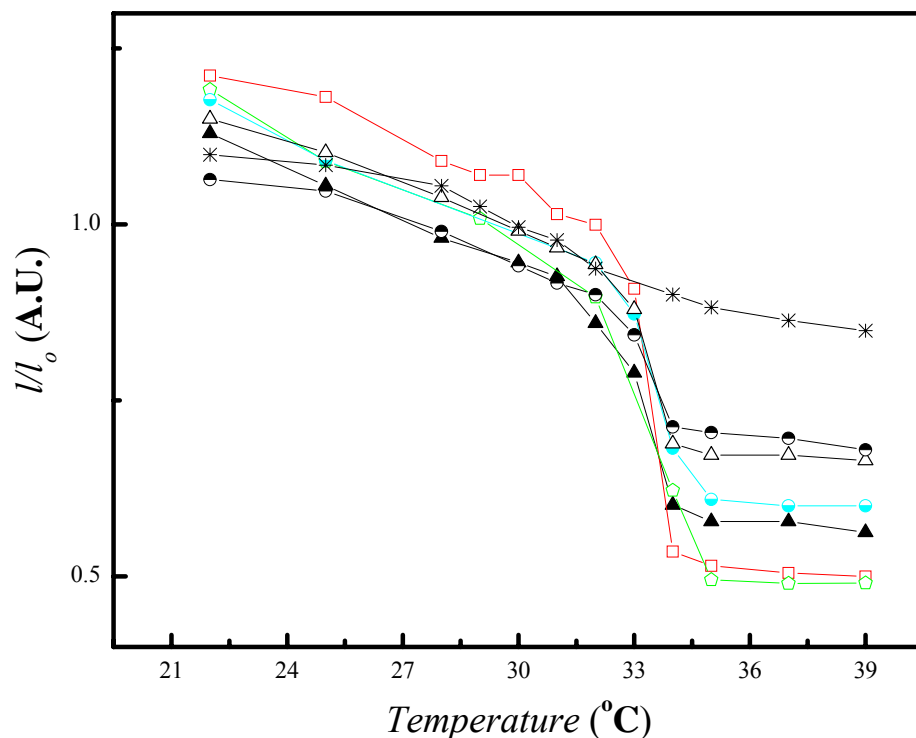
Dr. Z. Hu

Figure 4.2. Swelling ratio ( $d/d_0$ ) for the PNIPAM gel and its composites at 23°C, where  $d$  is the equilibrium gel filament diameter and  $d_0$  is the capillary diameter. The shear moduli of Na-MLS/PNIPAM composites are also shown in the figure, measured at 23°C.

Figure 4.2 shows the equilibrium swelling ratio  $d/d_0$  and shear modulus of gel composites as a function of Na-MLS concentration at 21°C, where  $d$  and  $d_0$  are, respectively, the diameter of the filaments in water at room temperature and the inner diameter of the capillary tubing. The value of  $d/d_0$  increased sharply from 1.12 of pure PNIPAM to the highest value 1.2 of 0.5 w% Na-MLS incorporated composite. In this low Na-MLS concentration range, Na-MLS are easily ionized and evenly distributed in the PNIPAM gel. This enhances the hydrophilicity of PNIPAM gel and makes it swell more. However, in the higher Na-MLS concentrations above 1.0

w%, the  $d/d_0$  decreases linearly with the increasing of Na-MLS concentration. This is partly due to the strong binding of sodium cations to the negatively charged MLS associates. These counter-ions are not free and cannot contribute to the osmotic pressure, resulting in the shrinkage of the gel.

Let us now discuss the mechanical properties of the gel composites. The dependence of the shear modulus  $G$  on the Na-MLS concentration is also shown in Figure 4.2. Adding Na-MLS in the region of small concentrations leads to the decrease of the  $G$  values from 1880 Pa of the pure PNIPAM to the minimum 865 Pa of 0.5 wt% Na-MLS composite. Further increase of Na-MLS concentration from 0.5 to 4.0 wt% is accompanied by the increase of the shear modulus from 865 Pa to 4320 Pa. Clearly, below 0.5 wt%, the Na-MLS are well separated and their hydrophilic property plays a major role. Above 0.5 wt%, the Na-MLS is associated to strengthen the gel network, resulting in the increase of the shear modulus. Specially, we have identified a narrow Na-MLS concentration ranging from 2.0 to 3.2wt%. In this range, the gel has larger swelling ratio and stronger mechanical strength than those for a pure PNIPAM, this is a significant result because an increase in swelling ratio is usually accompanied by a decrease in shear modulus for a non-composite gel.



Dr. Z. Hu

Figure 4.3. Temperature dependence phase transition of the PNIPAM gel and its composite with up to 4.0 wt% of Na-MLS in water, in which ▲ stands for pure PNIPAM; □ for PNIPAM + .5% Na-MLS; ◻ for PNIPAM + 1% Na-MLS; ● for PNIPAM + 2% Na-MLS; △ for PNIPAM + 2.5% Na-MLS; ● for PNIPAM + 3% Na-MLS; \* for PNIPAM + 4% Na-MLS.

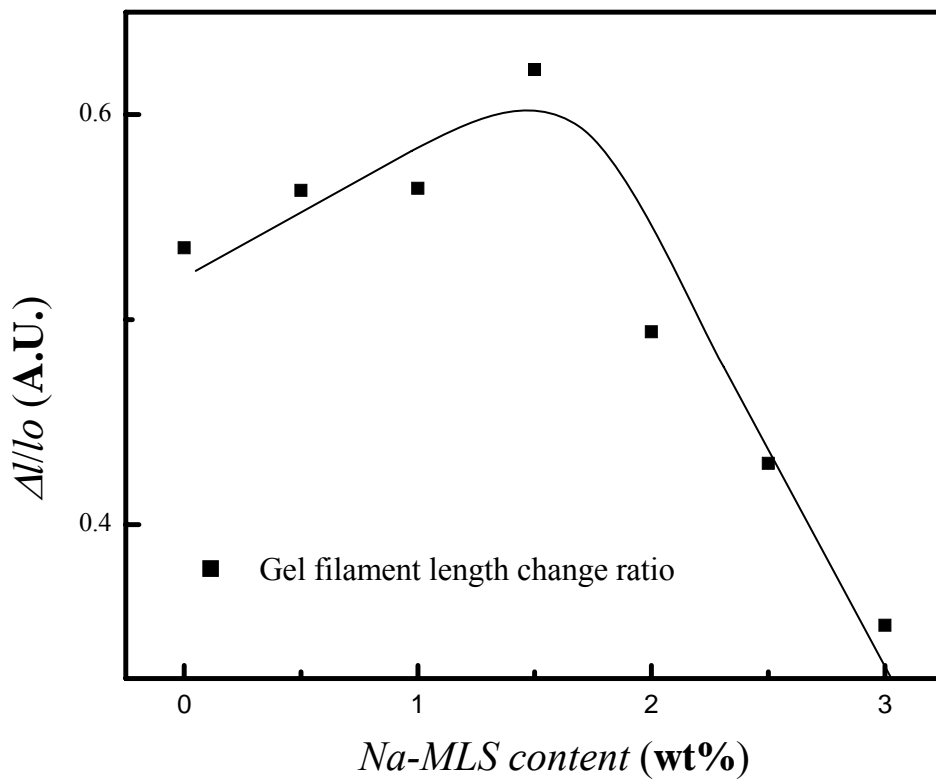
The temperature induced-volume phase transitions were tested for all Na-MLS/PNIPAM composites in water. The Na-MLS/PNIPAM filaments in water were heated gradually from 21°C to 39°C using a home made temperature controller with an accuracy of 0.5°C. The lengths of the filaments were measured at each temperature after it reaches the equilibrium value about 2 hours. Volume variation of the gel filament is represented by the change of  $l/l_0$ , where  $l_0$  is the length of filament when it is formed in the capillary tubing, and the  $l$  is temperature dependent length. Typical temperature induced volume phase transition

curves of pure PNIPAM gel filament and its composites, with up to 4.0 w% of Na-MLS, are shown in Figure 4.3. By comparing these curves it is apparent that the  $T_c$  ( $\sim 34^\circ\text{C}$ ) of the neutral PNIPAM gel in water is unaffected by the presence of Na-MLS in the concentration ranging from 0 to 4.0%. It is well known that increasing the cross-linker concentration could substantially increase the gel mechanical strength, however, it could also bring the  $T_c$  to a slight higher temperature.<sup>25</sup>

It can be seen that the presence of Na-MLS in neutral PNIPAM gels hinders the degree of the temperature-induced shrinkage at the  $T_c$  in water. This effect is more pronounced for the gels with higher Na-MLS content (above 4.0 w%). The plausible explanation is that the charged MLS start to sterically obstruct and electrically repulse one another. The strong collapse force of the PNIPAM gel is consequently being weakened.

The changes of the filament length  $\Delta l/l_0$  for the PNIPAM gel and its composites are compared and shown in Figure 4.4, where  $\Delta l$  is the filament length difference below and above the  $T_c$  ( $\sim 34^\circ\text{C}$ ) and  $l_0$  is the equilibrium filament length at  $22^\circ\text{C}$ . This parameter is defined to numerically represent the extent of gel volume change induced by the temperature at the  $T_c$ . It is interesting to observe that the volume change of the PNIPAM is increased first by Na-MLS additives in the range of 0-1.5 wt%, and then decreased linearly as more Na-MLS are incorporated. The extent of gel volume change at the  $T_c$  is the balance of competition between two contradictory driving forces: one is increased hydrophilicity arising from the well-dispersed Na-MLS, and the other is the strong self-association tendency from increasing amount of Na-MLS. This phenomenon is well explained by the morphology of the Na-MLS shown in Figure 4.1. At low additive concentration below 1.5 w%, the contribution from well-separated small Na-MLS aggregates is dominant as shown in Figure 4.1 (b) and (c). It therefore leads to the

enhanced volume change. As Na-MLS concentration increased above 1.5 w%, however, the self-associate force of MLS is overwhelming and causes a reduction in the volume change.



Dr. Z.Hu

Figure 4.4. The relative size change ( $\Delta l/l_0$ ) over the volume phase transition temperature for the PNIPAM gel and its composites, where  $\Delta l$  and  $l_0$  are the filament length difference between 22°C and 37°C and equilibrium filaments length at 22°C, respectively.

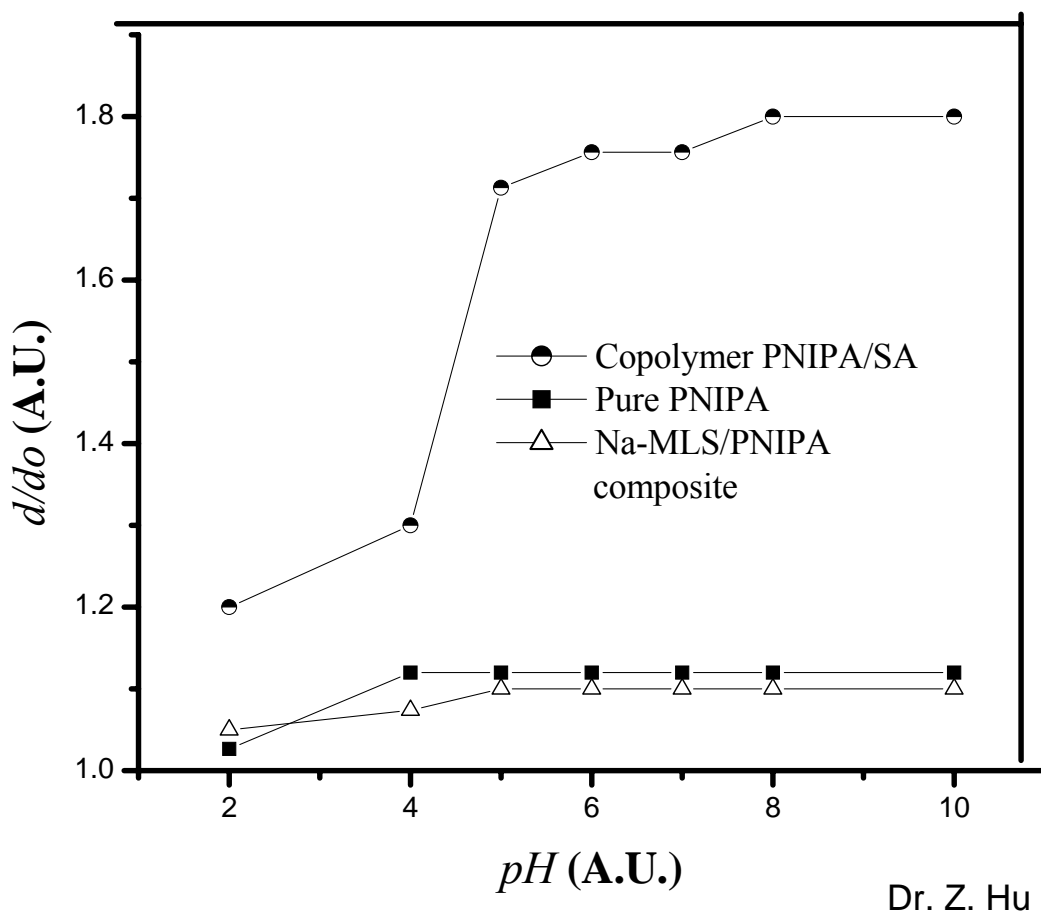


Figure 4.5. pH sensitivity of NIPA-SA copolymer <sup>26</sup>, pure PNIPAM and Na-MLS/PNIPAM composite gels. The weight ratios of NIPA to SA in NIPA-SA copolymer and PNIPAM to Na-MLS in Na-MLS/PNIPAM composite are 1/0.048 and 1/0.385, respectively.

It has been reported that the copolymer gels comprising *N*-isopropylacrylamide (NIPA) and sodium acrylate (SA) are sensitive to a pH change <sup>26</sup>. The Na-MLS/PNIPAM composites, however, exhibit no such sensitivity to pH conditions. The swelling ration  $d/d_o$  was kept almost constant as the pH environment changes from 2 to 10 at 21°C as shown in Figure 4.5. This suggests that Na-MLS is physically entrapped rather than chemically bonded into the gel network.



#### 4.4 CONCLUSION

Clay-polymer hydrogel composites have been synthesized based on poly(*N*-isopropylacrylamide) (PNIPAM) gels containing 0.25 to 4 wt% of the expandable smectic clay Na-montmorillonite layered silicates (Na-MLS). Their structure and property relationship has been investigated combining measurements of morphology, shear modulus, and swelling ratio as a function of temperature and Na-MLS concentration. Specifically, a polarized optical microscopy study has revealed that Na-MLS form aggregates in the PNIPAM gel and the size of aggregates increases with Na-MLS concentration. Incorporation of Na-MLS clay into a neutral PNIPAM network improves the gel mechanical properties, while does not change its volume phase transition temperature. The shear modulus of the gel composite first decreases and then increases with the increasing Na-MLS concentration, exhibiting a distinct minimum. In Na-MLS additive concentrations ranging from 2.0 to 3.2 w%, both swelling ratio and shear modulus of the composite gels have been improved comparing with the pure PNIPAM gel. The difference in gel volume below and above  $T_c$  can be enhanced by adding small amount of Na-MLS (<1.5 w%). The composite gel does not response to the pH change, indicating that Na-MLS is physically entrapped inside the gel matrix.

## CHAPTER REFERENCES

1. Xia, X., Yih, M.J., Dsouza, N., Hu, Z., *Polymer*, **2003**, 44, 3387
2. Hirotsu, S., Hirokawa, Y., Tanaka T. *J. Chem. Phys.* **1987**, 87, 1392
3. Li, Y., Tanaka, T. *Annu. Rev. Mat. Sci.* **1992**, 22, 243
4. Shibayama, M., Tanaka, T., Han, C.C. *J. Chem. Phys.* **1992**, 97, 6829
5. Liao, G., Xie, Y., Ludwig, K.F., Bansil, R., Gallagher, P. *Phys. Rev. E* **1999**, 60, 4473
6. Dong, L., Hoffman A.S. *J Control Release* **1986**, 4, 223
7. Osada, Y., Okuzaki, H., Hori, H. *Nature* **1992**, 355, 242
8. Hu, Z., Zhang, X., Li, Y. *Science* **1995**, 269, 525
9. Hu, Z., Chen, Y., Wang, C., Zheng, Y., Li, Y. *Nature* **1998**, 393, 149
10. Hu, Z., Lu, X., Gao, J., Wang, C. *Advanced Materials* **2000**, 12, 1173
11. Beebe, D.J., Moor, J.S., et al. *Nature* **2000**, 404, 588
12. Shinde, V.S., Badiger, M.V., Lele, A.K. Mashelkar, R.A. *Langmuir* **2001**, 17, 2585
13. Zhang, X., Zhuo, R., Yang, Y. *Biomaterials*, **2002**, 23, 1313
14. Takigawa, T., Yamawaki, T., Takahashi, K. Masuda, T. *Polymer Gels and Networks*, **1997**, 5, 585
15. Xue, W., Champ, S. Huglin, M.B. *Polymer* **2001**, 42, 3665
16. Lu, X., Hu, Z., Gao, J. *Macromolecules* **2000**, 33, 8698
17. Gao, D., Heimann, R.B. *Polymer Gels and Networks* **1993**, 1, 225
18. Churochkina, N.A., Starodoubtsev, SG., Khokhlov, AA. *Polymer Gels and Networks* **1998**, 6, 205
19. Phillip, B., Messersmith, Znidarsich, F. *Mat. Res. Soc. Symp.* **1997**, 457
20. Haraguchi, K., Takehisa, T. *Adv. Mat.* **2002**, 14, 1120

21. Lvov, Y., Ariga, K., Ichinose, I., Kunitake, T. *Langmuir* **1996**, 12, 3038
22. Ranade, A., D'Souza, N.A., Gnade, B. *Polymer*, **2002**, 43, 3759
23. Butzloff, P., D'Souza, N.A., Golden, T.D., Garrett, D. *Polym Engng Sci* **2001**, 41, 1794
24. Schramm, L.L. "Suspensions: fundamentals and applications in the petroleum industry"  
*American Chemical Society*, Washington, DC **1996**.
25. Harsh, D.C., Gehrke, S.H.. *J. Controlled Rel.* **1991**, 17, 175
26. Motonaga, T., Shibayama, M. *Polymer* **2001**, 42, 8925

## CHAPTER 5

### FORMATION AND VOLUME PHASE TRANSITION OF HYDROXYPROPYL CELLULOSE MICROGELS IN SALT SOLUTION <sup>1§</sup>

#### 5.1 INTRODUCTION

The volume phase transition in polymer gels can be induced by many external stimuli such as temperature, solvent composition, light, electric field, and pH value.<sup>2-3</sup> Hydroxypropyl cellulose (HPC), one of the thermally responsive gels similar to the poly(*N*-isopropylacrylamide) (PNIPAM),<sup>3-4</sup> has received considerable attention because of its biocompatibility.<sup>5-9</sup> Bulk HPC hydrogels and its derivatives with various forms including homogeneous gel, porous gel, and gel beads have been extensively studied.<sup>8-9</sup> Our group has reported the synthesis of HPC microgel particles<sup>10-11</sup> using a precipitation polymerization method. For polymer chains like the HPC that contain both hydrophobic and hydrophilic portions, changing the properties of the solvent by other ways may also induce self-association, leading to the formation of colloidal particle aggregates. It is known that addition of salt can lower the phase transition temperature in ionic and nonionic gels.<sup>12-14</sup> This effect is caused by the competing interactions between salt and water and between water and polymer chains.

Here we show that HPC microgel particles have been synthesized at room temperature by adding salt into HPC-water solution. In contrast to a previous method<sup>10</sup> that requires to heat HPC-water solution above the low critical solution temperature (LCST) of the HPC at about 41°C, the current method is to first reduce the LCST of HPC polymer chains from 41°C to room

§ Reproduced with permission from [Xia, X., Tang, S., Lu, X., Hu, Z. *Macromolecules* **2003**, 36, 3695] Copyright [2003] American Chemical Society.

temperature by adding salt into the HPC-water solution and then to bond HPC globules without surfactant at room temperature. These microgels may be used as building blocks for the formation of nanoparticle networks<sup>15-16</sup> and as carriers for controlled drug delivery. The volume phase transition of the resultant microgels has been investigated using light scattering techniques. The results have been discussed in terms of Flory-Huggins swelling equilibrium of gels and compared with the previous study of bulk PNIPAM gels.<sup>17</sup>

## 5.2 EXPERIMENTAL

*Materials:* Dry hydroxypropyl cellulose (HPC) powder (average  $M_w = 1.0 \times 10^6$ ), divinyl sulfone (DVS), sodium hydroxide (NaOH) pellets, and sodium chloride (NaCl) were purchased from Aldrich Chemical Co. and used as received. The substitution level of the HPC polymer for this study was  $MS = 3.9$ , where MS is the average number of molecules of propylene oxide combined per anhydroglucose unit.<sup>9</sup> Water for all reactions, solution preparation, and polymer purification was distilled and purified to a resistance of 18 M $\Omega$  using a Millipore system and filtered through a 0.22  $\mu$ m filter to remove particulate matter.

*HPC Microgel Synthesis:* 0.5 g of HPC powder was mixed in 99.5 g of water to form 0.5 wt % HPC solution by gentle stirring for a week to ensure it thoroughly dissolved. We first prepared HPC polymer solution (5 g of 0.5 wt % HPC) and NaCl solution (3.80 g (0.065 mol) of sodium chloride in 45 mL of distilled water). Then NaCl solution was injected to the polymer solution using a pipet. After mixing completely, the color of the HPC solution changed from clear to light blue, indicating the formation of HPC colloids. Then 0.075 g of cross-linker divinyl sulfone (DVS) was added to the HPC/NaCl solution. After 2 h, 0.25 g of 2 M NaOH solution was added

to make the pH value of HPC/NaCl solution equal to 12. The cross-linking reaction between DVS and HPC colloids was carried out for 24 h. The resultant microgels were then dialyzed for 1 week to remove NaCl and NaOH. The same procedure was used to prepare a series of HPC microgels with polymer concentrations ranging from 0.03 to 0.1wt % at various sodium chloride concentrations.

*LCST Determination:* The lower critical solution temperature (LCST) of un-cross-linked HPC polymer chains at various salt concentrations was determined by measuring the scattering intensity at 90° scattering angle. Here HPC (1000 ppm) was dissolved in a given concentration of a sodium chloride solution at 15°C. The cell holder in light scattering apparatus was thermally controlled using a refrigerating circulator. The temperature was gradually raised from 15 to 45°C by turning on the heater. The LCST of the HPC in a salt chloride solution was defined as the temperature at which scattering light intensity exhibits a sharp rise.

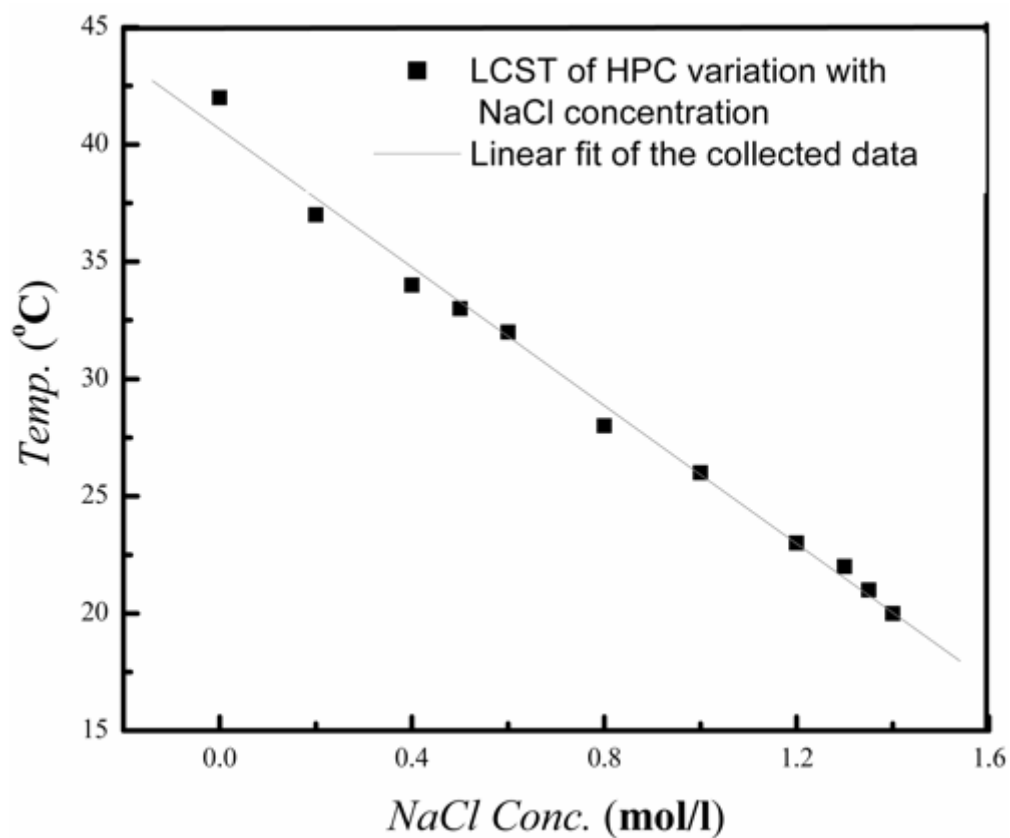


Figure 5.1. The LCST of un-cross-linked HPC decreases with increasing sodium chloride concentration, where the LCST was obtained from the midpoint of the sharpest light scattering intensity change.

### 5.3 RESULTS AND DISCUSSION

*5.3.1. Synthesis of HPC Microgels in Salt Solution.* The LCST of the HPC is plotted against NaCl concentration as shown in Figure 4.1. A linear relationship is obtained between the two, indicating that an increase of sodium chloride lowers the LCST of the HPC solution. It is known that the pure HPC is more soluble in water at the temperatures below LCST ( $\sim 41^{\circ}\text{C}$ ) than it is at

the temperatures above the LCST.<sup>19-21</sup> Here adding NaCl apparently weakens the hydrogen bonding between HPC and water, leading the LCST of the HPC to a lower temperature.

Our experiment demonstrated that HPC colloids can form at room temperature only within a narrow sodium chloride concentration ranging from 1.3 to 1.4 M. Below 1.3 M, HPC hydrophilic property is dominant, and HPC chains unable to form globules. Above 1.4 M, HPC colloids can grow bigger through hydrophobic interaction and eventually lead to precipitation. After finding the relationship between the LCST and the salt concentration, we carried out the experiment to synthesize surfactant free HPC microgels by cross-linking the self-associated chains in salt solution using divinyl sulfone at pH = 12 at room temperature.

It is found that three reaction factors affect the final HPC microgel particle size and size distribution: polymer concentration, salt concentration, and reaction temperature. Let us keep HPC concentration at 0.03 wt %, while changing the NaCl concentration from 1.4 to 1.3 M. As shown in Figure 5.2 (a), the higher NaCl concentration leads to the smaller average radii  $\langle R_h \rangle$  of the microgels. The main  $R_h$  peak positions for microgels synthesized in 1.4, 1.35, and 1.3 M NaCl solutions are 540, 570, and 830 nm, respectively. This suggests that more compact microgels were formed in higher salt concentrations. Furthermore, the radius distribution becomes broader with the increase of the salt concentration. PDI for the HPC microgels synthesized at 1.40, 1.35, and 1.30 M NaCl solutions are calculated respectively to be 1.5, 1.3, and 1.2. This indicates lowering NaCl concentration tends to form narrower size distribution. The formed globules are apt to precipitate as their density getting higher, while the steric effect from less condensed globules help to stabilize the colloidal dispersion. When NaCl concentration



was increased above 1.4 M, however, the steric effect could no longer be strong enough to balance the precipitation force contributed from the growing population of larger particles.

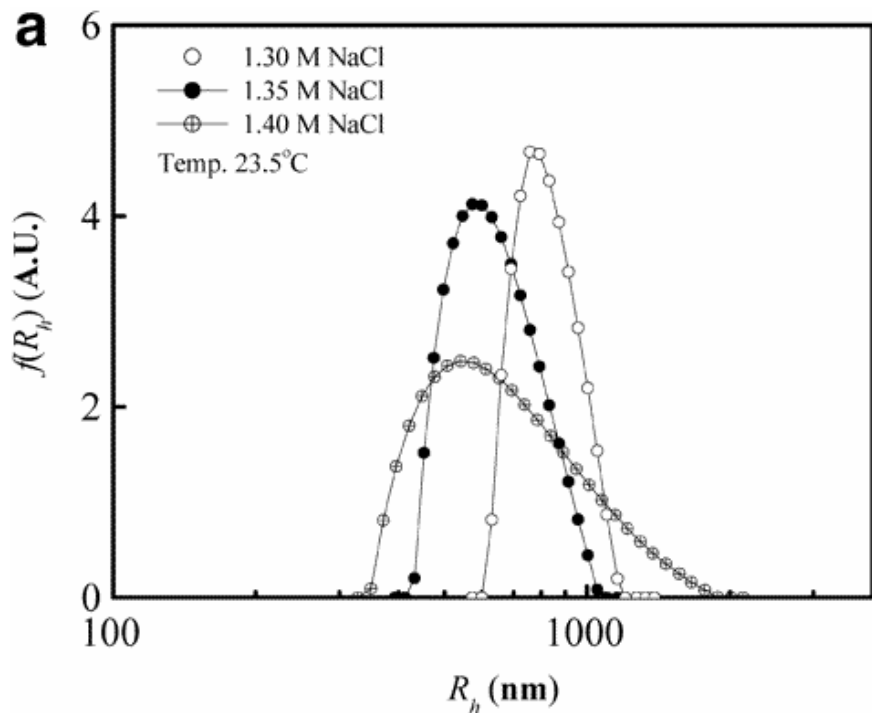


Figure 5.2(a) Hydrodynamic radius distributions ( $f(R_h)$ ) of HPC microgel particles ( $C = 5.0 \times 10^{-5}$  g/mL) in deionized water at 23.5°C. The HPC microgels were prepared in various NaCl concentrations, while the HPC polymer chains concentration and reaction temperature were kept at 0.03 wt % and 23.5°C, respectively.

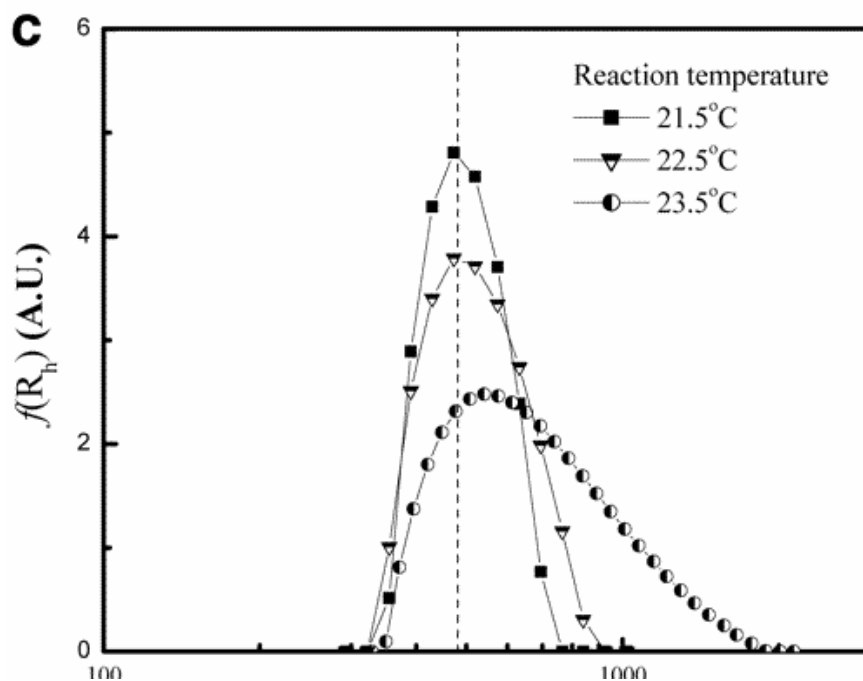
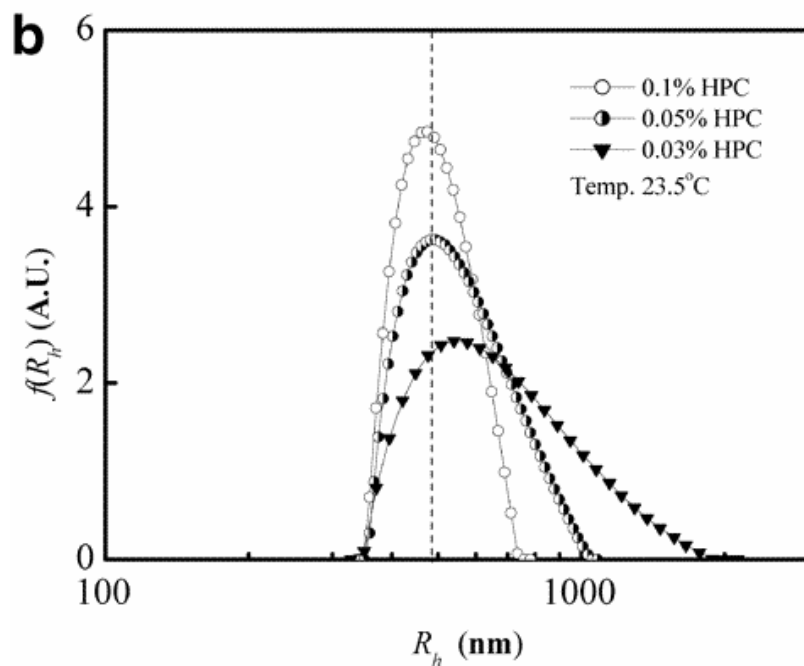


Figure 5.2. Hydrodynamic radius distributions ( $f(R_h)$ ) of HPC microgel particles ( $C = 5.0 \times 10^{-5}$  g/mL) in deionized water at 23.5°C (b) The HPC microgels were made at 23.5°C in various HPC polymer concentrations, while NaCl concentration was kept at 1.4 M. (c) The HPC microgels

were made at different temperatures, while HPC polymer concentration and NaCl concentrations were kept at 0.03% and 1.4 M.

The HPC microgel size distribution was then investigated as HPC concentration was varied from 0.03 to 0.1 wt %, while the NaCl concentration and the reaction temperature were kept at 1.4 M and 23.5°C, respectively. Figure 4.2 (b) shows hydrodynamic radius distributions ( $f(R_h)$ ) of resultant HPC microgels ( $C = 5 \times 10^{-5}$  g/mL). The average radii  $\langle R_h \rangle$  of the microgels show no significant change: 470 nm for 0.1 wt % HPC, 480 nm for 0.05 wt % HPC, and 540 nm for 0.03 wt % HPC. However, the radius distribution becomes narrower with the increase of HPC concentration. The PDI values for 0.03, 0.05, and 0.1 wt % HPC are 1.5, 1.3, and 1.3, respectively.

Figure 5.2 (c) shows the HPC microgel size distribution at different reaction temperatures. Here polymer and sodium chloride concentrations are kept at 0.03 wt % and 1.4 M. The reaction temperatures selected here are higher than the LCST of the HPC in 1.4 M NaCl solution ( $\sim 20.5^\circ\text{C}$ ) by 1, 2, and 3°C, respectively. As shown in Figure 5.2 (c), the particle size does not change significantly and are 470, 470, and 540 nm for 21.5, 22.5, and 23.5 °C, respectively. However, the size distribution becomes narrower as  $\Delta T = T - \text{LCST}$  decreases. As  $\Delta T$  increases, the salt association becomes faster so that polymer chains do not have time to relax themselves to the most favorable states. As a result, the particle size distribution becomes broader.

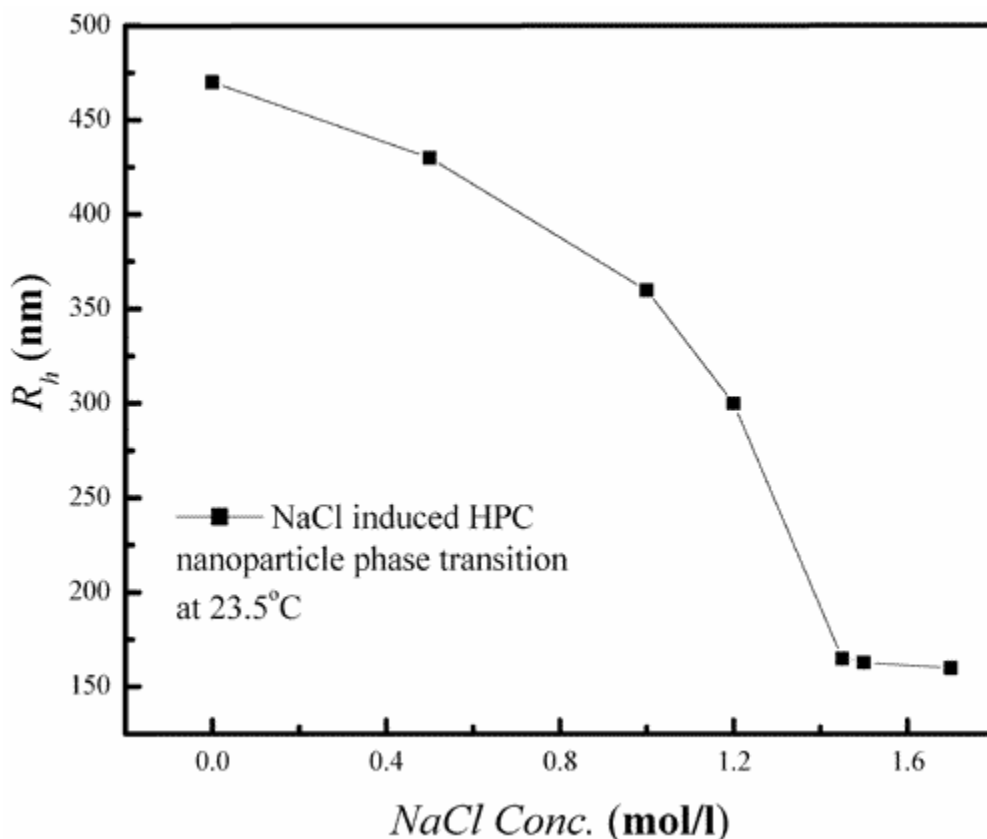


Figure 5.3. Sodium chloride induced HPC microgel particles ( $C = 5.0 \times 10^{-5}$  g/mL) volume phase transition at 23.5°C. The hydrodynamic radius was measured by dynamic light scattering.

5.3.2. *The Volume Phase Transition of HPC Microgels.* Like its polymer chain counterpart, the resultant surfactant-free HPC microgels exhibit both the temperature and salt sensitive volume phase transition behaviors. The average hydrodynamic radius of HPC microgels (synthesized at 23.5°C with polymer and salt concentration 0.1 wt % and 1.4 M, respectively) is plotted as a function of salt concentration at 23.5°C as shown in Figure 5.3. The HPC microgel hydrodynamic radius  $R_h$  dropped from 470 to 160 nm as the environment was changed from pure water to 1.4 M salt concentration. The critical sodium chloride concentration,  $C_c$ , is defined as the one that causes the sharpest change in gel volume. We found the  $C_c$  for HPC microgels is also between 1.3 and 1.4 M, similar to the value that we obtained for HPC chains. This suggests

that salt-induced volume change at room temperature and temperature-induced volume change in water are closely related.

The  $\langle R_h \rangle$  of HPC microgels plotted against temperature at various sodium chloride concentrations are shown in Figure 5.4. It can be seen that, at each sodium chloride concentration, the  $R_h$  of the gel sharply decreases at a certain temperature, which agrees well with the LCST of un-cross-linked HPC chains at different NaCl concentrations. As NaCl concentration increases, the volume transition temperature decreases.

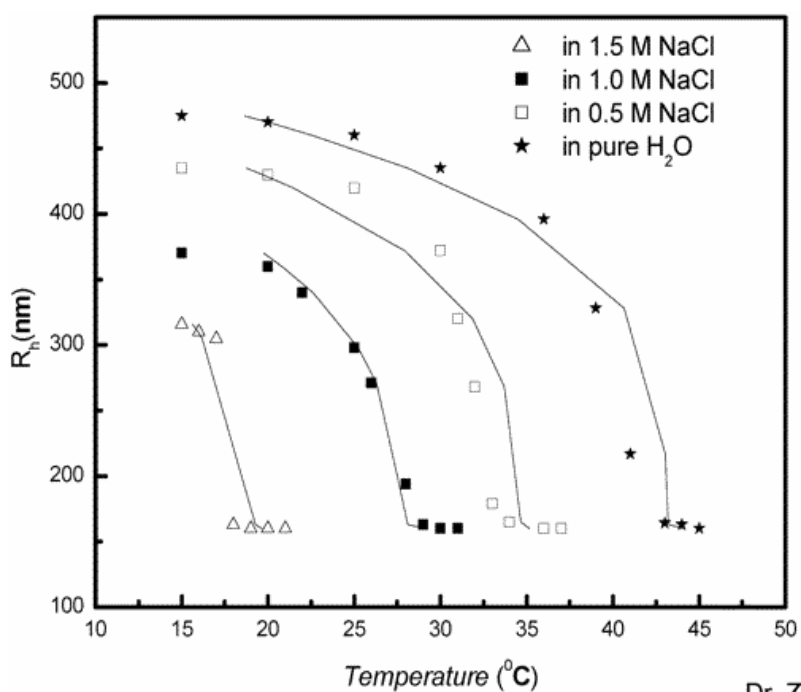


Figure 5.4. Temperature-induced volume phase transition of HPC microgel particles ( $C = 5.0 \times 10^{-5}$  g/mL) under different sodium chloride concentrations. The solid lines are the theoretical fitting curves based on the mean-field theory.

Let us turn our attention to understanding experimental results in Figure 5.4 in terms of Flory-Huggins free energy theory. According to this mean-field theory,<sup>22-23</sup> an equation relating the equilibrium concentration of a gel to the temperature can be written as<sup>17</sup>

$$\frac{\Delta H - T\Delta S}{T} = \frac{\Delta F}{T} = k \left\{ \frac{v_1 v}{N\phi^2} \left[ (2f + 1) \left( \frac{\phi}{\phi_0} \right) - 2 \left( \frac{\phi}{\phi_0} \right)^{1/3} \right] - \frac{2}{\phi} - \frac{2 \ln(1 - \phi)}{\phi^2} \right\} \quad (2)$$

where  $\phi$  is the volume fraction of polymer network,  $\Delta F$  is the free energy difference, and  $\Delta H$  and  $\Delta S$  are the corresponding enthalpy and entropy, respectively.  $v$  is the total number of chains in the gel,  $v_1$  the molar volume of the solvent,  $k$  the Boltzmann constant,  $T$  the absolute temperature,  $N$  Avogadro's number, and  $f$  the number of counterions per chain.

In this work,  $f$  is zero because of the neutral property of HPC chains. The volume fraction of gels  $\phi$  is varied on the basis of different salt concentrations.  $\Delta F$  can be expressed as  $\Delta F = \Delta F_0 + \Delta F_1 + \Delta F_2$ ,<sup>24</sup> where  $\Delta F_0$  is the change of the free energy of chains in pure water,  $\Delta F_1$  is the change of the free energy due to the disturbance of structured water molecules by salt, and  $\Delta F_2$  is the free energy change due to the disturbing or inducing the contacts of ionic polymer chains by hydrated ions. Since there is no ion in the HPC polymer chains,  $\Delta F_2$  is neglected.  $\Delta F_1$  is approximately represented as<sup>24</sup>

$$\Delta F_1 = \alpha C \quad (3)$$

where  $\alpha$  is a material constant.  $\Delta F_0 = \Delta H - T\Delta S$ , Combining eqs 2 and 3, we obtain

$$\frac{\Delta F_0 + \Delta F_1}{kT} = \frac{\Delta H - T\Delta S + \alpha C}{kT} = \frac{v_1 v}{N\phi^2} \left[ (2f+1) \left( \frac{\phi}{\phi_0} \right) - 2 \left( \frac{\phi}{\phi_0} \right)^{1/3} \right] - \frac{2}{\phi} - \frac{2 \ln(1-\phi)}{\phi^2} \quad (4)$$

Thus

$$\frac{\Delta H + \alpha C}{T} = k \left\{ \frac{v_1 v}{N\phi^2} \left[ (2f+1) \left( \frac{\phi}{\phi_0} \right) - 2 \left( \frac{\phi}{\phi_0} \right)^{1/3} \right] - \frac{2}{\phi} - \frac{2 \ln(1-\phi)}{\phi^2} \right\} + \Delta S = Y \quad (5)$$

$$T = \frac{\Delta H + \alpha C}{Y} \quad (6)$$

The values of  $\phi_0$  are calculated from the equilibrium swelling ratio of microgels at room temperature. They are 0.038, 0.050, 0.081, and 0.13 respectively for pure water, 0.5, 1.0, and 1.5 M NaCl solutions. The value of  $v$  is  $4.0 \times 10^{24} l^{-1}$ , estimated from the molar ratio (as initial concentration) between DVS cross-linker and HPC polymer. In equation (6),  $Y$  is a function of volume fraction  $\phi$  and  $\phi_0$ , it thus related to the particle size  $\langle R_h \rangle$ .  $\Delta H$ ,  $\Delta S$ , and  $\alpha$  are varied to fit the  $\langle R_h \rangle$  vs  $T$  curves for HPC microgels in Figure 5.4 and are found to be  $-5.56 \times 10^{-18} \text{ J}$  (average error 6%),  $-1.76 \times 10^{-20} \text{ J K}^{-1}$  (average error 6%), and  $27.9 \times 10^{-20} \text{ J/M}$  (average error 11%), respectively. The theoretical curves are shown in Figure 4 as solid lines and are in good agreement with the experimental data. It is noted that our  $\Delta H$  and  $\Delta S$  values are very close to those ( $\Delta H = -5.4 \times 10^{-18} \text{ J}$  and  $\Delta S = -1.8 \times 10^{-20} \text{ J K}^{-1}$ ) obtained for PNIPAM bulk gels,<sup>16</sup> even though HPC and PNIPAM have different chemical structures and different volume phase

transition temperatures in water. There are some discrepancies between the prediction of Eq 6 and the experimental results. This may be due to oversimplification of the theoretical modeling. For example, the effects of loops and free branches have not been considered.

#### 5.4 CONCLUSION

Surfactant-free HPC microgels have been synthesized by chemically cross-linking hydroxypropyl cellulose (HPC) linear macromolecules. The controllable synthesis parameters-salt concentration, HPC concentration, and reaction temperature-were varied to determine the effects on the size and size distribution of the microgels as monitored using dynamic laser light scattering techniques. It is found that the microgels can form at room temperature within a narrow NaCl concentration range from 1.3 to 1.4 M. As the HPC concentration increases from 0.03 to 0.1 wt %, or temperature varied from 23.5 to 21.5 °C, or sodium chloride concentrations decreased from 1.4 to 1.3 M, the particle size distribution of resultant HPC microgels become narrower. The formation of microgels may be explained by the breakdown of hydrogen bonding between water and HPC chain with the addition of electrolyte. The fitting curves based on the Flory-Huggins mean-field theory are in good agreement with the experimental results.



## CHAPTER REFERENCES

1. Xia, X., Tang, S., Lu, X., Hu, Z. *Macromolecules* **2003**, 36, 3695
2. Tanaka, T. *Phys. Rev. Lett.* **1978**, 40, 820
3. Shibayama, M., Tanaka, T. *Adv. Polym. Sci.* **1993**, 1, 109
4. Hu, Z. B., Zhang, X. M., Li, Y. *Science* **1995**, 269, 525
5. Kluc, E. D. *J. Polym. Sci.* **1971**, 36, 491
6. Drummond, C., Albers, S., Furlong, D. N. *J. Colloids Surf.* **1992**, 62, 75
7. Winnik, F. M., Tamai, N., Yonezawa, J., Nishimura, Y., Yamazaki, I. *J. Phys. Chem.* **1992**, 96, 1967
8. Kabra, B. G., Gehrke, S. H., Spontak, R. J. *Macromolecules* **1998**, 31, 21668
9. Harsh, D. C., Gehrke, S. H. *J. Controlled Release* **1991**, 17, 175
10. Lu, X., Hu, Z. B., Gao, J. *Macromolecules* **2000**, 33, 8698
11. Gao, J., Haidar, G., Lu, X., Hu, Z. *Macromolecules* **2001**, 34, 2242
12. Ohmine, I., Tanaka, T. *J. Chem. Phys.* **1982**, 77, 5725
13. Park, T., Hoffman, A. S. *Macromolecules* **1993**, 26, 5045
14. Zhang, X., Hu, Z., Li, Y. *J. Appl. Polym. Sci.* **1997**, 63, 1851
15. Hu, Z. B., Lu, X., Gao, J., Wang, C. *Adv. Mater.* **2000**, 12, 1173
16. Hu, Z. B., Lu, X., Gao, J. *Adv. Mater.* **2001**, 13, 1708
17. Hirotsu, S., Hirokawa, Y., Tanaka, T. *J. Chem. Phys.* **1987**, 87, 1392
18. Chu, B. *Laser Light Scattering*, 2nd ed.; Academic Press: New York, **1991**
19. Karlstrom, G., Carlsson, A., Lindman, B. *J. Phys. Chem.* **1990**, 94, 5005
20. Ahlnas, T., Karlstrom, G., Lindman, B. *J. Phys. Chem.* **1987**, 91, 4030
21. Karlstrom, G. *J. Phys. Chem.* **1985**, 89, 4962

22. Tanaka, T., Fillmore, D., Sun, S., Nishio, I., Swislow, G., Shah, A. *Phys. Rev. Lett.* **1980**, 45, 1636
23. Flory, P. J. *Principles of Polymer Chemistry*; Cornell University Press: Ithaca, NY, **1963**.
24. Suzuki, A. *Adv. Polym. Sci.* **1993**, 110, 201

## CHAPTER 6

### LIGHT SCATTERING STUDY OF SELF-ASSOCIATION BEHAVIOR OF LONG CHAIN BRANCHED POLY(2-ETHYLOXAZOLINE) IN SOLVENTS <sup>15</sup>

#### 6.1 INTRODUCTION

A new architectural class of polymeric materials known as dendritic materials, including dendrimers and their more readily accessible but less structurally-defined counterparts known as hyperbranched polymers (HBPs) and long chain branched polymers (LCBPs) have received a great deal of interest in the last decade. <sup>2-8</sup> Work on dendrimers, HBPs and LCBPs have primarily focused on their synthesis and chemical modification with an eye toward micelle mimics, nanoscale building blocks and drug-delivery agents. <sup>9-10</sup> At the same time, intensive efforts have been made to study fundamental properties of these macromolecules using various analytic tools including NMR, <sup>11</sup> rheology, <sup>12</sup> small angle neutron scattering and light scattering, <sup>13-15</sup> atomic force microscopy, <sup>16</sup> TEM, <sup>17</sup> fluorescence Probing. <sup>18</sup>

The effect of solvent quality on dendrimer conformation has been investigated and it was found that the average dimension of dendrimers has a small but significant dependence on the solvent quality, which consequently leads to large variations of average segment density. <sup>15, 19-20</sup> Recently, a novel CH<sub>3</sub>-(CH<sub>2</sub>)<sub>17</sub> surface modified LCB-poly (2-ethyloxazoline) (PEOx) polymer, was synthesized using a cationic polymerization method. With the internal tertiary amide functional group on repeat ethyloxazoline units and external C<sub>18</sub> chains, it possesses a hydrophilic core and a hydrophobic shell. The grafted hydrophobic C<sub>18</sub> chains aim to act as a smart arm to move intelligently according to solvent environment. This unique architecture may

\$ Reproduced with permission from [Xia, X., Hu, Z., Gao, J., Qin, D., Durst, D.H., Yin, R., *Langmuir*, **2002**, 18, 8302] Copyright [2003] American Chemical Society.

provide us a model system to study solvent quality effect on LCBP conformation and its self-association in different solvents. The study may lead to not only better understanding of self-association of macromolecules in general, but also to potential applications in the fields of nanoscale catalysts, reactors, and controlled drug delivery.

Self-association is a well-known self-assembling phenomenon often found in diblock or triblock copolymer/solvent systems,<sup>21-22</sup> where the selective solvent to specific polymer blocks can lead to the formation of nanoparticles or chain aggregates without precipitation. Linear polymer self-association processes and mechanisms have been well studied. For example, it was found that in concentrated solutions, neutral poly (N-isopropylacrylamide) (PNIPAM) homopolymer chains self-associate above their lower critical solution temperature (LCST, ~32°C) to stable aggregates instead of undergoing the expected precipitation.<sup>23</sup> In these processes, chain collapse accompanied chain association, forming stable aggregates of different sizes at different temperatures and concentrations. Our previous studies revealed that the driving force leading to hydropropylcellulose (HPC) self-association results from hydrophobic attraction between hydrophobic moieties of HPC linear chains when water becomes a poor solvent above the LCST of the HPC.<sup>24</sup> It is thus reasonable to rationalize that, for the hyper-branched polymers containing both hydrophobic and hydrophilic portions, changing the properties of the solvent may induce self-association, leading to the formation of stable LCBP aggregates.

In this work, light scattering techniques were used to study the LCBP self-associate processes because the scattering light intensity is very sensitive to particle size. We demonstrated that long chain branched-PEOx can self-associate at different critical aggregation concentrations (cac) and form metastable aggregates in ethanol, methanol and tetrahydrofuran. The cac depends strongly on solvent polarity. Below the cac, static light scattering measurements revealed

properties of individual long chain branched-PEOx macromolecules including its molar mass and second virial coefficient. Heating a dilute long chain branched-PEOx ethanol solution to higher temperatures leads to significant shrinkage of the hydrodynamic radius of the macromolecules.

## 6.2 EXPERIMENTAL

*Materials:* Long chain branched poly (2-ethyloxazoline) (PEOx) with  $\text{CH}_3\text{-(CH}_2\text{)}_{17}$  ( $\text{C}_{18}$ ) chains modified surface was synthesized using cationic polymerization method.<sup>25-28</sup> The ratio of the initiator (1-Bromooctadecane) to the 2-ethyloxazoline is 1:20. The schematic chemical structure is shown in Fig. 6.1

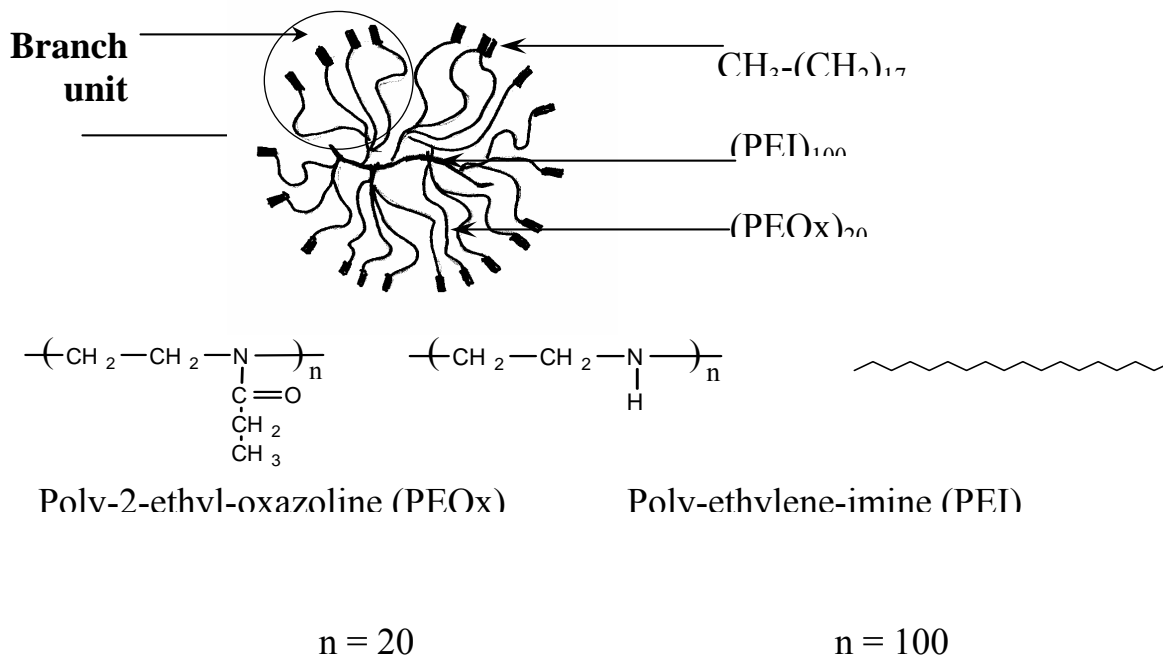


Figure 6.1 A schematic diagram of the chemical structure of the long chain branched poly (2-ethyloxazoline).

The center core is a linear polyethyleneimine (PEI) with the repeating units of 100. The internal branches are PEOx chains with the repeating units of 20. The side chain units that consist of 3 to 4 branches are grafted on the center PEI linear chain. The synthesis and characterization of PEOx have been reviewed.<sup>25-27</sup> The external shell consists of CH<sub>3</sub>-(CH<sub>2</sub>)<sub>17</sub> chains. The polymerization and grafting processes have been previously reported<sup>29-31</sup> and detailed analysis of chemical structures will be published elsewhere. Considering the molar mass ratio of C<sub>18</sub>- chains and branched-PEOx chains, the hydrophobic content of the samples were about 10 wt %. Ethanol (dehydrated 200) was purchased from Pharmco. Tetrahydrofuran (THF) and Methanol were bought from Aldrich and Fisher Chemical Company, respectively. All solvents were purified by repeatedly injecting them through 0.22 μm pore sterile filters to remove dust. Water for sample preparation was distilled and deionized to a resistance of 18.2 MΩ by a MILLIPORE system, and filtered through a 0.22μm filter to remove particulate matter.

*Sample Preparation:* The long chain branched PEOx samples were weighed using an analytical balance, and immersed in ethanol at room temperature under stirring for 3 days to make 1.0x10<sup>-3</sup> g/ml solution. Then the solution was diluted to 5.0 x 10<sup>-4</sup>, 2.5 x 10<sup>-4</sup>, 1.0 x 10<sup>-4</sup>, 5.0 x 10<sup>-5</sup>, and 2.5 x 10<sup>-5</sup> g/ml, respectively. The same method was used to prepare methanol solutions of 1.0 x 10<sup>-2</sup>, 5.0 x 10<sup>-3</sup>, 4.0 x 10<sup>-3</sup>, 2.0 x 10<sup>-3</sup>, 1.0 x 10<sup>-3</sup> g/ml, aqueous solutions of 2.0 x 10<sup>-2</sup>, 1.5 x 10<sup>-2</sup>, 1.0 x 10<sup>-2</sup> g/ml, and THF solutions of 2.0 x 10<sup>-3</sup>, 1.0 x 10<sup>-4</sup>, 1.0 x 10<sup>-5</sup>, 1.0 x 10<sup>-6</sup> g/ml, respectively. Visual inspection revealed that the LCBP quickly dissolved in water and methanol within 30 seconds, whereas about 12 hours in ethanol, and 48 hours in THF. Before experiments, all samples with the hydrodynamic radius ( $\langle R_h \rangle$ ) less than 150 nm were treated with dust free

devices, by which the samples were repeatedly filtered through 0.22  $\mu\text{m}$  pore sterile filters purchased from Millipore.

### 6.3 RESULTS AND DISCUSSION

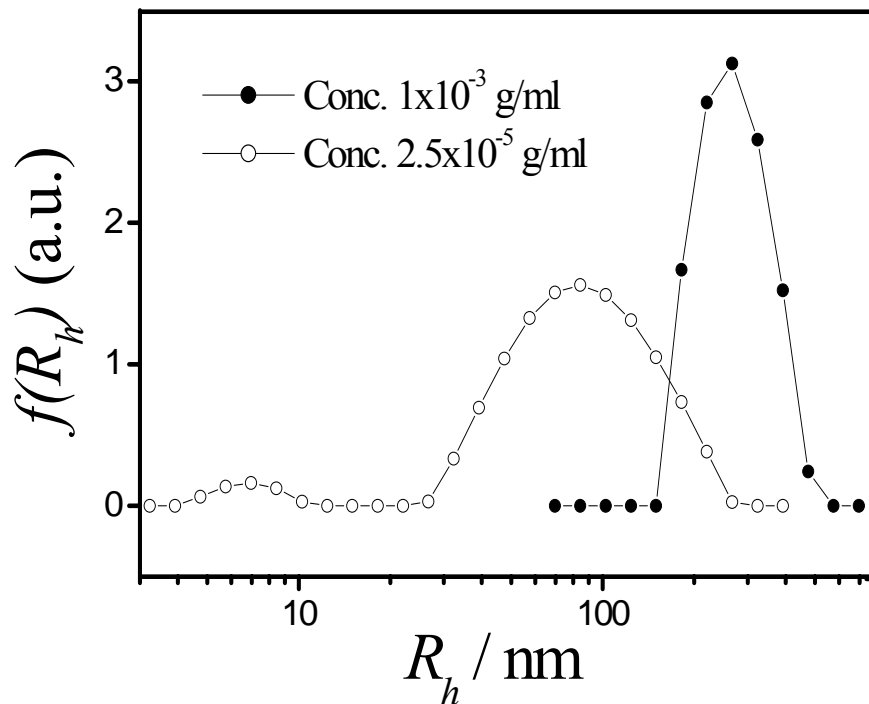


Figure 6.2. Hydrodynamic radius distribution profiles of the long chain branched-PEOx in ethanol at 23°C. At a higher polymer concentration of  $1.0 \times 10^{-3}$  g/ml, there is a single peak centered around 304 nm due to the formation of aggregates. At a lower polymer concentration of  $2.5 \times 10^{-5}$  g/ml, the large- $R_h$  peak centered around 80 nm and small- $R_h$  peak at 6 nm are attributed to individual long chain branched polymers and uncoupled intermediates respectively.

Overall hydrodynamic radius distribution profiles of the long chain branched-PEOx in ethanol at 23°C are shown in Figure 6.2. At the higher polymer concentration of  $1.0 \times 10^{-3}$  g/ml, there is a single peak centered around 300 nm. At the lower polymer concentration of  $2.5 \times 10^{-5}$  g/ml, there are two peaks centered around 80 nm and 6 nm. For the reasons that will be given

below, the single peak at the higher concentration is attributed to stable aggregates of the long chain branched-PEO<sub>x</sub>, while the large- $R_h$  peak and small- $R_h$  peak at the lower concentration are attributed to individual long chain branched-PEO<sub>x</sub>, and ungrafted precursor polymers, respectively. In the following paragraphs, we will first discuss how the long chain branched-PEO<sub>x</sub> self-associate into aggregates, then how individual polymers behave, and finally how the unreacted intermediates are incorporated into individual long chain branched-PEO<sub>x</sub> macromolecules.

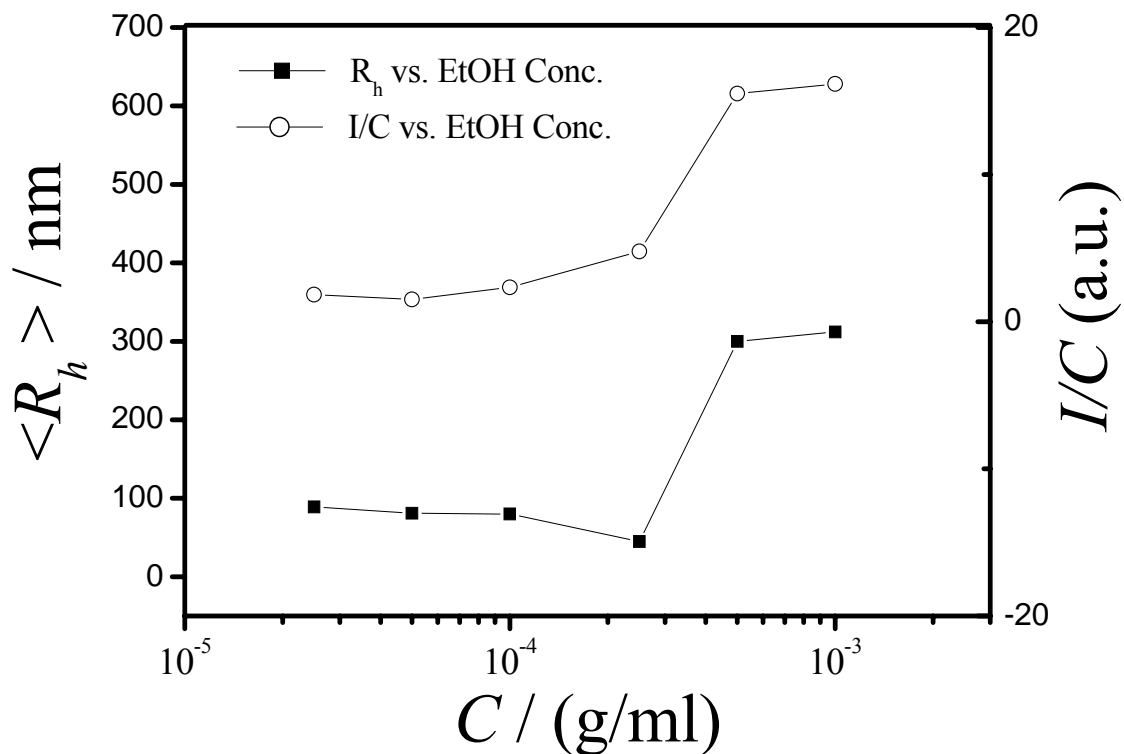
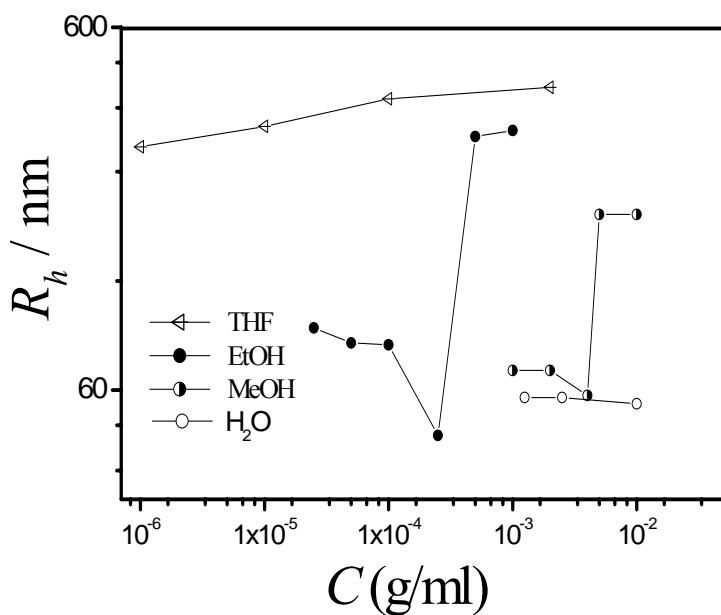


Figure 6.3. The change in hydrodynamic radius  $\langle R_h \rangle$  and normalized scattering light intensity ( $I/C$ ) of long chain branched-PEO<sub>x</sub> in ethanol as a function of polymer concentration at 23°C. The polymer concentration ranges from  $2.5 \times 10^{-5}$  g/ml to  $1 \times 10^{-3}$  g/ml.

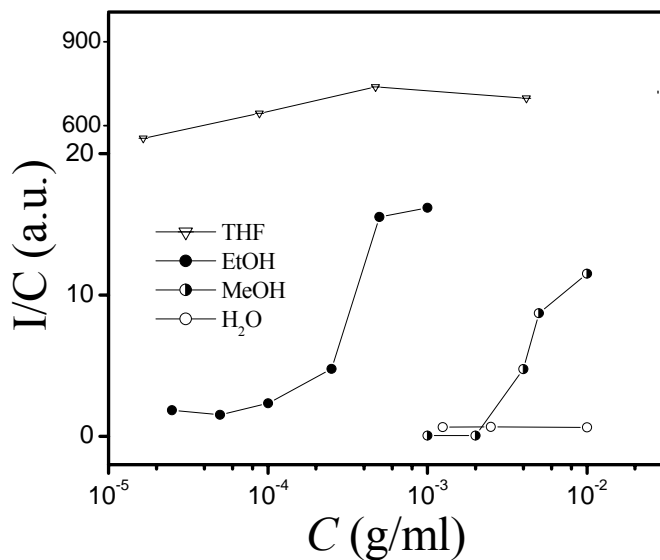


6.3.1. *Self-association of Long Chain Branched-PEOx Macromolecules.* Figure 6.3 shows average hydrodynamic radius ( $R_h$ ) of long chain branched-PEOx in ethanol at 23°C as a function of polymer concentration. At low concentrations ranging from  $2.5 \times 10^{-5}$  to  $1.0 \times 10^{-4}$  g/ml,  $R_h$  has a small value between 93 nm and 80 nm. When polymer concentration increases above  $2.5 \times 10^{-4}$  g/ml,  $R_h$  jumps to 304 nm. This gives us the first evidence that self-association occurs around  $2.5 \times 10^{-4}$  g/ml. To further confirm this observation, light scattering intensity (I) was measured and normalized by polymer concentration (C) as shown in Figure 6.2. The normalized scattering intensity (I/C) increases about 15 times as the concentration increases from  $1.0 \times 10^{-4}$  to  $5.0 \times 10^{-4}$  g/ml. From  $R_h$  and I/C data, the value of  $2.5 \times 10^{-4}$  g/ml is determined to be the critical aggregation concentration (cac) of the polymer in ethanol. Above the cac, the value of  $\langle R_h \rangle$  did not change with time within 2 weeks. After three months, it shrank 30% but the dispersion remained stable without phase separation. The slow shrinkage of  $\langle R_h \rangle$  may be caused by reorganization of polymer chains inside individual aggregates.

The aggregates have a narrow size distribution revealed by the small value of the polydispersity index (PD.I.) of 1.29. PD.I is referred as  $1 + \frac{\mu_2}{\langle \Gamma \rangle^2}$ , where  $\Gamma$  is the average line width and  $\mu_2 = \int_0^\infty G(D)(D - \langle D \rangle)^2 dD$ ,  $D = \frac{K_b T}{6\pi\eta \langle R_h \rangle}$ . PD.I for LCBP aggregates in methanol and THF were calculated to be 1.83 and 1.183, respectively, indicating long chain branched-PEOx aggregates were narrowly distributed in less polar solvents (i.e. THF), while moderately distributed in more polar solvents (i.e. methanol). A narrow distribution of meta-stable aggregates again indicates that this is a self-associating process, in contrast to simply packing individual molecules that usually leads to aggregates with a broad size distribution.



(a)



(b)

Figure 6.4 Comparison of the hydrodynamic radius  $\langle R_h \rangle$  and normalized light scattering intensity as a function of polymer concentration for water, methanol, ethanol, and THF at 23°C. (a) The change in hydrodynamic radius; (b) The normalized light scattering intensity.

Figure 6.4(a) summarizes the hydrodynamic radius  $\langle R_h \rangle$  as a function of the LCBP concentration in four different solvents. The corresponding normalized scattering light intensity

(I/C) is shown in Figure 6.4(b). In both methanol and ethanol, the sharp increase of hydrodynamic radius accompanies the increase of scattering light intensity, giving the cac value. In THF, the large- $R_h$  and high values of I/C exhibit little change with concentration. This suggests that the LCBPs form aggregates even at the extremely low concentration of  $1.0 \times 10^{-6}$  g/ml. Therefore, the cac of long chain branched-PEOx in THF, if it exists, must be much lower than that in ethanol ( $2.5 \times 10^{-4}$  g/ml). In water, the low- $R_h$  accompanied by the low value of I/C indicates that there are no aggregates in the concentrations ranging from 0.001 to 0.01 g/ml. Below 0.001 g/ml, signals are too weak and above 0.01 g/ml, the interaction between polymeric molecules prevents the obtaining of reliable light scattering data. From the shift of the cac value, it is apparent that the quality of the solvents for the long chain branched-PEOx ranks from good to poor in the sequence of water, methanol, ethanol, and THF. This result follows the order of solvents' polarity.

Based on dynamic light scattering observation, conformation of individual polymers and their aggregates in various solvents are proposed as shown in Figure 6.5.

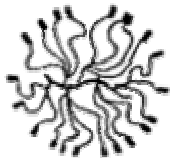
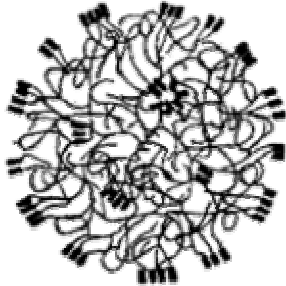

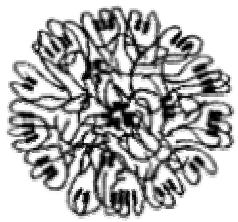
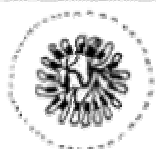
Solvent	Concentration increase $\longrightarrow$		Solvent
THF			
Alcohol			Polarity increase
H <sub>2</sub> O			$\downarrow$
	Single LCBP	LCBP aggregated	

Figure 6.5. The sketch of conformation of individual long chain branched-PEOx and their aggregates in various solvents. The short darker lines indicate C<sub>18</sub> chains and the long lighter lines indicate polar moieties (poly(2-ethyloxazoline) branched chains). The long dark line indicates the PEI linear chain.

We will first discuss individual polymers. In non-polar solvent such as THF, the non-polar moiety of C<sub>18</sub> chains on the long chain branched-PEOx surface tend to stretch outward to reduce exposure of interior polar polyethyloxazoline moiety of the macromolecules to the solvent. As polarity of the solvent increases, C<sub>18</sub> chains back-fold from the outside surface towards the interior, pushing the interior polyoethylxazoline branches to the surface. At the same time, the inward-moving C<sub>18</sub> chains can cause the interior materials (i.e.

polyethyloxazoline branches) to move with them, causing shrinkage in the overall size. In Figure 6.5, the short/darker lines indicate C<sub>18</sub> chains, the long/lighter lines indicate the polar moiety (polyethyloxazoline branches) and the long dark line indicates the PEI linear chain. The folding of the PEOx chains due to the inward movement of C<sub>18</sub> chains in a polar solvent makes the long chain branched-PEOx smaller. The more polar the solvent, the more inward pushing force on the C<sub>18</sub> chains, and that is why individual polymer has smaller  $\langle R_h \rangle$  (68 nm) in methanol than that in ethanol (80 nm). In water, the individual polymer was found to be only 55 nm in radius. This equilibrium size is a balance between the inward-bound force and the elasticity of the hyper-branched polymer core, which prevents complete collapse of the polymer in water.

We now turn our attention to self-association of the long chain branched-PEOx macromolecules. In a less-polar solvent such as THF, the number of C<sub>18</sub>-chains on the surface is not high enough to stabilize a single polymer that is dominated by the polar moieties of tertiary amide groups of ethyloxazoline repeat units in the interior. As a result, the macromolecules self-associate to a large aggregate that exhibits a high density of C<sub>18</sub> chains on the surface and concentrated polyethyloxazoline moieties in the interior. In the most polar solvents like water, C<sub>18</sub> chains enter deeply into the core of the polymer, leaving behind a hydrophilic polyethyloxazoline shell. That prevents aggregation even at the very high polymer concentration of  $1.0 \times 10^{-2}$  g/ml.

The most revealing effect of self-association may be observed in alcohols. As we will discuss later, our static light scattering measurement revealed that the second virial coefficient  $A_2$  of the polymer in ethanol is a small negative number, indicating that ethanol is a poor solvent. When polymer concentration increases, self-association of the long chain branched-PEOx indeed

takes place as shown in Figure 6.4(a). It is interesting to note that  $\langle R_h \rangle$  exhibit a minimum value at the cac. This suggests at the beginning of the aggregation, only small number of the polymers self-associate into compact spheres with hydrodynamic radius smaller than that of individual long chain branched-PEOx macromolecules. Self-association in the long chain branched-PEOx appears to two competing processes of intra-chain and inter-chain interactions. The shrinkage is due to the association of  $C_{18}$  within a single polymer, and due to a lack of enough polymer neighbors to form the aggregate. When the cac is reached, sufficient number of neighbors exists to allow the aggregation to occur instead of continual shrinkage.

*6.3.2. Individual Long Chain Branched-PEOx Macromolecules.* Static light scattering was carried out for the polymer in ethanol below its cac. Figure 6.6 shows the Zimm plot of the polymer in ethanol at 23°C. The value of  $dn/dc$  used here is  $0.133 \text{ cm}^3/\text{g}$  as measured by a refractometer (Dawn DSP, Wyatt Technology Corporation). From the extrapolation of  $KC/R_{vv}(q)$  in Eq. (2-10) to the zero angle and zero concentration, the molar mass  $M_w$ , the second virial coefficient  $A_2$ , and the radius of gyration  $\langle R_g \rangle$  were determined to be  $5.68 \times 10^5 \text{ g/mol}$ ,  $-2.4 \times 10^{-6} \text{ mol} \cdot \text{cm}^3/\text{g}^2$ , and 48 nm, respectively. Our separated measurements using matrix assisted laser desorption ionization time-of-flight mass spectrometry (Thermobioanalysis, Inc., Model Vision 2000 mass spectrometer) showed that the average  $M_w$  of a side chain PEOx unit is 8714. Here the matrix solution consisted of 10mg/ml 2.5 dihydroxybenzoic acid in 20:80 acetonitrile/water containing 0.1% trifluoroacetic acid. From these data, the average  $M_w$  (4300) of the center PEI chain, and the  $M_w$  for the long chain branched polymer, we found that there are about 50 side chain PEOx units on each PEI linear polymer core.

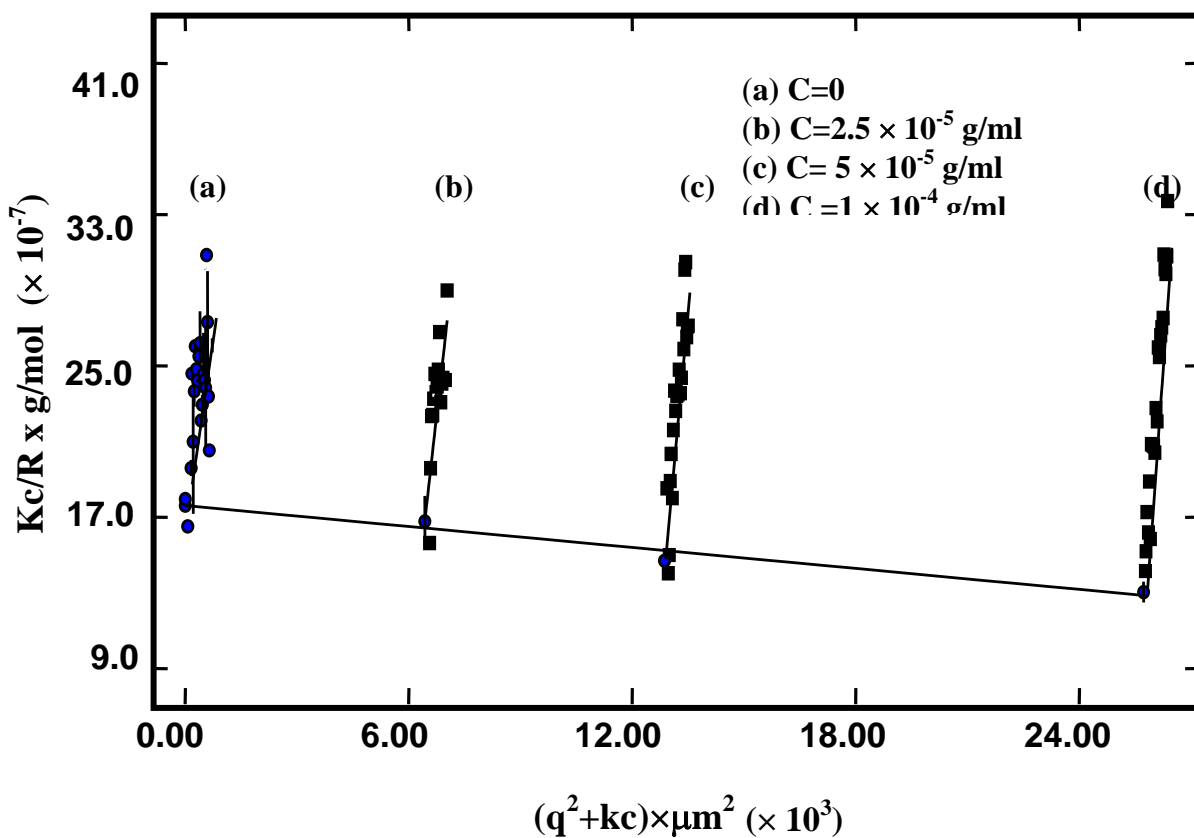


Figure 6.6. Zimm plot of the long chain branched-PEOx in ethanol at 23°C, where the polymer concentration ranges from  $2.5 \times 10^{-5} \text{ g/ml}$  to  $1 \times 10^{-4} \text{ g/ml}$ .

By combining DLS and SLS results, the ratio of  $\langle R_g \rangle / \langle R_h \rangle$  was found to be 0.60. This value is lower than the theoretical value of  $(3/5)^{1/2}$  for uniform hard spheres, indicating the polymer concentration in the surface region of individual HBP molecules is not as dense as in the central region. The density of HBP ( $\rho$ ) in ethanol may be estimated according to the relation  $4/3 \cdot \pi R^3 \rho = M_w / N_A$ , where  $R$  is  $R_h$  from DLS, the molar mass,  $M$ , is  $M_w$  from SLS, and  $N_A$  is Avogadro's number. Thus the calculated average polymer density in each polymer sphere is about  $2.65 \times 10^{-3} \text{ g/cm}^3$  at 23°C in ethanol. It is noted that the density ( $\rho$ ) obtained here is only an approximate value due to non-uniform distribution of polymer within an individual polymer. In

dynamic light scattering, the Laplace inversion of Eq (3) gives the line-width distribution  $G(\Gamma)$ . For a diffusive relaxation,  $\Gamma$  is normally a function of both  $C$  and  $\theta$ , which can be expressed as <sup>33</sup>

$$\Gamma/q^2 = D_0(1 + K_d C)(1 + f \langle R_g^2 \rangle_z q^2) \quad (5)$$

where  $K_d$  is the diffusion second virial coefficient and  $f$  is a dimensionless number. As  $C \rightarrow 0$  and  $\theta \rightarrow 0$ ,  $\Gamma/q^2 \rightarrow D_0$ . Since all the measurements were performed at the same scattering angle ( $90^\circ$ ), we may use  $D_1 = D_0(1 + f \langle R_g^2 \rangle_z q^2)$ . Eq (5) is therefore transformed roughly to simplified version as  $D = \Gamma/q^2 = D_1(1 + K_d C)$ , in which  $D$  can be calculated from Eq (4) as  $k_B T / (6\pi\eta R_h)$  for each concentration. A linear relationship between  $D$  and  $C$  is expected and the intercept should be the value of  $D_1$ . From the slope and intercept, we obtain  $K_d = 5.4 \times 10^3$  ml/g. The same calculations were made for the long chain branched-PEOx in methanol solution and  $K_d$  was determined to be  $0.76 \times 10^3$  ml/g.

The temperature dependent conformation change of the long chain branched-PEOx in ethanol has been studied. From Fig. 6.7(a), we can see that the radius  $\langle R_h \rangle$  of the single macromolecules decreases from 81 nm to 56 nm as the sample was heated from  $20^\circ\text{C}$  to  $45^\circ\text{C}$ . The normalized scattering light intensity data as shown in Fig. 6.7(b) indicate that aggregation did not occur in the polymer solution as temperature increasing. Note that there is a very large change of 37% shrinkage in size, indicating the solvent becomes poorer as temperature increases. This radial reduction is substantial and indicates that this long chain branched polymer may be used as a smart trap that can either entrap or release bio-molecules depending on environmental temperatures. Furthermore, the polymer may act as a solvent reservoir because it can shrink very quickly and expel solvent from its structure upon heating.<sup>34</sup> This may lead the temperature-induced change in rheological properties.



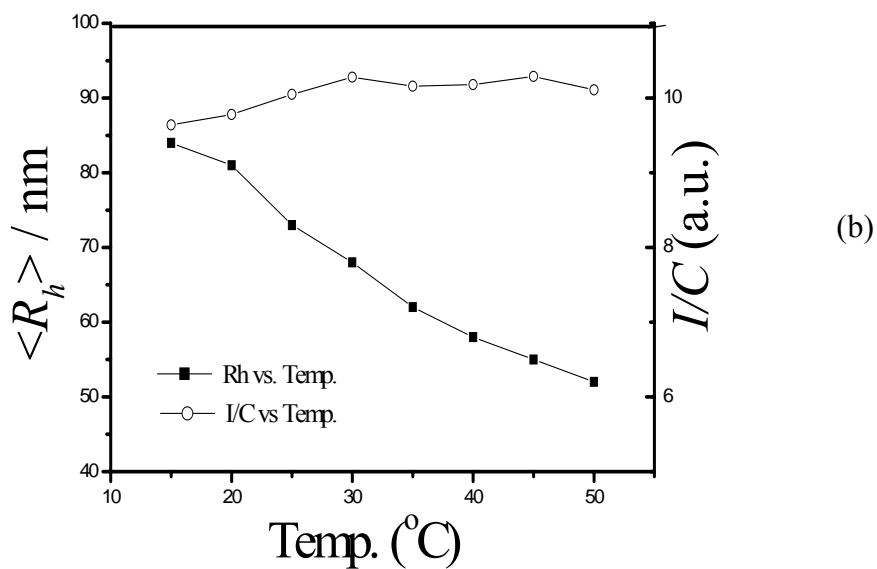
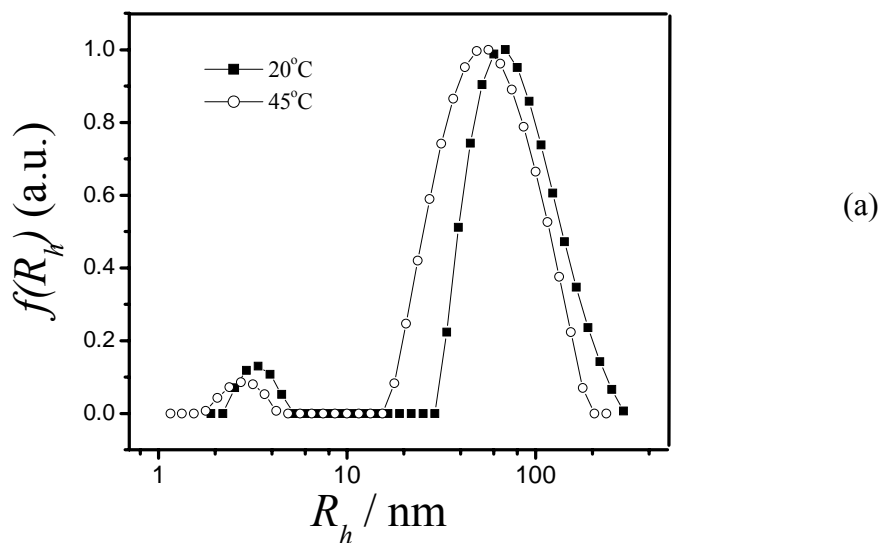


Figure 6.7. The temperature dependent conformation change of the individual long chain branched-PEOx in ethanol. (a) Hydrodynamic radius  $R_h$  distribution of  $1.0 \times 10^{-4}$  g/ml polymer concentration in ethanol at  $20^\circ\text{C}$  and  $45^\circ\text{C}$ , respectively. (b) Temperature dependence of the average hydrodynamic radius  $\langle R_h \rangle$  in multi-step heating, where the concentration is  $1.0 \times 10^{-4}$  g/ml in ethanol.

*6.3.3. Ungrafted Polymer Precursors.* At a lower LCBP concentration of  $2.5 \times 10^{-5}$  g/ml in ethanol, there are two peaks in the hydrodynamic radius distribution profiles for the HBP as shown in Figure 6.8. Also shown in Figure 6.8 are the hydrodynamic radius ( $R_h$ ) distributions of individual polymer at  $1.0 \times 10^{-3}$  g/ml in methanol and  $1.0 \times 10^{-2}$  g/ml in water for comparison. It is interesting to observe two peaks for the long chain branched polymer in all these solvents. In ethanol, the large- $R_h$  peak around 80 nm is attributed to individual polymer, while the smaller- $R_h$  peak around 6 nm is attributed to ungrafted products. The nature of the grafting reaction often results in a small amount of ungrafted intermediates. In this case, the ungrafted intermediates were still present in the final products due to the one pot synthesis process. Therefore, both grafted long chain branched and ungrafted polymers co-exist in the samples. It is noted that the ungrafted products yield a small sized light scattering peak around 6 nm, which is well separated from the large-sized peak around 80 nm. As a result, removing these ungrafted intermediates using solvent fractionation will not significantly affect the light scattering data on the large sized peak that is our major interest here. We found that the ratio ( $A_L/A_s$ ) of the single long chain branched polymer peak area ( $A_L$ ) to the ungrafted intermediate peak area ( $A_s$ ) in ethanol is 9.69, which is much greater than 0.37 in methanol and 1.86 in water. This suggests that the ungrafted intermediates were entrapped inside an individual macromolecule in ethanol but were released in the presence of a better solvent such as methanol. That is, higher solubility enables more hydrophilic linear molecules to move out from the long chain branched polymer interior. The ratio of  $A_L/A_s$  in water is larger than that in methanol because partially collapsed  $C_{18}$  chains can inhibit the release of the entrapped ungrafted intermediates. This mechanism may be used as a guide for designing long chain branched polymer nanoencapsules for controlled drug delivery.

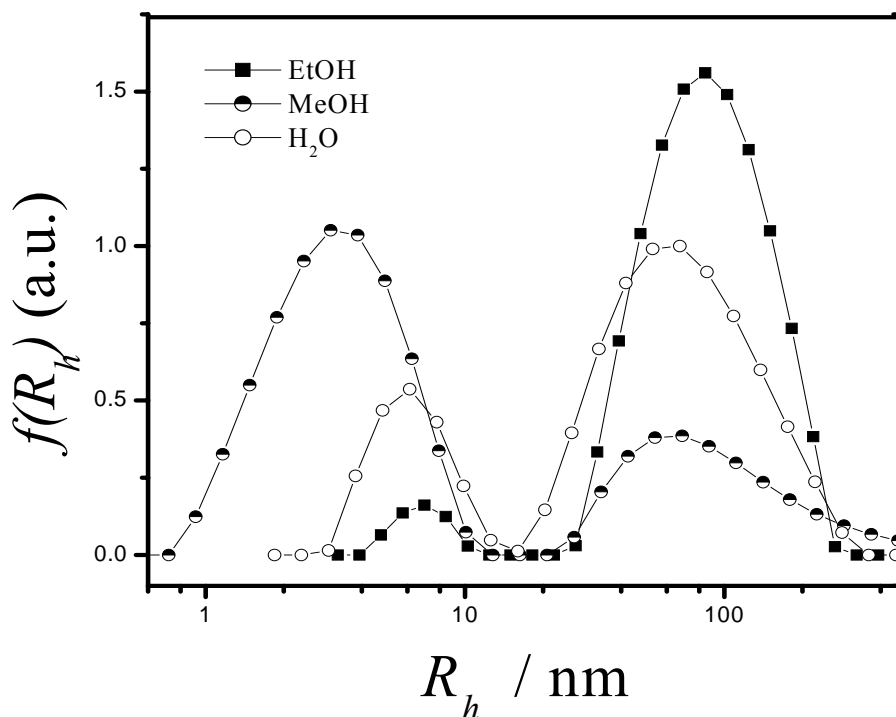


Figure 6.8. Comparison of hydrodynamic radius distribution profiles for the long chain branched-PEOx in ethanol, methanol, and water at 23°C. The polymer concentration is  $1 \times 10^{-2}$  g/ml in H<sub>2</sub>O,  $1 \times 10^{-3}$  g/ml in methanol and  $2.5 \times 10^{-5}$  g/ml in ethanol, all below their own cac. Two peaks are observed for all three solvents. The large- $R_h$  and the small- $R_h$  peaks are attributed to individual long chain branched polymers and ungrafted polymer precursors, respectively.

## CONCLUSION

The self-association behavior of long chain branched-PEOx in various solvents has been investigated using laser light scattering techniques. It was found that this long chain branched polymer can form meta-stable, narrowly size-distributed aggregates through self-association not only in a less-polar solvent such as THF, but also in more polar solvents such as ethanol and methanol. The cac of the HBP in water, methanol, ethanol and THF at 23°C were determined to be larger than 0.01,  $4.0 \times 10^{-3}$ ,  $2.5 \times 10^{-4}$ , and less than  $1.0 \times 10^{-6}$  g/ml, respectively. From the shift of the cac value, it is apparent that the quality of the solvents for the

long chain branched-PEOx ranks from good to poor in the sequence of water, methanol, ethanol, and THF. This result follows the order of solvents' polarity.

Based on light scattering measurements, conformation of individual long chain branched-PEOx and their aggregates in various solvents are proposed. As polarity of the solvent increases, C<sub>18</sub> chains move from the outside surface to the interior. Inward-moving C<sub>18</sub> chains can bring coupled PEOx chains to move with them, causing shrinkage of the hydrodynamic radius. The equilibrium size of individual long chain branched polymer is a balance between the inward-bound force and the elasticity of the polymer core, which prevents complete collapse of the polymer in water. Self-association in the long chain branched-PEOx appears to consist of two competing processes of intra-chain and inter-chain interactions. The shrinkage is due to the association of C<sub>18</sub> within a single long chain branched polymer, and due to a lack of enough polymer neighbors to form the aggregate. When the cac is reached, sufficient number of neighbors exists to allow the aggregation to occur instead of continual shrinkage.

Static LLS revealed that the molar mass of an individual long chain branched-PEOx is  $5.68 \times 10^5$  g, and its average density in ethanol is about  $2.65 \times 10^{-3}$  g/cm<sup>3</sup> at 23°C. The hydrodynamic radius of an individual polymer in ethanol shrinks from 81 nm to 56 nm as the temperature increases from 20°C to 45°C. During this process no aggregation occurs. A dynamic LLS study of individual molecules showed that some unreacted intermediates can be entrapped into or released from the core of the long chain branched polymer, depending on the polarity of the solvent.

## CHAPTER REFERENCES

1. Xia, X., Hu, Z., Gao, J., Qin, D., Durst, D.H., Yin, R., *Langmuir*, **2002**, 18, 8302
2. Moore, J.S. *Acc. Chem. Res.*, **1997**, 30, 402
3. Tomalia, D. A., Baker, H., Dewald, J., Hall, M., Kallos, G., Martin, S., Roeck, J., Ryder, J., Smith, P. *Polym. J.*, **1985**, 17, 117
4. Tomalia, D.A., Baker, H., Dewald, J., Hall, M., Kallos, G., Martin, S., Roeck, J., Ryder, J., Smith, P. *Macromolecules* **1986**, 19, 2466
5. Hawker, C.J., Frechet, J.M. *J. Am. Chem. Soc.* **1990**, 112, 7638
6. Kawaguchi, T., Walker, K.L., Wilkins, C.L., Moore, J.S. *J. Am. Chem. Soc.* **1995**, 117, 2159
7. Yin, R., Zhu, Y., Tomalia, D.A., *J. Amer. Chem. Soc.* **1998**, 120, 2678
8. Aoki, A., Ghosh, P., Crooks, R.M. *Langmuir* **1999**, 15, 7418
9. Guan, Z., Cotts, P. M., McCord, E. F., McLain, S. J. *Science* **1999**, 283, 2059
10. Tomalia, D.A., Naylor, A.M., Goddard, W.A. *Angew. Chem. Int. Ed. Engl.* **1990**, 29, 138
11. Dagani, R. *Chemical and Engineering News* **1996**, 1
12. Meltzer, A. D., Tirrell, D. A., Jones, A. A. *Macromolecules* **1992**, 25, 4541
13. Uppuluri, S., Keinath, S. E., Dvornic, P. R. *Macromolecules* **1998**, 31, 4498
14. Topp, A., Bauer, B.J., Prosa, T.J., Scherrenberg, R., Amis, E.J. *Macromolecules* **1999**, 32, 8923
15. Bauer, B., Topp, A., Prosa, T.J., Amis, E.J., Yin, R., Qin, D., Tomalia, D.A. *ACS PMSE Proc.* **1997**, 77, 87
16. Topp, A., Bauer, B.J., Tomalia, D.A., Amis, E.J. *Macromolecules* **1999**, 32, 7232
17. Li, J., Piehler, L.T., Meier, D.J. *Langmuir* **2000**, 16, 5613
18. Ottaviani, M. F., Favuzza, P., Tomalia, D. A. *Langmuir* **2000**, 16, 7368

19. Pistolis, G., Malliaris, A., Tsiourvas, D., *Langmuir* **1997**, 13, 5870
20. Ishizu, K., Takeda, H. *Eur. Polym. J.* **2001**, 37, 2073
21. Bayouhd, S., Laschewsky, A., Wishcherhoff, E. *Coll. Polym. Sci.* **1999**, 277, 519
22. Zhou, Z., Chu, B., Nace, V. M. *Langmuir* **1996**, 21, 5016
23. Yu, J.M., Jerome, R. *Macromolecules* **1996**, 29, 8371
24. Li, M., Wu, C. *Macromolecules* **1999**, 32, 4311
25. Gao, J., Haidar, G., Lu, X., Hu, Z. *Macromolecules* **2001**, 34, 2242
26. Tomalia, D.A., Huffines, E.F. *U.S. Pat.* 4,261,925, **1981**, April 14
27. Aoi, K., Okada, M. *Prog. Polym. Sci.* **1996**, 21, 151
28. Kobayashi, S., *Prog. Polym. Sci.* **1990**, 15, 751
29. Kennedy, J. P. *Trip*, **1995**, 3, 386
30. Qin, D., Yin, R., Li, J., Piehler, L., Tomalia, D.A., Durst, H. D., Hagnauer, G. *Poly. Prepr.* **1999**, 40, 171
31. Yin, R., Qin, D., Tomalia, D.A., Kukowoska-Latallo, J., Baker, J.R. Jr. *PMSE*, **1997**, 77, 206
32. Yin, R., Swanson, D.R., Tomalia, D.A. *PMSE*, **1995**, 73, 277
33. Stockmayer, W. H., Schmidt, M. *Pure Appl. Chem.* **1982**, 54, 407; *Macromolecules* **1984**, 17, 509
34. Pelton, R. H. *Advances in Colloid Interface Sci.* **2000**, 85, 1

## CHAPTER 7

### CONCLUSION

This dissertation elaborates on the synthesis and properties of novel temperature sensitive bulk polymer hydrogel and gel nanoparticles including long chain branched-PEOX, FDA approved HPC microgels, PNIPAM/Na-MLS polymer-clay composite, PNIPAM-PAA IPN microgels. The main conclusions are described as follows:

(1) The self-association behavior of long chain branched-PEOX in various solvents has been investigated using laser light scattering techniques. It was found that this long chain branched polymer can form meta-stable, narrowly size-distributed aggregates through self-association not only in a less-polar solvent such as THF, but also in more polar solvents such as ethanol and methanol. The cac of the HBP in water, methanol, ethanol and THF at 23°C were determined to be larger than 0.01,  $4.0 \times 10^{-3}$ ,  $2.5 \times 10^{-4}$ , and less than  $1.0 \times 10^{-6}$  g/ml, respectively. From the shift of the cac value, it is apparent that the quality of the solvents for the long chain branched-PEOX ranks from good to poor in the sequence of water, methanol, ethanol, and THF. This result follows the order of solvents' polarity.

Based on light scattering measurements, conformation of individual long chain branched-PEOX and their aggregates in various solvents are proposed. As polarity of the solvent increases, C<sub>18</sub> chains move from the outside surface to the interior. Inward-moving C<sub>18</sub> chains can bring coupled PEOx chains to move with them, causing shrinkage of the hydrodynamic radius. The equilibrium size of individual long chain branched polymer is a balance between the inward-bound force and the elasticity of the polymer core, which prevents complete collapse of the polymer in water. Self-association in the long chain branched-PEOX appears to consist of two

competing processes of intra-chain and inter-chain interactions. The shrinkage is due to the association of  $C_{18}$  within a single long chain branched polymer, and due to a lack of enough polymer neighbors to form the aggregate. When the cac is reached, sufficient number of neighbors exists to allow the aggregation to occur instead of continual shrinkage.

Static LLS revealed that the molar mass of an individual long chain branched-PEOx is  $5.68 \times 10^5$  g, and its average density in ethanol is about  $2.65 \times 10^{-3}$  g/cm<sup>3</sup> at 23°C. The hydrodynamic radius of an individual polymer in ethanol shrinks from 81 nm to 56 nm as the temperature increases from 20°C to 45°C. During this process no aggregation occurs. A dynamic LLS study of individual molecules showed that some unreacted intermediates can be entrapped into or released from the core of the long chain branched polymer, depending on the polarity of the solvent.

(2) Surfactant-free HPC microgels have been synthesized by chemically cross-linking hydroxypropyl cellulose (HPC) linear macromolecules. The controllable synthesis parameters-salt concentration, HPC concentration, and reaction temperature-were varied to determine the effects on the size and size distribution of the microgels as monitored using dynamic laser light scattering techniques. It is found that the microgels can form at room temperature within a narrow NaCl concentration range from 1.3 to 1.4 M. As the HPC concentration increases from 0.03 to 0.1 wt %, or temperature varied from 23.5 to 21.5°C, or sodium chloride concentrations decreased from 1.4 to 1.3 M, the particle size distribution of resultant HPC microgels become narrower. The formation of microgels may be explained by the breakdown of hydrogen bonding between water and HPC chain with the addition of electrolyte. The fitting curves based on the Flory-Huggins mean-field theory are in good agreement with the experimental results.



(3) Clay-polymer hydrogel composites have been synthesized based on poly(N-isopropylacrylamide) (PNIPAM) gels containing 0.25 to 4 wt% of the expandable smectic clay Na-montmorillonite layered silicates (Na-MLS). Their structure and property relationship has been investigated combining measurements of morphology, shear modulus, and swelling ratio as a function of temperature and Na-MLS concentration. Specifically, a polarized optical microscopy study has revealed that Na-MLS form aggregates in the PNIPAM gel and the size of aggregates increases with Na-MLS concentration. Incorporation of Na-MLS clay into a neutral PNIPAM network improves the gel mechanical properties, while does not change its volume phase transition temperature. The shear modulus of the gel composite first decreases and then increases with the increasing Na-MLS concentration, exhibiting a distinct minimum. In Na-MLS additive concentrations ranging from 2.0 to 3.2 w%, both swelling ratio and shear modulus of the composite gels have been improved comparing with the pure PNIPAM gel. The difference in gel volume below and above  $T_c$  can be enhanced by adding small amount of Na-MLS (<1.5 w%). The composite gel does not response to the pH change, indicating that Na-MLS is physically entrapped inside the gel matrix.

(4) Monodisperse IPN nanoparticles composed of poly-acrylic acid (PAA) and poly(N-isopropylacrylamide) (PNIPAM) interpenetrating networks are for the first time synthesized. The kinetics of IPN formation is obtained by measuring the turbidity variation and particle hydrodynamic radius change as a function of time. Individual IPN and PNIPAM nanoparticles are studied and compared using both dynamic and static light scattering techniques. The semidilute IPN nanoparticle dispersion possesses the advantage of thermosensitive property and the single IPN nanoparticle exhibits a relatively high equilibrium water content and also showed

the multiple and reversible sensitivity to both pH and temperature. Those properties may be explored for the application in controlled drug delivery.

#### CHAPTER REFERENCES:

1. Xia, X., Hu, Z., Gao, J., Qin, D., Durst, H. D., Yin, R. *Langmuir* **2002**, 18, 8302
2. Xia, X., Tang, S., Lu, X., Hu, Z. *Macromolecules* **2003**, 36, 3695
3. Xia, X., Yih, M.J., Dsouza, N., Hu, Z. *Polymer* **2003**, 44, 3387
4. Hu, Z., Xia, X. *Adv. Mater.* **2003**, (in press)
5. Xia, X., Hu, Z. *Langmuir* **2003**, (submit)

## BIBLIOGRAPHY

1. Ahlnas, T., Karlstrom, G., Lindman, B. *J. Phys. Chem.* **1987**, 91, 4030
2. Alexandridis, P., Hatton, T. A. *Colloidal Surfaces A: Physicochem. Eng. Aspects* **1995**, 96, 1
3. Allcock, H. R., Lampe, F. W. *Contemporary Polymer Chemistry, 2nd edition* Prentice-Hall, Ins.: New Jersey, **1990**
4. Almgren, M., Bahadur, P., Jansson, M., Li, P., Brown, W., Bahadur, A. J. *Colloid & Interface Sci.* **1992**, 151, 157
5. Aoi, K., Okada, M. *Prog. Polym. Sci.* **1996**, 21, 151
6. Aoki, A., Ghosh, P., Crooks, R.M. *Langmuir*, **1999**, 15, 7418
7. Bauer, B., Topp, A., Prosa, T.J., Amis, E.J., Yin, R., Qin, D., Tomalia, D.A. *ACS PMSE Proc.* **1997**, 77, 87
8. Bayouhd, S., Laschewsky, A., Wishcherhoff, E. *Coll. Polym. Sci.* **1999**, 277, 519
9. Beebe, D.J., Moor, J.S., et al. *Nature* **2000**, 404, 588
10. Benee, L. S., Snowden, M. J., Chowdhry, B. Z., *Langmuir*, **2002**, 18, 6025
11. Berne, B. J., Pecora, R. *Dynamic Light Scattering*; John Wiley & Sons, Inc: NewYork, **1976**
12. Bouillot, P., Vincent, B. *Colloid and Polymer Science* **2000**, 278, 74
13. Brown, W. *Dynamic Light Scattering*; Oxford University Press: Oxford, **1993**
14. Butzloff, P., D'Souza, NA, Golden, T.D., Garrett, D. *Polym Engng Sci* **2001**, 41, 1794
15. Chen, L., Gong, J., Osada, Y. *Macromolecular Rapid Communications* **2002**, 23, 171

16. Churochkina, N.A., Starodoubtsev, S.G., Khokhlov, A.A. *Polymer Gels and Networks* **1998**, 6, 205
17. Chu, B. *Laser Light Scattering*, 2nd edition; Academic Press, **1991**
18. Dagani, R. *Chemical and Engineering News* **1996**, 1
19. Dong, L., Hoffman A.S. *J Control Release* **1986**, 4, 223
20. Drummond, C., Albers, S., Furlong, D. N. *J. Colloids Surf.* **1992**, 62, 75
21. Durand, A., Hourdet, D. *Polymer*, **1999**, 40, 17, 4941
22. Everett, D. H. *Basic Principles of Colloid Science*, Royal Society of Chemistry, London **1998**
23. Flory, P. J. *Principles of Polymer Chemistry* Cornell University Press: Ithaca, NY, **1963**
24. Gao, J., Frisken, B. J., *Langmuir*, **2003**, 19, 5217
25. Gao, D., Heimann, R.B. *Polymer Gels and Networks*, **1993**, 1, 225
26. Gao, J., Haidar, G., Lu, X. H., Hu, Z. B. *Macromolecules* **2001**, 34, 2242
27. Gao, J., Hu, Z. *Langmuir*, **2002**, 18 (4), 1360
28. Guan, Z., Cotts, P. M., McCord, E. F., McLain, S. J. *Science*, **1999**, 283, 2059
29. Gutowska, Y.H., Bae, H., Jacobs, J., Feijen, Sung Wan Kim, *Macromolecules*, **1994**, 27, 4167
30. Han C. K., Bae, Y. H. *Polymer* **1998**, 39, 2809
31. Haraguchi, K., Takehisa, T. *Adv. Mat.* **2002**, 14, 1120
32. Harsh, D. C., Gehrke, S. H. *J. Controlled Release* **1991**, 17, 175
33. Hawker, C.J., Frechet, J.M. *J. Am. Chem. Soc.* **1990**, 112, 7638
34. Hirotsu, S., Hirokawa, Y., Tanaka, T. *J. Chem. Phys.* **1987**, 87, 1392
35. Hu, Z. B., *Adv. Mat. Adv. Mater.* **2001**, 13, 1708

36. Hu, Z. B., Lu, X., Gao, J. *Adv. Mater.* **2001**, 13, 1708
37. Hu, Z. B., Lu, X., Gao, J., Wang, C. *Adv. Mater.* **2000**, 12, 1173
38. Hu, Z. B., Zhang, X. M., Li, Y. *Science* **1995**, 269, 525
39. Hu, Z., Chen, Y., Wang, C., Zheng Y., Li, Y. *Nature* **1998**, 393, 149
40. Hu, Z., Xia, X., *Adv. Mat.* **2003** (in press)
41. Ilmain, F., Tanaka, T., Kokufuta, E. *Nature* **1991**, 349, 400
42. Ishizu, K., Takeda, H. *Eur. Polym. J.* **2001**, 37, 2073
43. Jeffrey, G.A., Saenger, W. *Hydrogen Bonding in Biological Structures*. Springer-Verlag, New York, **1991**
44. Jeong, B., Kim S. W., Bae, Y. H. *Adv. Drug Del. Rev.* **2002**, 54, 37
45. Jones, C. D., Lyon, L.A. *Macromolecules* **2000**, 33, 8301
46. Kabra, B. G., Gehrke, S. H., Spontak, R. J. *Macromolecules* **1998**, 31, 21668
47. Harsh, D. C., Gehrke, S. H. *J. Controlled Release* **1991**, 17, 175
48. Karlstrom, G. *J. Phys. Chem.* **1985**, 89, 4962
49. Karlstrom, G., Carlsson, A., Lindman, B. *J. Phys. Chem.* **1990**, 94, 5005
50. Katono, H., Sanui, K., Ogata, N., Okano, T., Sakurai, Y. *Polym J* **1991**, 23, 1179-1189;  
Katono, H., Maruyama, A., Sanui, K., Ogata, N., Okano, T., Sakurai, Y. *J Control Rel* **1991**, 16, 215
51. Kato, T., Yokoyama, M., Takahashi, A. *Colloid & Polym. Sci.* **1978**, 256, 15
52. Kawaguchi, T., Walker, K.L., Wilkins, C.L., Moore, J.S. *J. Am. Chem. Soc.* **1995**, 117, 2159
53. Kennedy, J. P. *Trip* **1995**, 3, 386
54. Kluc, E. D. *J. Polym. Sci.* **1971**, 36, 491

55. Kobayashi, S. *Prog. Polym. Sci.* **1990**, 15, 751
56. Li, J., Piehler, L.T., Meier, D.J. *Langmuir* **2000**, 16, 5613
57. Li, M., Wu, C. *Macromolecules* **1999**, 32, 4311
58. Li, Y., Tanaka, T. *Annu. Rev. Mat. Sci.* **1992**, 22, 243
59. Liao, G., Xie, Y., Ludwig, K.F., Bansil, R., Gallagher, P. *Phys. Rev. E* **1999**, 60, 4473
60. Lu, X., Hu, Z., Gao, J. *Macromolecules* **2000**, 33, 8698
61. Lvov, Y., Ariga, K., Ichinose, I., Kunitake, T. *Langmuir* **1996**, 12, 3038
62. Meltzer, A. D., Tirrell, D. A., Jones, A. A. *Macromolecules* **1992**, 25, 4541
63. Motonaga, T., Shibayama, M. *Polymer* **2001**, 42, 8925
64. Moore, J.S. *Acc. Chem. Res.* **1997**, 30, 402
65. Murry, M. J., Snowden, M. J. *Adv. Colloid Interface Sci.* **1995**, 54, 73
66. Ohmine, I., Tanaka, T. *J. Chem. Phys.* **1982**, 77, 5725
67. Osada, Y., Okuzaki, H., Hori, H. *Nature* **1992**, 355, 242
68. Ottaviani, M. F., Favuzza, P., Tomalia, D. A. *Langmuir* **2000**, 16, 7368
69. Park, T. G., Choi, H. K. *Macromol. Rapid Commun.* **1998**, 19, 167
70. Park, T., Hoffman, A. S. *Macromolecules* **1993**, 26, 5045
71. Pelton, R. *Adv. Colloid Interface Sci.* **2000**, 85, 1
72. Phillip, B., Messersmith, Znidarsich, F. *Mat. Res. Soc. Symp.* **1997**, 457
73. Pistolis, G., Malliaris, A., Tsiourvas, D., *Langmuir* **1997**, 13, 5870
74. Provencher, S. W. *Biophys. J.* **1976**, 16, 29
75. Provencher S. W. *Makromol. Chem.* **1979**, 180, 201
76. Qin, D., Yin, R., Li, J., Piehler, L., Tomalia, D.A., Durst, H. D., Hagnauer, G. *Poly. Prepr.* **1999**, 40, 171

77. Ranade, A., D'Souza, N.A., Gnade, B. *Polymer*, **2002**, 43, 13, 3759
78. Routh, A. F., Vincent, B., *Langmuir*, **2002**, 18, 5366
79. Russel, W. B., Saville, D. A., Schowalter, W.R. *Colloidal Dispersions*, Cambridge University Press, Cambridge **1989**
80. Saunders, B. R., Vincent, B. *Adv. Colloid Interface Sci.* **1999**, 80, 1
81. Schmidt, M., Stockmayer, W. H. *Macromolecules* **1984**, 17, 509
82. Schramm, L.L. "Suspensions: fundamentals and applications in the petroleum industry" *American Chemical Society*, Washington, DC **1996**
83. Senff, H., Richtering, W., Norhausen, C., Weiss, A., Ballauff, M. *Langmuir* **1999**, 15, 102
84. Senff, H., Richtering, W. *J. Chem. Phys.* **1999**, 111, 1705
85. Shibayama, M., Ikkai, F., Inamoto, S., Nomura, S., Han, C.C. *J. Chem. Phys.* **1996**, 105, 8
86. Shibayama, M., Tanaka, T. *Advances in Polymer Science* **1993**, 109, 1
87. Shibayama, M., Tanaka, T., Han, C.C. *J. Chem. Phys.* **1992**, 97, 6829
88. Shinde, V.S., Badiger, M.V., Lele, A.K., Mashelkar, R.A. *Langmuir* **2001**, 17, 2585
89. Sperling, L. H. *Adv. Chem. Ser.* **1994**, 239, 12
90. Stockmayer, W. H., Schmidt, M. *Pure Appl. Chem.* **1982**, 54, 407
91. Suzuki, A. *Adv. Polym. Sci.* **1993**, 110, 201
92. Takigawa, T., Yamawaki, T., Takahashi, K., Masuda, T. *Polymer Gels and Networks*, **1997**, 5, 585
93. Tanaka, T. *Phys. Rev. Lett.* **1978**, 40, 820
94. Tanaka, T. *Experimental Methods in Polymer Science* Academic Press, **2000**

95. Tanaka, T., Fillmore, D. J., Sun, S.T., Nishio, I., Swislow, G., Shah, A. *Phys. Rev. Lett.* **1980**, 45, 1636
96. Tanaka, T., Nishio, I., Sun, S. T., Ueno-Nishio, S. *Science* **1982**, 218, 467-469
97. Tomalia, D. A., Baker, H., Dewald, J., Hall, M., Kallos, G., Martin, S., Roeck, J., Ryder, J., Smith, P. *Polym. J.* **1985**, 17, 117
98. Tomalia, D.A., Baker, H., Dewald, J., Hall, M., Kallos, G., Martin, S., Roeck, J., Ryder, J., Smith, P. *Macromolecules*, **1986**, 19, 2466
99. Tomalia, D.A., Huffines, E.F. *U.S. Pat.* 4,261,925, **1981**, April 14
100. Tomalia, D.A., Naylor, A.M., Goddard, W.A. *Angew. Chem. Int. Ed. Engl.* **1990**, 29, 138
101. Topp, A., Bauer, B.J., Tomalia, D.A., Amis, E.J. *Macromolecules* **1999**, 32, 7232
102. Topp, A., Bauer, B.J., Prosa, T.J., Scherrenberg, R., Amis, E.J. *Macromolecules* **1999**, 32, 8923
103. Uppuluri, S., Keinath, S. E., Dvornic, P. R. *Macromolecules* **1998**, 31, 4498
104. Wang, C. J., Hu, Z. B., Chen, Y. Y., Li, Y. *Macromolecules* **1999**, 32, 1822-1827
105. Winnik, F. M., Tamai, N., Yonezawa, J., Nishimura, Y., Yamazaki, I. *J. Phys. Chem.* **1992**, 96, 1967
106. Woodward, N. C., Chowdhry, B. Z., Snowden, M. J., Leharne, S. A., Griffiths, P. C., Winnington, A. L., *Langmuir*, **2003**, 19, 3202
107. Wu, C., Chan, K. K., Xia, K. Q. *Macromolecules* **1995**, 28, 1032
108. Wu, C., Zhou, S. *Macromolecules* **1996**, 29, 1574
109. Xia, X. Hu, Z. *Langmuir* **2003**, (submit)
110. Xia, X., Hu, Z., Gao, J., Qin, D., Durst, H. D., Yin, R. *Langmuir* **2002**, 18, 8302



111. Xia, X., Tang, S., Lu, X., Hu, Z. *Macromolecules* **2003**, 36, 3695
112. Xia, X., Yih, M.J., Dsouza, N., Hu, Z. *Polymer* **2003**, 44, 3387
113. Xue, W., Champ, S., Huglin, M.B. *Polymer* **2001**, 42, 3665
114. Yin, R., Qin, D., Tomalia, D.A., Kukowoska-Latallo, J., Baker, J.R. Jr. *PMSE* **1997**, 77, 206
115. Yin, R., Swanson, D.R., Tomalia, D.A. *PMSE* **1995**, 73, 277
116. Yin, R., Zhu, Y., Tomalia, D.A. *J. Amer. Chem. Soc.* **1998**, 120, 2678
117. Yu, J.M., Jerome, R. *Macromolecules* **1996**, 29, 8371
118. Zhang, G., Wu, C. *J. Am. Chem. Soc.* **2001**, 123, 1376
119. Zhang, X., Hu, Z., Li, Y. *J. Appl. Polym. Sci.* **1997**, 63, 1851
120. Zhou, Z., Chu, B., Nace, V. M. *Langmuir* **1996**, 21, 5016
121. Zhang, X., Zhuo, R., Yang, Y. *Biomaterials* **2002**, 23, 1313

## APPENDIX

### List of Abbreviations

APS	Ammonium Persulfate
BIS	Methylene-bis-acrylamide
CAC	Critical Aggregation Concentration
DLS	Dynamic Light Scattering
HPC	Hydroxypropyl Cellulose
IPN	Interpenetrating Polymer Networks
LCB-PEOx	Long Chain Branched Poly(2-ethyloxazoline)
LCST	Lower Critical Solution Temperature
LLS	Laser Light Scattering
Na-MLS	Sodium Montmorillonite Layered Silicates
PAAc	Poly(Acrylic Acid)
PAAM	Polyacrylamide
PBS	Phosphate Buffer Saline
PDI	Polydispersity Index
PNIPAM	Poly(N-isopropylacrylamide)
PSC	Photon Correlation Spectroscopy
R <sub>g</sub>	Radius of Gyration
R <sub>h</sub>	Hydrodynamic Radius
SDS	Sodium Dodecyl Sulfate
SLS	Static Light Scattering
THF	Tetrahydrofuran